The Role of Sex Hormones in Male-biased Influenza Virus Infections

A dissertation

for the doctoral degree of

DOCTOR RERUM NATURALIUM

Faculty of Mathematics, Informatics and Natural Sciences

Department of Biology

at the University of Hamburg

by

Tian Bai

From Sichuan, China

Hamburg, 2023

Date of Oral Defense: September 27, 2023

First reviewer:

Prof. Dr. Gülşah Gabriel

Research Department Viral Zoonoses-One Health, Leibniz Institute of Virology (LIV), Hamburg, Germany; University of Veterinary Medicine, Hannover, Germany.

Second reviewer:

Prof. Dr. Thomas Dobner

Research Department Viral Transformation, Leibniz Institute of Virology (LIV), Hamburg, Germany; Department of Biology, University of Hamburg, Hamburg, Germany

Publications related to this study (as of March 2023):

Tian Bai*, Yongkun Chen*, Sebastian Beck*, Stephanie Stanelle-Bertram, Nancy Kouassi Mounogou, Tao Chen, Jie Dong, Bettina Schneider, Tingting Jia, Jing Yang, Lijie Wang, Andreas Meinhardt, Antonia Zapf, Lothar Kreienbrock, Dayan Wang, Yuelong Shu, Gülsah Gabriel. H7N9 infection in men is associated with testosterone depletion. *Nat Commun* **13**, 6936 (2022).

Maria Schröder*, Berfin Schaumburg*, Zacharias Müller, Ann Parplys, Dominik Jarczak, Kevin Roedl, Axel Nierhaus, Geraldine de Heer, Joern Grensemann, Bettina Schneider, Fabian Stoll, **Tian Bai**, Henning Jacobsen, Martin Zickler, Stephanie Stanelle-Bertram, Kristin Klaetschke, Thomas Renne, Andreas Meinhardt, Jens Aberle, Jens Hiller, Sven Peine, Lothar Kreienbrock, Karin Klingel, Stefan Kluge, Gülşah Gabriel. High estradiol and low testosterone levels are associated with critical illness in male but not in female COVID-19 patients: a retrospective cohort study. *Emerg Microbes Infect* **10**, 1 (2021).

Berfin Tuku*, Stephanie Stanelle-Bertram*, Julie Sellau, Sebastian Beck, **Tian Bai**, Nancy Mounogou Kouassi, Annette Preuß, Stefan Hoenow, Thomas Renné, Hanna Lotter, Gülşah Gabriel. Testosterone Protects Against Severe Influenza by Reducing the Pro-Inflammatory Cytokine Response in the Murine Lung. *Frontiers in Immunology* **11**, 697 (2020).

Other publications (as of March 2023):

Yongkun Chen*, Laura Graf*, Tao Chen*, Qijun Liao*, **Tian Bai**, Philipp P. Petric, Wenfei Zhu, Lei Yang, Jie Dong, Jian Lu, Ying Chen, Juan Shen, Otto Haller, Peter Staeheli, Georg Kochs, Dayan Wang, Martin Schwemmle, Yuelong Shu. Rare variant MX1 alleles increase human susceptibility to zoonotic H7N9 influenza virus. *Science* **373**, 6557 (2021)

Chen Yongkun*, **Bai Tian***, Shu Yuelong. Poultry to Human Passport: Cross-species Transmission of Zoonotic H7N9 Avian Influenza Virus to Humans. *Zoonoses* **2**,1 (2022)

Chen, Liling, Levine, Min Z, Zhou, Suizan, **Bai, Tian**, Pang, Yuanyuan, Bao, Lin, Tan, Yayun, Cui, Pengwei, Zhang, Ran, Millman, Alexander J., Greene, Carolyn M., Zhang, Zhongwei, Wang, Yan, Zhang, Jun. Mild and asymptomatic influenza B virus infection among unvaccinated pregnant persons: Implication for effectiveness of non-pharmaceutical intervention and vaccination to prevent influenza. *Vaccine* **41**, 3 (2023)

Stephanie Stanelle-Bertram, Sebastian Beck, Nancy Kouassi Mounogou, Berfin Schaumburg, Fabian Stoll, **Tian Bai**, Martin Zickler, Georg Beythien, Kathrin Becker, Madeleine de la Roi, Fabian Heinrich, Claudia Schulz, Martina Sauter, Susanne Krasemann, Philine Lange, Axel Heinemann, Debby van Riel, Lonneke Leijten, Lisa Bauer, Thierry P.P. van den Bosch, Boaz Lopuhaä, Tobias Busche, Daniel Wibberg, Dirk Schaudien, Torsten Goldmann, Hanna Jania, Zacharias Müller, Vinicius Pinho dos Reis, Vanessa Krupp-Buzimkic, Martin Wolff, Chiara Fallerini, Margherita Baldassarri, Simone Furini, Katrina Norwood, Christopher Käufer, Nina Schützenmeister, Maren von Köckritz-Blickwede, Maria Schroeder, Dominik Jarczak, Axel Nierhaus, Tobias Welte, Stefan Kluge, Alice C. McHardy, Frank Sommer, Jörn Kalinowski, Susanne Krauss-Etschmann, Franziska Richter, Jan von der Thüsen, Wolfgang Baumgärtner, Karin Klingel, Benjamin Ondruschka, GEN-COVID Multicenter Study , Alessandra Renieri and Gülsah Gabriel. *CYP19A1* mediated sex hormone metabolism promotes severe SARS-CoV-2 disease outcome in males. *Cell Reports Medicine* (in revision)

Tian Bai*, Sebastian Beck, Gülsah Gabriel. Replication of influenza A virus in Leydig cells. *Zoonoses* (manuscript in preparation)

*: First or co-first author

1 Table of contents

2 List of Abbrevations

The abbreviations of amino acids, chemical elements/compounds (e.g. NaCl, sodium chloride) and SI units are considered to be known according to common literature and are therefore not listed here.

°C	Degree Celsius
µg	Microgram
µl	Microliter
AA	Amino acid
AIV	Avian influenza virus
ACE2	Angiotensin converting enzyme 2
APS	Ammonium peroxidisulfate
AR	Androgen receptor
ARE	Androgen receptor element
BCS	Basic cleavage site
BMI	Body mass index
BSA	Bovine serum albumin
BSL	Biosafety level
C-	Carboxy-terminal
C/C	Cytokines and chemokines
cDNA	Complementary DNA
CDC	Center for disease control and prevention
CNIC	Chinese National Influenza Center
CO_2	Carbon dioxide
CoV	Corona viruses
COVID-19	Corona virus disease 2019
cRNA	Complementary RNA
cRNP	Complementary ribonucleoprotein
DC	Dendritic cell
d p.i.	Days post infection
DBD	DNA-binding domain
ddH_2O	Double distilled H_2O
DMEM	Dulbecco's Modified Eagle's Medium
DMSO	Dimethylsulfoxide
DNA	Deoxyribonucleic acid
dNTP	2'-deoxynucleotide-5'-triphosphate
DTT	Dithiotreitol
DHT	Dihydrotestosterone
E2	17β-estradiol
e.g.	example given
EDTA	Ethylendiaminetetraacetate
EGF	Epidermal growth factor
ER	Estrogen receptor
ERE	Estrogen receptor element
FBS	Fetal bovine serum
fwd	Forward

g	Gram
GAPDH	Glycerinealdehyde 3‘-phosphate dehydrogenase
GC	Guanine – cytosine
G-CSF	Granulocyte colony-stimulating factor
GM-CSF	Granulocyte-macrophage colony-stimulating factor
h	Hour
H&E	Hematoxylin and eosin
h p.i.	Hours post infection
h p.t.	Hours post transfection
H_2O	Water
HA_0	Hemagglutinin precursor protein
HA_1	Hemaggluttinin subunit 1
HA_2	Hemaggluttinin subunit 2
HPAIV	Highly pathogenic avian influenza virus
HPG	Hypothalamic-pituitary-gonadal axis
HRT	Hormone replacement therapy
i.e.	id est
kb	Kilo base pairs
kDa	Kilodalton
IAV	Influenza A virus
IBV	Influenza B virus
IP-10	Interferon gamma-induced protein 10
IFN	Intereron
IL	Interleukin
IL-RA	Interleukin receptor antagonist
L	Liter
LC	Leydig cells
LBD	Ligand-binding domain
LIV	Leibniz Institute of Virology
LPAIV	Low pathogenic avian influenza virus
LRR	Leucine-rich repeat
LRT	Lower respiratory tract
M	Molar
M1/2	Matrix protein 1/2
MCP-1	Monocyte chemoattractant protein-1
MEM	Minimum Essential Medium
mg	Milligram
min	Minute
Mio.	Million
MIP	Macrophage inflammatory protein
ml	Milliliter
mM	Millimolar
MOI	Multiplicity of infection
mRNA	Messenger RNA
MSM	Men who have sex with men
N-	Amino-terminal
NA	Neuraminidase
NAIs	Neuraminidase inhibitors

NEP	Nuclear export protein
NF-κB	Nuclear factor κB
NK cell	Natural killer cells
NLS	Nuclear localization signal
NTD	N-terminal domain
nm	Nanometer
nM	Nanomolar
NP	Nucleoprotein
NPC	Nuclear pore complex
NS	Non-structural protein (influenza virus)
ORF	Open reading frame
P/S	Penicillin–streptomycin
PA	Polymerase acidic protein
PB1/2	Polymerase basic protein 1/2
PBS	Phosphate buffered saline
PBS-T	PBS, supplemented with Tween-20
PCR	Polymerase chain reaction
PEI	Polyethylenimine
PFA	Paraformaldehyde
PFU	Plaque-forming units
pmol	Picomol
PMSF	Phenylmethylsulfonylfluoride
Poly (I:C)	Polyinosinic:polycytidylic acid
PRR	Pattern recognition receptor
PT	Plaque test
qRT-PCR	Quantitative reverse transcription PCR
RBS	Receptor binding site
RdRp	RNA-dependent RNA polymerase
rev	Reverse
RNA	Ribonucleid acid
RNP	Ribonucleoprotein
RP	Reversed phase
rpm	Rounds per minute
RT	Reverse transcriptase
RT	Room temperature
RT-PCR	Reverse transcription PCR
SA	Sialic acid
SARS-CoV	Severe acute respiratory syndrome-associated-coronavirus
SARS-CoV-2	Severe acute respiratory syndrome-associated-coronavirus type 2
SD	Standard deviation
SDM	Site-directed mutagenesis
SDS	Sodium dodecylsulfate
SDS-PAGE	SDS polyacrylamide gel electrophoresis
sec	Second
SHBG	Sex hormone-binding globulin
SOFA	Sequential organ failure assessment
SNP	Single nucleotide polymorphism

snRNA	Small nuclear RNA
SOP	Standard operating procedure
TAE	Tri-acetate-EDTA
TBS	Tris buffered saline
TEMED	Tetramethylethylendiamine
TF	Transfection
TLR	Toll-like receptor
TPCK	L-(tosylamido-2-phenyl) ethyl chloromethyl ketone
TMPRSS2	Transmembrane serine protease 2
TK	Thymidine kinase
T_M	Melting temperature
TMD	Transmembrane domain
TNF	Tumour necrosis factor
Tris	Tris(hydroxymethyl)aminomethane
U	Unit (enzymatic activity)
URT	Upper respiratory tract
V	Volt
VEGF	Vascular endothelial growth factor
VPD	Viral pathogenicity determinant
vRNA	Viral RNA
vRNP	Viral RNP
WB	Western blot
WHO	World health organization
XCI	X-chromosome inactivation

3 List of Figures

4 List of Tables

5 Zusammenfass

Das aviäre Influenza-A-Virus (H7N9) galt vor der aktuellen Coronavirus-Erkrankung 2019 (COVID-19) Pandemie als das Virus mit dem höchsten Potenzial, die nächste Pandemie auszulösen. Im Frühjahr 2013 wurden erstmals menschliche Infektionen mit dem H7N9-Virus in Ostchina gemeldet. Es hat in fünf aufeinanderfolgenden Winter-Frühling-Saisons auf dem chinesischen Festland insgesamt 1568 Fälle mit einer Letalitätsrate von 39% verursacht. Während der fünf Epidemiewellen zeigten H7N9-Infektionen wiederholt eine höhere Inzidenz bei Männern als bei Frauen. Um die Mechanismen hinter den geschlechtsspezifischen Infektionen zu entschlüsseln, konzentrierte sich diese Studie auf die Rolle von Sexualhormonen bei der Anfälligkeit für und Schwere von H7N9-Infektionen.

In dieser Studie wurden Sexualhormone sowie Entzündungsmarker von H7N9-Patienten systematisch analysiert und mit gesunden Kontrollpersonen sowie Patienten mit saisonaler Grippe verglichen. Eine multivariable Analyse ergab, dass eine H7N9-Infektion spezifisch die Hormonachse bei Männern, aber nicht bei Frauen beeinflusst. Bei Männern führte eine H7N9-Infektion zu niedrigen Testosteronspiegeln, die mit Schweregrad und tödlichem Ausgang einhergingen. Eine Verringerung der Testosteronwerte bei Männern wurde auch bei hospitalisierten saisonalen Influenza-Fällen beobachtet, jedoch in geringerem Ausmaß als bei einer H7N9-Infektion. Die lineare Regressionsanalyse ergab ferner, dass niedrige Testosteronspiegel bei H7N9-infizierten Männern mit induzierten Zytokinspiegeln, insbesondere IL-6 und IL-15, korrelierten. Weiterhin bestätigt diese Studie, in welcher Mausmodelle verwendet wurden, den kausalen Zusammenhang zwischen der H7N9-Infektion und dem Testosteronmangel bei Männern. Darüber hinaus replizierte sich das H7N9-Influenzavirus in Nagetier-Leydig-Zellen und den Hoden von Mäusen und induzierte systemische und testikuläre Entzündungsreaktionen, die wahrscheinlich die Testosteronsynthese beeinträchtigen.

Diese Studie liefert neue Erkenntnisse darüber, dass das H7N9-Influenzavirus der Atemwege spezifisch die metabolische Hypothalamus-Hypophysen-Gonaden-Achse (HPG) treffen kann, was zur Schwere der Erkrankung bei männlichen Patienten beiträgt. Dies könnte teilweise erklären, weshalb Männer vermehrt von einer H7N9-Infektion betroffen sind. Angesichts der aktuellen COVID-19-Pandemie, die das männliche Geschlecht eindeutig als Risikofaktor für die Schwere der Erkrankung betont, könnte unsere Studie als Blaupause für zukünftige Untersuchungen an Personen angesehen werden, die mit neu auftretenden Atemwegsviren infiziert sind. Darüber hinaus legt diese Studie auch nahe, dass die personalisierte Behandlung infizierter Patienten geschlechtsspezifische Milderungsstrategien berücksichtigen sollte.

6 Abstract

Avian influenza A (H7N9) virus was considered having the highest potential to cause next pandemic prior to the current coronavirus disease 2019 (COVID-19) pandemic. In early spring of 2013, human infections with H7N9 virus were first reported in Eastern China. It has caused a total of 1568 cases with a high fatality rate of 39% in five successive Winter-Spring seasons in mainland China. During the five epidemic waves, H7N9 infections showed repeated higher incidence in males than females. To unravel the mechanisms behind the male-biased infections, this study focused on the role of sex hormones in susceptibility and severity of H7N9 infections.

This study systematically analyzed sex hormones as well as inflammatory markers from H7N9 patients and compared to healthy controls as well as seasonal influenza patients. Multivariable analysis revealed H7N9 infection specifically affects the hormone axis in men but not women. In men, H7N9 infection mediated low testosterone levels that associated with severity and fatal outcome. Reduction of testosterones in males was also observed in hospitalized seasonal influenza cases but to a lower extent than H7N9 infection. Linear regression analysis further revealed that low testosterone levels in H7N9-infected men correlated with induced inflammatory cytokine levels, particularly IL-6 and IL-15. This study utilized the murine models further confirmed the causal link between H7N9 infection and testosterone depletion in males. Additionally, H7N9 influenza virus replicated in rodent Leydig cells and the testes of mice, and induced systemic and testicular inflammatory responses that likely interferes with testosterone synthesis.

This study provides new knowledge that respiratory H7N9 influenza virus can specifically hit the metabolic hypothalamic–pituitary–gonadal (HPG) axis contributing to disease severity in male patients, which could partially explain the male-biased H7N9 infections. Given the current pandemic of COVID-19 that clearly emphasizes that male sex has a higher risk of developing poor outcomes, this study might be considered as a blueprint for future investigation in individuals infected with emerging respiratory viruses. Furthermore, this study also suggests that personalized treatment of infected patients should consider sex-specific mitigation strategies.

7 Introduction

7.1 Influenza virus

7.1.1 Taxonomy and classification

Influenza viruses are classified into the Orthomyxoviridae family, which includes four types: Alphainfluenzavirus (such as Influenza A virus, IAV), Betainfluenzavirus (such as Influenza B virus, IBV), Gammainfluenzavirus (such as Influenza C virus, ICV) and Deltainfluenzavirus (such as Influenza D virus, IDV). All genera (species) of influenza A, B, C virus can infect mammals and are highly transmissible respiratory viruses in humans[1,2]. IDV circulates in cattle and swine with little known about its impact in humans[3]. The haemagglutinin (HA) and neuraminidase (NA) proteins are two major surface antigens of influenza viruses. Based on those two glycoproteins, there are 18 HA (H1-H18) and 11 NA (N1-N11) subtypes of IAV[4,5] and two recent lineages ('Victoria' and 'Yamagata') of IBV. IAV is considered as the greatest threat in public health as it has broadest host range and can cause pandemic or highly pathogenic strains that cause infections or deaths in humans.

7.1.2 Virion structure and genome organization

Since this study mainly focused on IAVs, their biology, epidemiology characteristics are described in detailed. The viral particle of IAVs has two major glycoproteins HA and NA embedded in the lipid envelope of virus with a ratio of about four to one[6] **(Figure 1A)**. Influenza viruses possess a limited number of M2 ion channels that span the lipid membrane, whereas the M1 matrix protein envelops the virion core. The M1 matrix protein is surrounded by the nuclear export protein (NEP, also known as non-structural protein 2, NS2) and the ribonucleoprotein (RNP) complexes. The eight segments of ribonucleoprotein (RNP) present in influenza A viruses are flanked by the 5' and 3' termini, which are bound by a viral RNA-dependent RNA polymerase (RdRp) consisting of two polymerase basic and one polymerase acidic subunits (PB1, PB2, and PA). These RNPs are coated with oligomeric viral nucleoprotein (NP). Morphologically, IAVs can either form spheres with a diameter of about 80-120nm or filaments that reach up to 20µm in length. However, the form of filaments is usually lost after passaging eggs or MDCK cells[7,8]. Influenza A virus genome consists of eight segments of negative-sense, single-stranded viral RNA (vRNA), which are arranged in descending order of length. Among those eight gene segments, segment 4 to 6 encode only single protein for HA, NP and NA, respectively. Other segments encode their main protein but also variants via adding alternate reading frame or mRNA splicing, such as the polymerase

subunit PB1-F2[9] or nuclear export protein/non-structural protein NEP/NS2[10]. In **Table 1**, all encoded proteins of each segment and their functions are summarized in detail for IAVs**.**

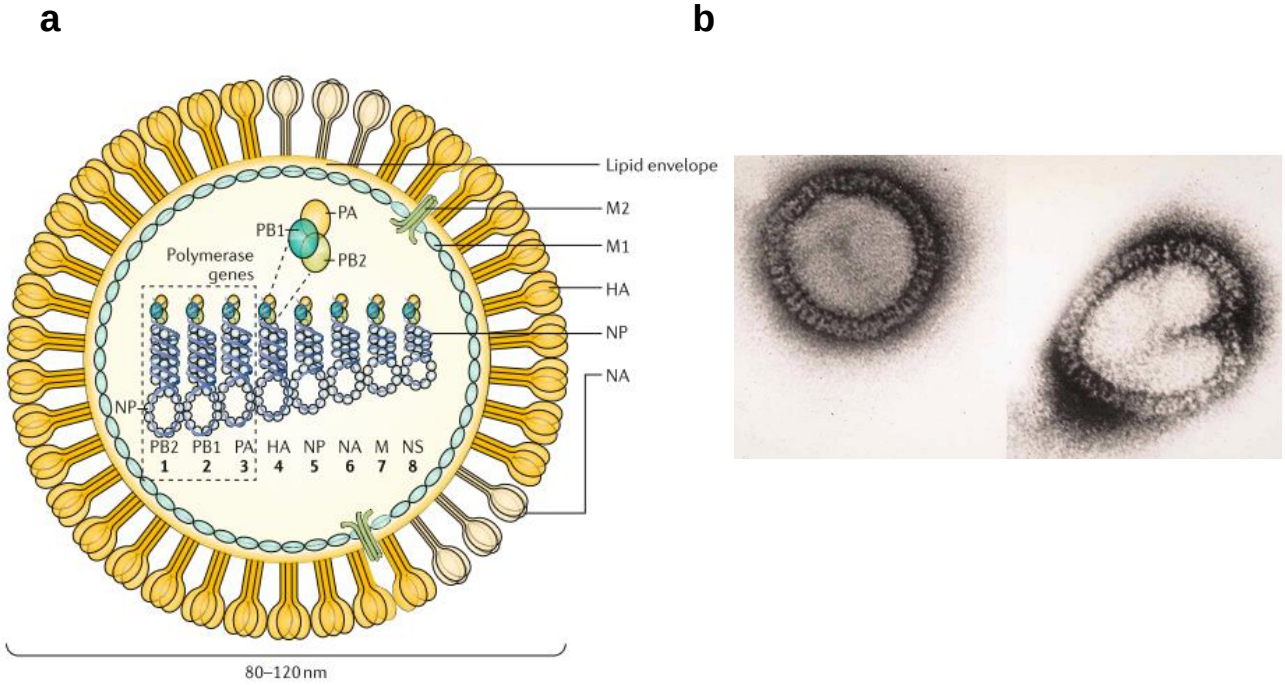

Figure 1. Structure of an influenza A virus.

(a) An illustration depicting the structure and components of an influenza A virus (adapted from[11]). (b) Electron micrograph of an influenza A virus particles. The virion is characterized by the presence of two spike-like surface glycoproteins, HA and NA. (adapted from[9])

Table 1. The genome and functions of influenza A virus.

Segment	vRNA (nt)	Viral Protein(s)	Length		Main Function	Ref
			aa	kDa		
1	2341	Polymerase basic protein 2 (PB2)	759	80	(a).Triggers the initiation of vRNA transcription by binding to the 5'-cap structure of cellular mRNA; (b). RIG-I activates the expression of interferons (IFNs) by interacting with mitochondrial antiviral signaling protein (MAVS)	6,12
		Polymerase basic protein 2, variant S1 (PB2-S1)	508	55	(a).Suppression of RIG-I-mediated interferon signaling pathway; (b). Disruption of RdRp function through competitive binding to PB1	13
2	2341	Polymerase basic protein 1 (PB1)	757	90	(a). The virus snatches the cap structure to initiate mRNA transcription; (b). The viral RNA-dependent RNA polymerase (RdRp) transcribes the viral RNA into a complementary RNA (cRNA) as a template for further viral RNA synthesis.	14,15

		Polymerase basic protein 1, variant F2 (PB1-F2)	87-90	~10	(a). Induce apoptosis activity; (b). Modulate host interferon response;	16,17
		Polymerase basic protein 1, variant N40 (PB1-N40)	718	~80	Balance the expression between PB1 and PB1-F2	18,19
3	2233	Polymerase acidic protein (PA)	716	83	RNA endonuclease cleaves the cap structure of small RNA molecules to generate primers for viral mRNA transcription	6
		Polymerase acidic protein, variant X (PA-X)	252	29	Manipulating the host immune response and viral pathogenicity	20–22
		Polymerase acidic protein, variant N155 (PA-N155)	561	62	Viral replication and pathogenicity	23,24
		Polymerase acidic protein, variant N182 (PA-N182)	534	60		
4	1778	Hemagglutinin (HA)	566	77	(a) The process of attaching to receptors and fusing with the host cell membrane; (b) The primary target of the host immune response due to its high variability and antigenicity.	6
5	1565	Necleoprotein (NP)	498	55	(a). vRNA binding; (b). vRNA synthesis; (c).Regulation of nuclear import of vRNP	6
6	1413	Neuraminidase (NA)	454	56	(a). Sialidase activity for virion progeny releasement; (b). Major antigen	6
7	1027	Matrix protein 1 (M1)	252	28	(a) Import and export of viral ribonucleoproteins (vRNPs) to and from the nucleus; (b) Assembly, budding, and morphogenesis of virions.	6,25
		Matrix protein 2 (M2)	97	15	(a). Ion channel activitiy; (b). Viral assembly	6,26
		Matrix protein 3 (M3)	9	Unknown	Unknown	27
		Matrix protein 4 (M4)	54	Unknown	Unknown	
		Matrix protein 42 (M42)	99	11	Complements to M2	
8	890	Non-structural protein 1 (NS1)	230	26	(a). Antagonizes cellular antiviral response (interferons); (b). vRNP entry by hijacking importin-α; (c).Regulates host gene expression; (d). Supports viral mRNA splicing, maturation and translation	28–30

	Nuclear export protein/Non-structural protein 2 (NEP/NS2)	121	~14	(a). vRNA nuclear export; (b). Regulates vRNA transcription and replication	[31–34]
	Non-structural protein 3 (NS3)	187	~20	Provides replicative gain-of-function for host adaptation	[35]

7.1.3 Influenza A virus replication

7.1.3.1. Viral entry and fusion

Influenza viruses primarily reproduce in the respiratory tract of vulnerable hosts' epithelial cells. The life circle starts with binding to sialic acids (SAs) residues present in the oligosaccharides of the glycoproteins at the cellular surface mediating with receptor-binding site in viral HA protein **(Figure 2, step 1)**. It is generally considered that human IAVs prefer receptors with α2,6-linked SAs (so called 'human-type' receptors), whereas avian IAVs prefer binding α2,3-linked SAs (so called 'avian-type' receptors)[36,37]. The HA-mediated attachment to SA receptors triggers endocytosis of the virion **(Figure 2, step 2)**. Upon trafficking to the endosome, the M2 ion channel is activated by the acidic environment of the endosomal compartment, leading to a conformational change of the HA protein and exposure of the fusion peptide located within the HA2 region of HA **(Figure 2, step 3)**. Opened M2 ion channel acidifies the internal environment of viral particle[38], allowing releasement of vRNPs from the viral matrix into the cellular cytoplasm following HA-mediated uncoating and membrane fusion[39–41].

7.1.3.2. Viral genome trafficking to host cell nucleus

Influenza virus RNA synthesis occurs exclusively within the nucleus. Newly released vRNPs from endosome are transported to the host cellular nucleus through 'nuclear localization signals' (NLSs) in viral proteins such as NP. Numerous studies suggest that released vRNPs utilize the importin-α-importin-β nuclear import pathway to enter the nucleoplasm. Importin-α serves as an adaptor protein that identifies nuclear localization signals (NLSs) present on vRNPs, and promotes their translocation into the nucleus through the involvement of importin-β and the nuclear pore complex. Comparing with viral entry and fusion which occurs very fast (about 10 min), nuclear import requires longer time (about 1h) observed from previous studies via imaging and RNA labelling techniques. The adaptation of viral proteins to specific isoforms of importin-α in a given species is critical for the success of influenza A virus infections.

7.1.3.3. vRNPs replication and transcription

The RdRp uses the negative-sense vRNA as a template to synthesize two types of positive-sense RNA in nucleus including the complementary RNA (cRNA) for transcription of more

copies of new vRNA, and mRNA for subsequent viral protein synthesis **(Figure 2, step 4-6, Figure 3)**. The cRNAs are produced through an unprimed process that relies on the complementary base pairing of free ribonucleoside tri-phosphate (rNTPs) with the 3' end of the vRNA template within the PB1 subunit from which the cRNA is elongated[42,43]. NP protein continually binds to the newly cRNA when it exits the polymerase promoting cRNP formation with newly synthesized viral polymerase (PB1, PB2 and PA). It is currently considered that multiple vRNA copies are generated in a mode similar to cRNA transcription based from cRNA formation[44]. Transcription of viral mRNA from vRNA is primed, which is more efficient than cRNA and vRNA transcription[45]. It is initiated by a 'cap-snatching' mechanism in PB2 subunit, where it binds to the 5'-cap sequence of a cellular mRNA[46] and the PA subunit endonuclease domain cleaves the short downstream of the 5'-cap sequence (about 10-13 nucleotides)[47]. Subsequently, the cap-binding domain of PB2 undergoes a conformational change, facilitating the presentation of the newly capped RNA primer to the PB1 subunit, which elongates the primer by utilizing the vRNA as a template. The transcription process is completed with the addition of a poly(A) tail to the mRNA through a repetitive copying process that occurs when the polymerase encounters the short poly(U) sequence at the 5' end of the vRNA, leading to the formation of a poly(A) tail in the mRNA[48,49].

7.1.3.4. Assembling and trafficking of vRNPs, maturation of viral membrane proteins and viral budding

The synthesis of IAV proteins is completely dependent on the translation machinery of the host cells. After exportation of viral mRNAs from nuclear, the translation is either by cytosolic ribosomes for internal proteins of PB1, PB2, PA, NP, NS1, NS2 and M1, or by endoplasmic reticulum (ER)-associated ribosomes for three membrane proteins including HA, NA and M2[44]. Due to the inefficient transcription of cRNA and vRNA, newly synthesized viral polymerase subunits (PB1, PB2, PA) and NP are imported back into the nucleus. Once new vRNPs are assembled, M1 and NS2, two viral proteins that are synthesized concurrently, can interact with the polymerase to promote the recruitment of CRM1, which facilitates the export of vRNPs from the nucleus to the cytoplasm[50,51]. The exported vRNPs are then trafficked by Rab11 toward to budding regions in cell surface where trafficking of HA, NA and M2 from ER are co-localized[52], but the underlying mechanisms of vRNPs trafficking are remain unknown **(Figure 2, step 7)**. Since HA traffics from the ER has incompetent fusion function (HA0), HA should be cleaved into HA1 and HA2 subunit in either monobasic or multibasic sites within the *trans-Golgi* network[53]. Seasonal influenza and low pathogenic avian IAVs encode with monobasic cleavage site whereas highly pathogenic avian IAVs commonly encode multibasic cleavage sites that is highly related to the difference of cell tropisms[54]. After budding, progeny virus can still bind to SA receptors through HA on the surface of infected cells. Then NA can release

newly viral particles by hydrolysing the glycosidic bond to the SAs[55]. Besides, NA also promotes separation of HA-mediated virus-virus binding[44]. In the respiratory tract where sialylated glycoproteins are abundant (i.e mucins) that can interact with HA of IAVs and slow viral movement to the uninfected neighbouring cells. Studies have shown that NA can hydroylize the binded SAs from mucins and facilitate the movement of virus in mucus layer to recipient cells nearby[56,57].

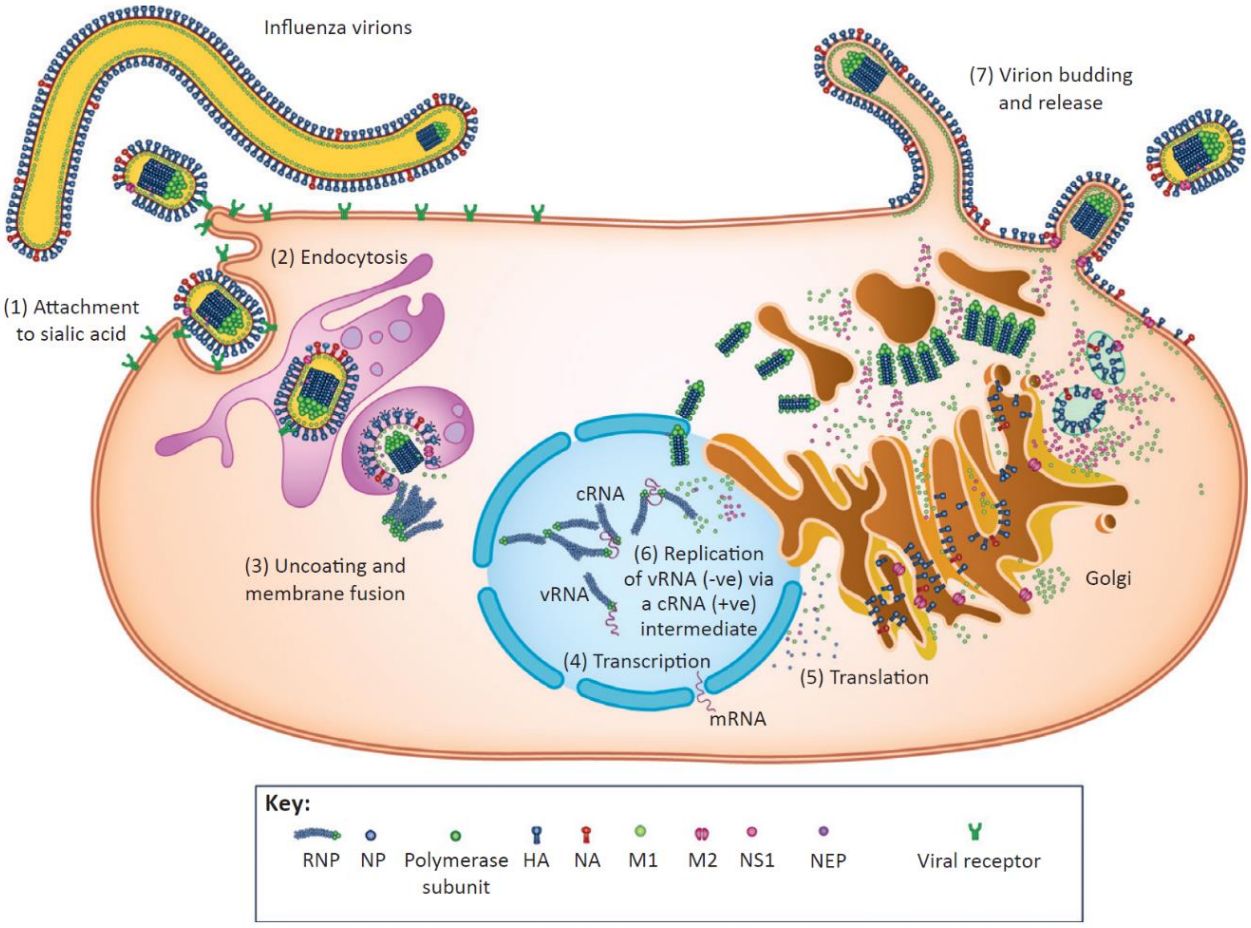

Figure 2. Life cycle of influenza A virus.

The process of influenza virus infection begins with the attachment of the virus to host cell receptors (α-2,3 and α-2,6 sialic acid), followed by endosomal uptake and subsequent release of negative-sense viral RNA (vRNA) through uncoating and membrane fusion. The vRNA is then imported into the nucleus for transcription into viral mRNA, which serves as a template for replication intermediated through positive-sense complementary RNA (cRNA). These viral mRNAs are translated into viral proteins in the cytoplasm and assembled into new virions with newly synthesized viral ribonucleoproteins (vRNPs) that can infect neighboring cells. RNP, ribonucleoprotein; NP, nucleoprotein; HA, haemagglutinin; NA, neuraminidase; M1, matrix protein; M2, membrane protein; NS1, non-structural protein; NEP, nuclear export protein (adapted from[1]).

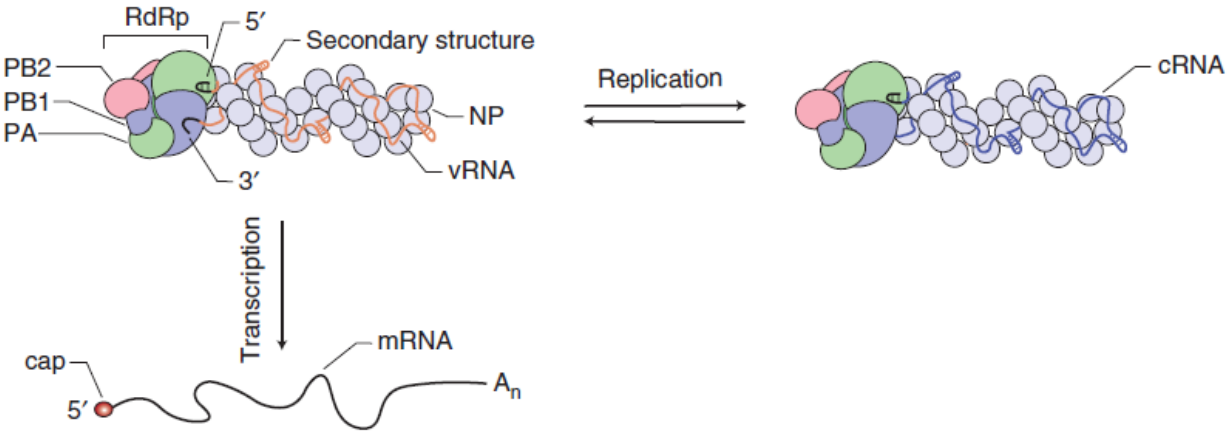

Figure 3. Schematic of influenza vRNA replication and transcription.

The influenza virus genome consists of segmented vRNA that assemble into vRNPs with multiple copies of NP and a single copy of the viral RNA-dependent RNA polymerase (RdRp), which is made up of PB1, PB2, and PA polymerase subunits. The RdRp binds to the conserved 5' and 3' vRNA termini and transcribes vRNA into viral mRNA that has a 5' cap structure and a 3' poly-(A) tail. The RNA polymerase also replicates vRNA through a negative-sense complementary RNA (cRNA) intermediate that becomes a positive-sense cRNP when assembled with NP and polymerase (adapted from[15]).

7.1.4 Inter-species transmission of avian influenza A viruses

Influenza A viruses can cause sporadic or sustained infection in a very wide range of hosts such as avian, human, swine, canine, equine and chiropteran making it an important prototype for emerging viruses of pandemic potential **(Figure 4)**. It is well known that wild aquatic birds are the natural reservoirs for influenza A viruses including all H1-H16 subtypes except for H17 and H18 that were identified from bats[5,58]. The migration nature of wild birds plays an important role in maintenance of this diverse gene pool of influenza viruses. Wild birds shed the viruses through their faeces and later acquired by other birds that contacted with the contaminated environment in the same habitat in the migration flyways. The orders of Anseriformes (e.g. ducks and geese) and Charadriiformes (e.g. shorebirds and gulls) are the main wild waterfowls harbouring influenza A viruses but with different prevalence of subtypes[59]. All influenza A viruses identified from domestic poultry and mammal species including humans have evolved directly or indirectly from wild aquatic birds. This procedure of crossing species barriers includes amino acid mutations and gene reassortment of viral proteins, which could increase the receptor binding affinity for the entry of mammalian cells, and enhance the replication or virulence in the new host. For example, influenza A viruses in birds mainly replicate in intestinal tract at a higher temperature (42C°) and prefer an HA binding receptor of α2,3-linked SAs ('avian-like' receptor) for the entry of host cells. However, α2,6-linked SAs ('human-like' receptor) are dominantly expressed in upper respiratory tract in humans[36]. It is believed

acquisition of ‘human-like’ receptor in HA is a fundamental feature for adaptation in mammalian hosts. Avian influenza viruses have limited ability to replicate in mammalian cells due to differences in their genomic structure. Therefore, specific genetic mutations in the viral polymerase, such as E627K or D701N in PB2, are required to adapt to mammalian hosts[60–62]. Several subtypes of avian influenza virus such as H1, H3, H5, H6, H7 and H9 are mostly low pathogenic avian infections (LPAI) in domestic poultry (chickens) without developing apparent symptoms or only can cause mild diseases[63]. Onthe other hand, certain subtypes of H5 and H7 that contains several basic residues in the HA gene can cause severe diseases or deaths in domestic poultry (chickens) and are therefor referred as highly pathogenic avian influenza (HPAI). Live poultry markets with mixed domestic poultry have been considered as the most important place harbouring a variety of avian influenza viruses. Viruses acquired features for mammalian adaptation can occasionally jump to other species such as swine, horse and human. In general, the occurrence of cross-species transmission of avian influenza viruses to humans is infrequent. In the past few decades, there have been occasional reports of human infections with various subtypes of avian influenza viruses including H5, H6, H7, H9, and H10 **(Figure 5)**. Many of these zoonoses have no subsequent transmission in humans and can only accumulate a small number of cases worldwide in a relatively long period. For example, the first human infection with HPAI H5N1 virus was identified in Hong Kong Special Administrative Region (SAR) of China in 1997 and followed with 17 subsequently confirmed cases[64]. Since 2003, HPAI H5N1 reemerged in Asia and caused a total of 868 cases in 21 countries as of 2023 in the past twenty years[65]. However, H7N9 avian influenza viruses caused over thousand cases in five successive Winter-Spring seasons since 2013 in China, making it the most ‘successful’ virus that caused interspecies transmission from poultry to human. In chapter 7.2, the molecular and epidemiological information of this inter-species epidemic are further described in detail.

a

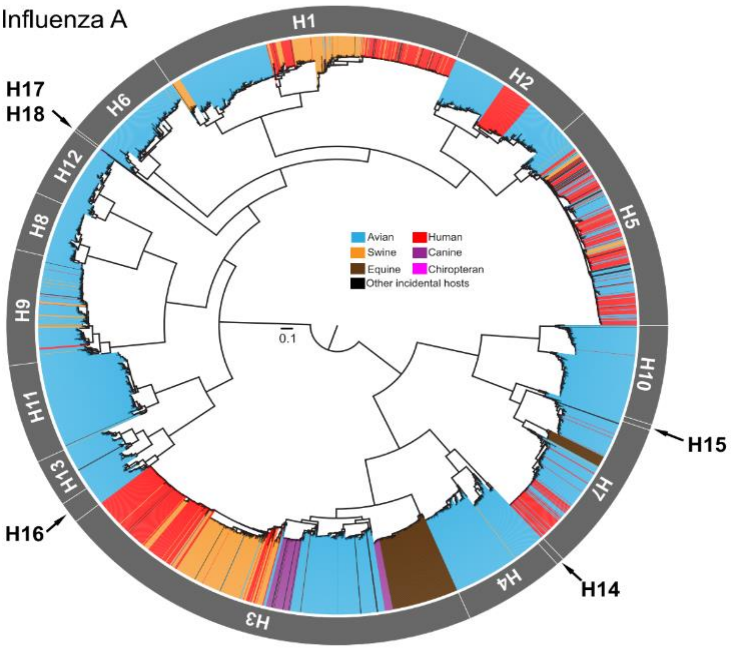

b

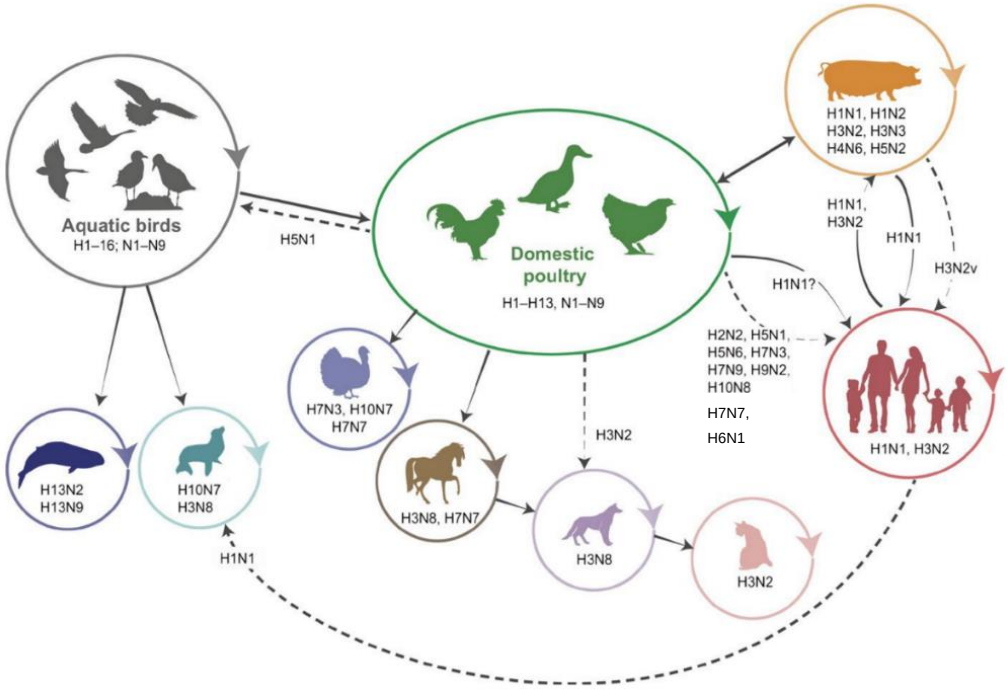

Figure 4. Host distribution and representative interspecies transmission of influenza A viruses.

(a). The haemagglutinin (HA) gene phylogenetic of all subtype of influenza A virus. The tree reconstruction was developed from randomly data set (NCBI GenBank database) including 200 isolates per subtype of each host. Branches are coloured for the major host groups: avian (blue), human (red), swine (orange), canine (purple), equine (brown), chiropteran (pink) and other incidental hosts (black). (b). The diagram of representative interspecies transmission of influenza A viruses. The solid arrows indicate established direct transmissions within the species, while the dashed arrows represent sporadic or infrequent infections (adopted from[63]).

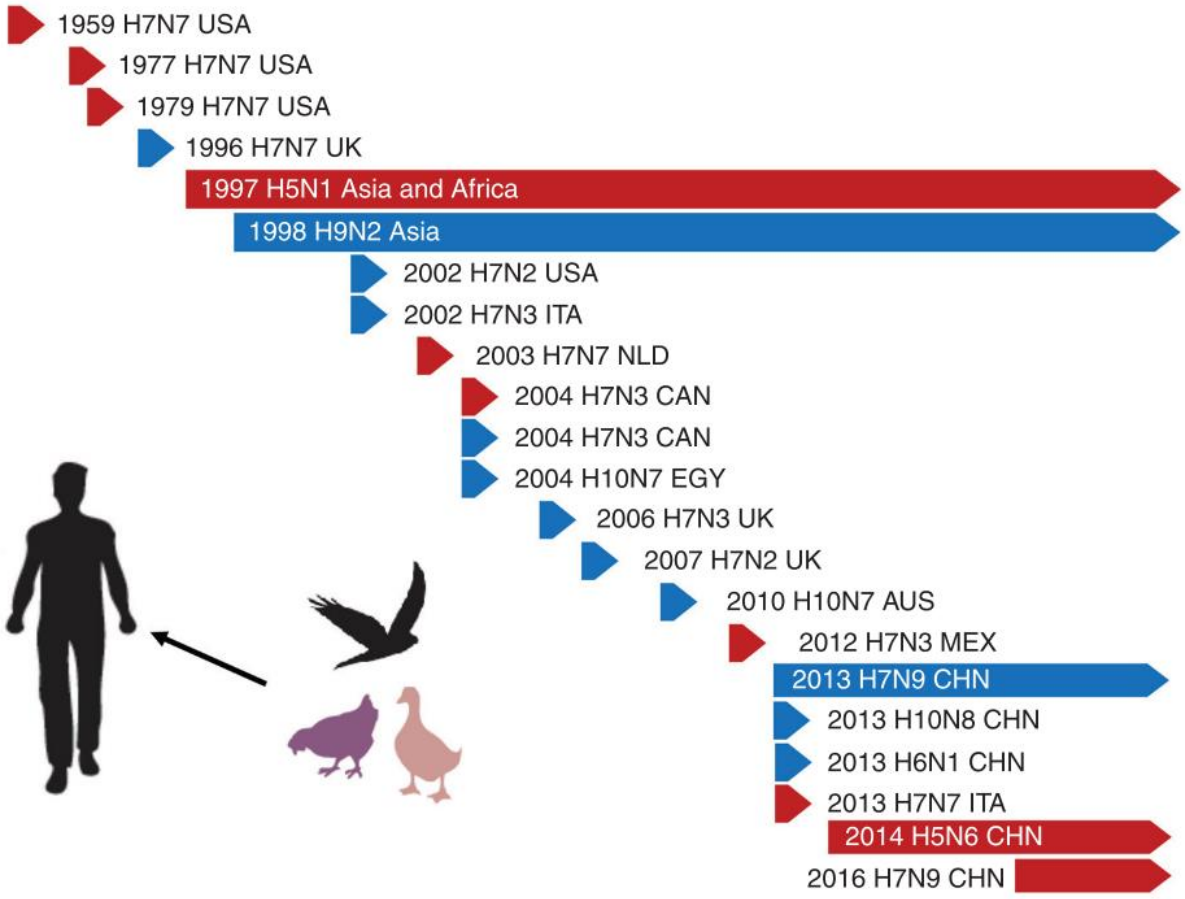

Figure 5. Historical human infections with avian influenza viruses.

Summary of historical human infections with LPAI (blue arrow) and HPAI (red arrow) in recent decades chronologically. USA (United States of America, UK (United Kingdom), ITA (Italy), NLD (Netherlands), CAN (Canada), EGY (Egypt), AUS (Australia), MEX (Mexico), CHN (China) (adapted from[66]).

7.2 Human influenza A (H7N9) virus

7.2.1 Epidemiology

The first reported human infections with a novel avian influenza A(H7N9) virus occurred in the Spring of 2013 in the Yangtze River Delta region of China[67]. The virus caused low pathogenic infections in domestic poultry with asymptomatic or mild disease but can cause severe human infections or deaths. It is ranked with the highest pandemic risk among all evaluated influenza viruses using USCDC's Influenza Risk Assessment Tool (IRAT)[68]. Exposure to poultry is considered as the main risk factor as approximately 70% patients reported historical poultry exposure before their infections[69], and closure of live poultry market limited the incidence of human infections

in short term[70]. Over 70% of H7N9 cases occurred in urban or semi-urban area in mainland China. This is different compared to human infections with avian influenza A(H5N1) virus, another zoonotic threat, where most cases are rural residents[71]. Outbreak of H7N9 infections followed a Winter-Spring seasonal trend with continuous five epidemic waves since 2013 in mainland China **(Figure 6)**. After the 2013-14 wave, the number of cases identified in subsequent waves was lower, until an upsurge was observed in the fifth wave with expanded geographic range since December 2016[72]. In early 2017, patients infected with H7N9 viruses that evolved into the highly pathologic influenza viruses were reported in Guangdong Province, China[73,74,75]. There were 1568 laboratory-confirmed cases (including two exported cases in Malaysia and Canada[76]) with the fatality rate of approximately 39%[77]. Overall, the middle-aged adults were the most affected populations and followed with elders aged above 60 years old, whereas individuals younger than 15 years old were less affected[69]. There were 40 clusters of H7N9 patients during the five epidemic waves. However, the cluster size is very small (range 2-3) and the overall effective reproductive number (R_e) is less than 0.12 (95%CI: 0.10, 0.14), indicated the sustained human-to-human transmission is very limited[78].

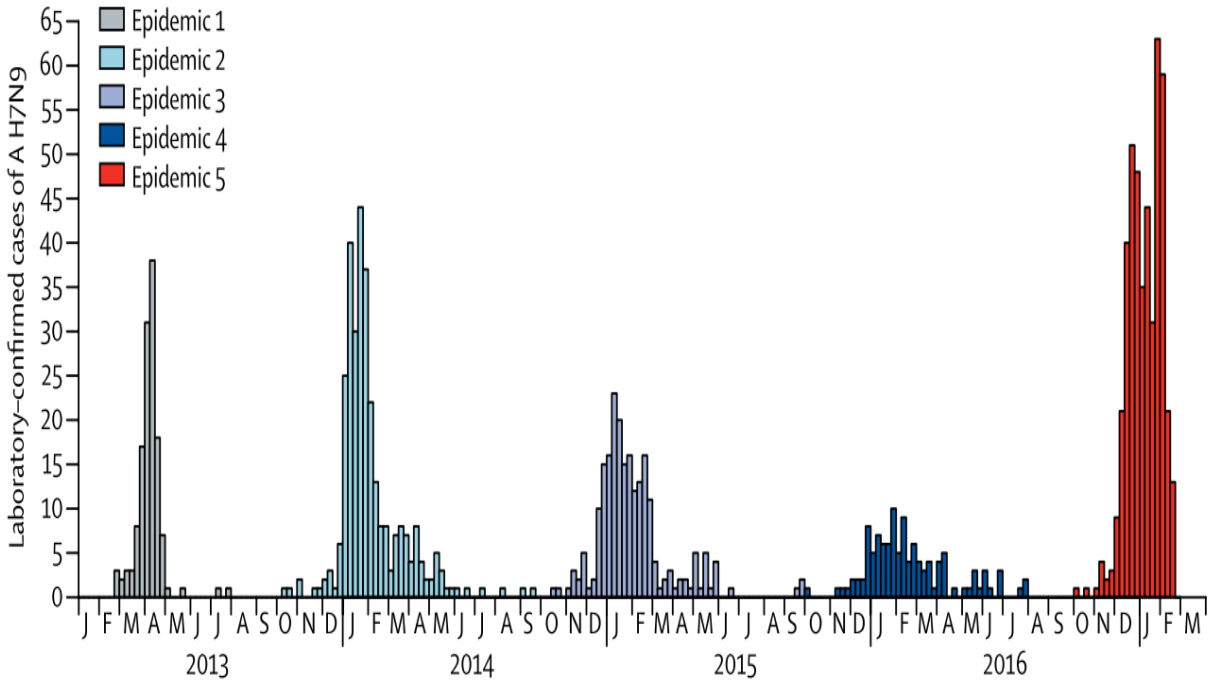

Figure 6. Temporal pattern of laboratory-confirmed H7N9 influenza cases from 2013-2017 in mainland China.

Showed with epidemic waves of H7N9 cases reported weekly in mainland China. Human infection with H7N9 influenza virus was first reported since the early Spring of 2013.Then followed with four successive winter-spring epidemics in 2013-2014, 2014-2015, 2015-2016, 2016-2017 (adapted from[69]).

7.2.2 Sex bias

Primary epidemiology studies revealed that 71% of H7N9 patients were male in the early stage of the epidemic[67,68]. The male-biased incidence was repeatedly observed during following epidemic waves in both young and older age groups **(Figure 7)**. Overall, males accounted 70% of all reported H7N9 cases[69]. The notable sex distribution is different to reported H5N1 cases where no sex difference were observed overall **(Figure 8a)**[71,79]. However, after further analysis by dividing cases identified from urban and rural areas, the higher incidence in men was also found from H5N1 cases from urban areas in mainland China[71] **(Figure 8c)**. Questions arose naturally regarding underlying reasons that may cause this remarkable sex difference in H7N9 infections. The gender-associated difference such as the proposed higher frequency of live poultry market exposure of men living in urban area was one possible explanation[79]. However, a modelling study indicated that increased risk of H7N9 infection in older men is not attributable to longer exposure to live poultry markets[81]. The differential health care access in both sexes that leads to surveillance bias was also discussed. Given the severity and high case fatality rate, high awareness of public health sectors for influenza-like illness surveillance network that covers all provinces at different levels, men were unlikely to be over detected. Since the incidence of H7N9 infection in males is repeatedly higher than in females from the early epidemic wave till the last. Biological difference between males and females may play an important role.

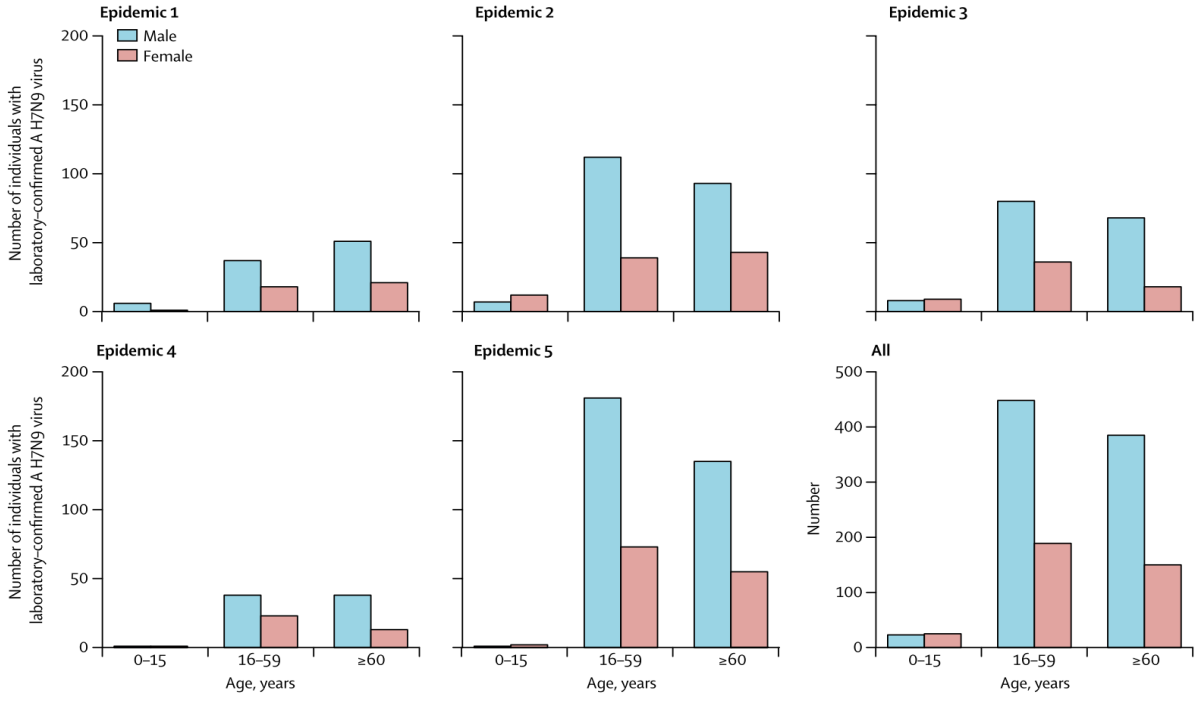

Figure 7. Sex distribution of laboratory-confirmed H7N9 influenza cases in five epidemic waves from 2013-2017 in mainland China.

Showed with sex distribution of H7N9 cases in 0-15 years, 16-59 years and ≥ 60 years age groups during the five epidemic waves (epidemic 1: 2013, epidemic 2: 2013-2014, epidemic 3: 2014-2015, epidemic 4: 2015-2016, epidemic 5: 2016-2017) (adapted from[69]).

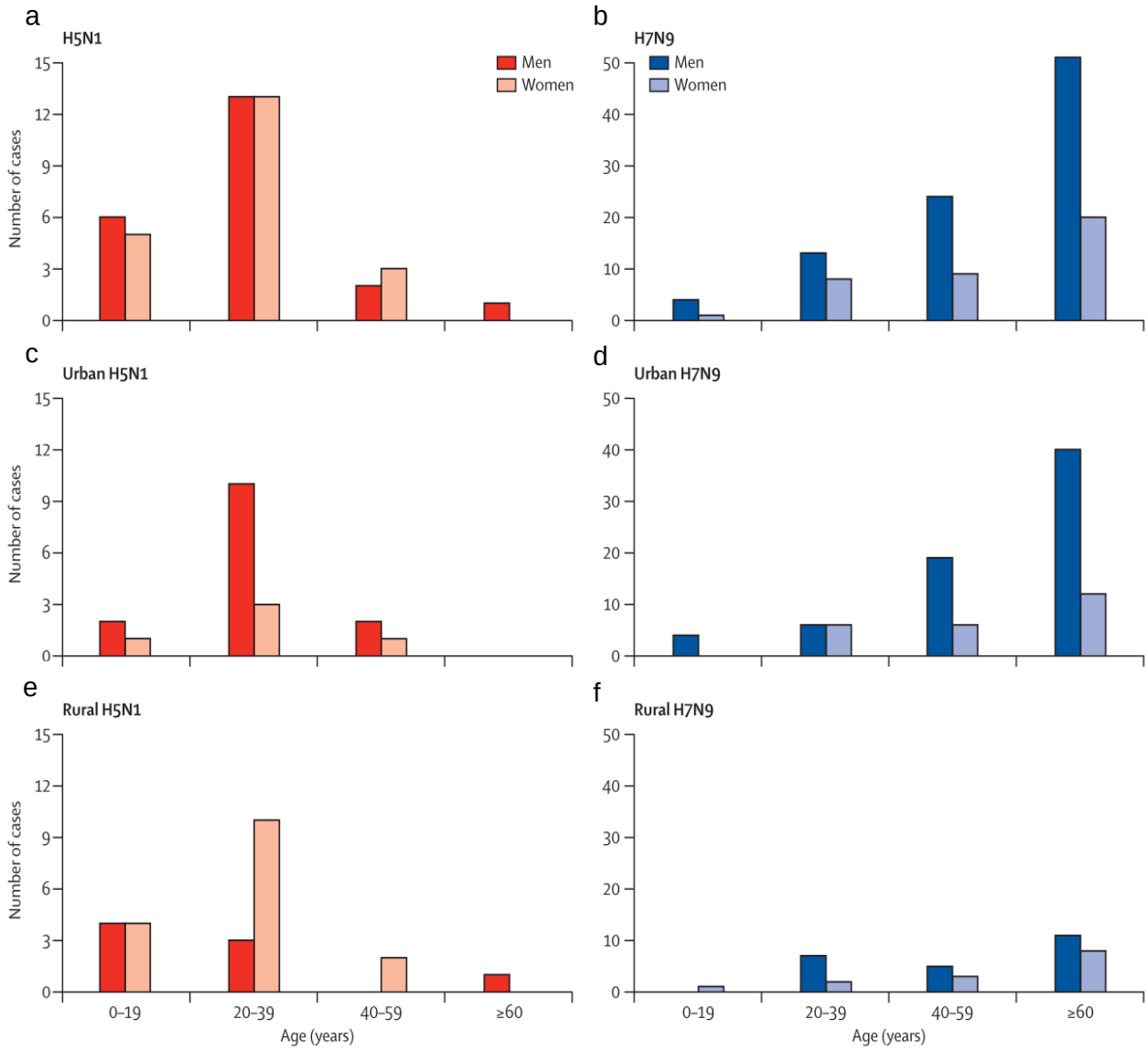

Figure 8. Comparison of age and sex distribution of laboratory-confirmed H5N1 and H7N9 cases in mainland China as of May 24, 2013.

(a, b). Demographic characteristics (age and sex) of all H5N1 and H7N9 cases in mainland China, (c, d). Demographic characteristics (age and sex) of H5N1 and H7N9 cases in Urban areas in mainland China, (e, f). Demographic characteristics (age and sex) of H5N1 and H7N9 cases in rural areas in mainland China (adapted from[71]).

7.2.3 Prevention and measurement

A Joint Prevention and Control Mechanism (JPCM) was established in China to lead the national wide response to H7N9 epidemic since April of 2013. The exposure to live bird markets was identified as a major origin of human H7N9 infections. Thus, a periodic closure of the market and environment disinfection was mandatorily conducted[80] **(Figure 9)**. The dramatic decline of human infections was a clear evidence that this measure efficiently prevented poultry to human transmissions. After a lower circulation of H7N9 virus in humans during the 2014-2015 and 2015-2016 season, the virus spread widely and caused a higher number of cases than before. Importantly, some low pathogenic H7N9 influenza strains evolved to highly pathogenic AIVs in southern China in the beginning of 2017, which posed greater threat to human and poultry industry. In order to prevent the spread of the epidemic, an H7N9 and H5N1 bivalent inactivated vaccine was developed[82]. After the efficacy and safety field test in three provinces, a national wide vaccination formally initiated in Chicken since September 2017[82]. Large-scale surveillance in poultry revealed the H7N9 isolation rate was dropped over 90% after the implementation of the massive vaccination program[82]. Only four human infections with H7N9 virus were identified postvaccination in poultry[83] **(Figure 10)**. This massive vaccination campaign successfully limited the prevalence of H7N9 virus infections in poultry and ended the epidemic in humans.

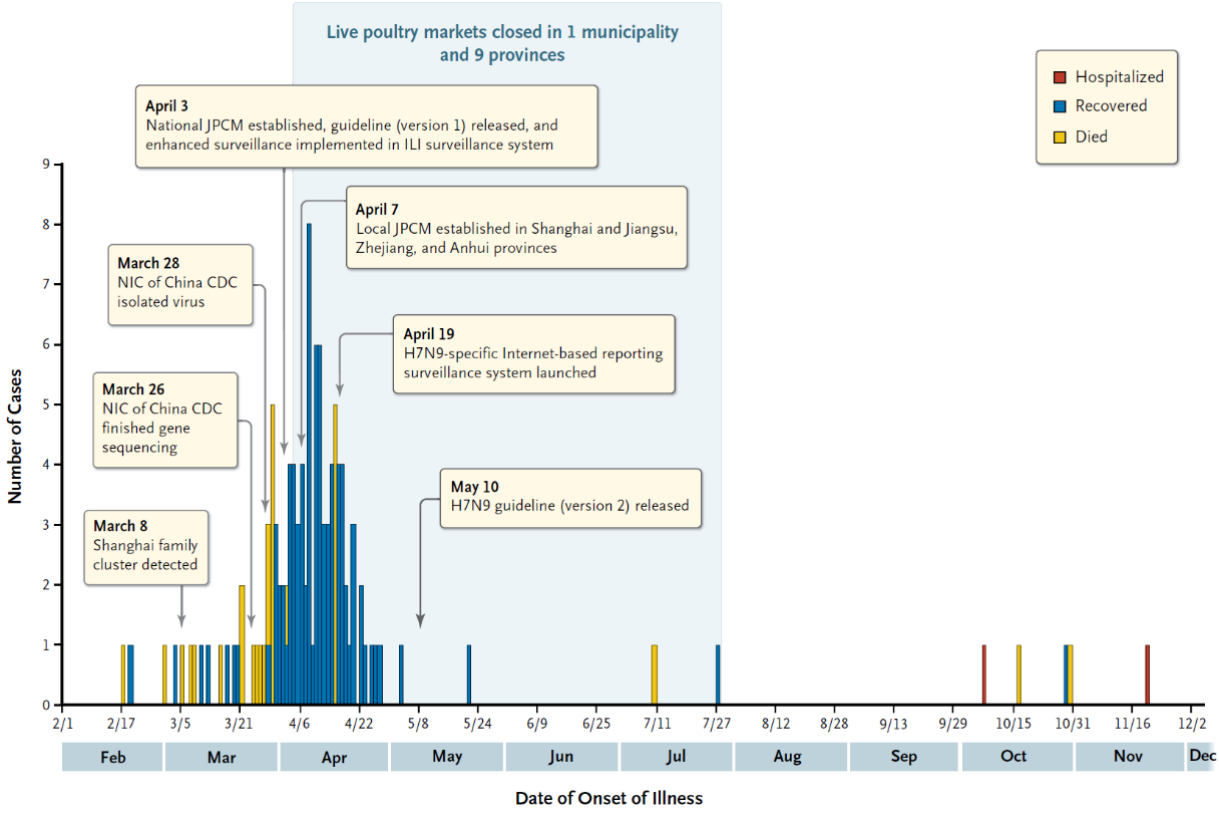

Figure 9. Epidemic dynamic of laboratory-confirmed H7N9 cases before and after live poultry market closure and emergency response.

Shown with the impact of prevention and control measures including establishment of emergency system and closure of live poultry market to the kinetic reduction of reported H7N9 cases in mainland China in 2013. NIC represents National Influenza Center, CDC represents Center for Disease control and Prevention, JPCM represents Joint Prevention and Control Mechanism (adapted from[80]).

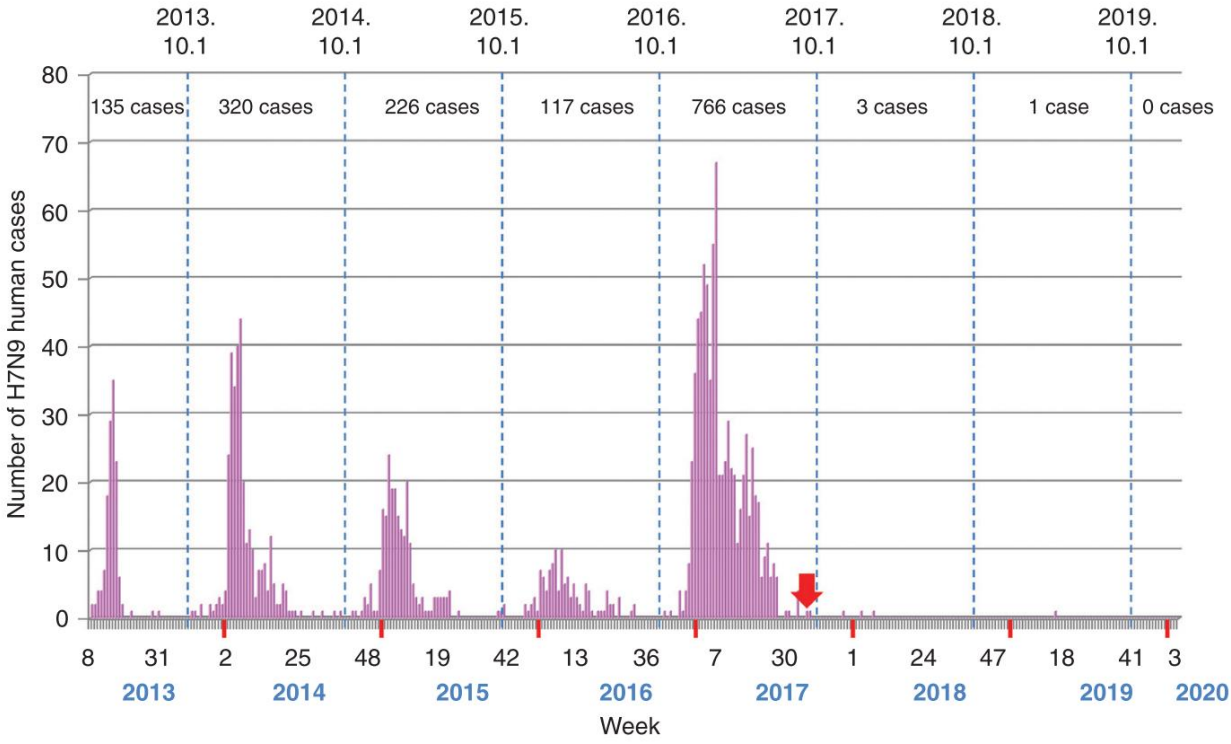

Figure 10. The effect of massive poultry vaccination (H5/H7 bivalent vaccine) in preventing human H7N9 infections.

Shown with laboratory-confirmed H7N9 cases from 2013 to 2020. The red arrow highlights the start of the administration of H5/H7 bivalent inactivated vaccine to poultry in mainland China (adopted from[83]).

8 Materials and Methods

8.1 Materials

8.1.1. Chemicals

Chemical	Manufacturer
Agarose	Serva
Ammoniumperoxodisulfate (APS)	Carl Roth
Avicel	FMC BioPolymer
Bouin’s fixative	Carl Roth
Bovine serum albumin (BSA)	Sigma-Aldrich/Merck
Chloroform	Geyer
Crystal violet	Merck
Diethylpyrocarbonate (DEPC)	Sigma-Aldrich/Merck
Dimethylsulfoxide (DMSO)	Sigma-Aldrich/Merck
Dithiothreitol (DTT)	Serva
Ethanol (denatured), for disinfection	Geyer Th. GmbH & Co.KG
Ethanol (pure)	Merck
Formaldehyde (37%)	Merck
Hydrochloric acid (37 %)	Merck
Hydrogen peroxide	Merck
Methanol	ChemSolute
Paraformaldehyde (PFA)	AppliChem
Phenylmethanesulfonyl fluoride (PMSF)	Sigma-Aldrich/Merck
Pursept-A Xpress, for disinfection	SCHÜLKE & MAYR AG
Sodium chloride	ChemSolute
Sodium dodecylsulfate (SDS)	Sigma-Aldrich/Merck
Sodium hydrogene phosphate	Merck
Sodium hydroxide (NaOH)	Merck
Sterilium, for hand disinfection	Bode
Tetramethylethylenediamine (TEMED)	Carl Roth

Tris (hydroxymethyl) amino methane	Merck
Triton X-100	Sigma-Aldrich/Merck
Trizol Reagent	Ambion RNA
Tween-20 (pure)	Serva
Virkon S, for disinfection (BSL-3 work)	DuPont

8.1.2. Buffers and solutions

Description	**Composition/Preparation notes**
4x Laemmli loading dye (*SDS-PAGE*)	0.2 M Tris-HCl pH 6.8 8% SDS 40% glycerol Trace of bromophenol blue 40 mM DTT (add shortly before usage)
APS (10%)	10% APS → filter sterilize (0.22µm)
Avicel solution	2.5% Avicel →autoclave
Blocking Buffer (*Western Blot*)	1x PBS-T 3% BSA
Blocking Buffer (I*mmunofluorescence*)	D-PBS 3% BSA
Blotting Buffer (10x) (*Western Blot*)	250 mM Tris base 1,92 M glycine → autoclave

Blotting Buffer (1x) (*Western Blot)*	Diluted from 10 x Blotting Buffer 20% methanol
Crystal violet solution	270 ml 37% formaldehyde 1 g crystal violet ad 1L ddH_2O
DEPC-ddH_2O	0.1% DEPC, in ddH_2O → soluble overnight at RT or >12h at 37°C →autoclave
DEPC-ethanol (70%)	100% ethanol (pure) → dilute to 70% ethanol with DEPC-ddH2O
DTT (1M)	1 M DTT
Lysis Buffer (*SDS-PAGE*)	50 mM HEPES (pH 8.0) 200 mM NaCl 0.5% Igepal (NP40) 25% Glycerol 1 mM PMSF 0.07 µl/ml β-mercaptoethanol 1 x HALT Protease & Phosphatase Inhibitor (100x; including EDTA, 100x add shortly before usage)
PFA (4%)	4% PFA, in PBS
Phosphate buffered saline (PBS) (1x)	Diluted from 10x PBS → autoclave

PBS (10x)	1.37 M NaCl 26.8 mM NaCl 51.3 mM Na_2HPO_4 x $2H_2O$ 17.6 mM KH_2PO_4 pH 7.2-7.4 → autoclave
SDS resolving gel buffer (4x) (*SDS-PAGE*)	1.5 M Tris base 0.4% SDS pH 8.8
SDS Running Buffer (10x) (*SDS-PAGE)*	250 mM Tris base 1.92 M glycine 1% SDS → autoclave
SDS Running Buffer (1x) (*SDS-PAGE)*	Diluted from 10x SDS Running Buffer
SDS stacking gel buffer (4x) (*SDS-PAGE*)	0.5 M Tris base 0.4% SDS pH 6.8
SDS (10%)	5 g ad 50 ml ddH_2O
Sodium chloride buffer (0.9%)	0.9% NaCl, in ddH_2O
Triton X-100 buffer (*Immunofluorescence*)	0.1% Triton X-100, in ddH_2O
Washing Buffer (PBS-T) (*Western Blot*)	1x PBS 0.1% Tween-20

8.1.3. Manufactured solutions, reagents and reaction system (kits)

Description	Manufacturer
Access Estradiol Assay (REF 33540)	BECKMAN COULTER
Access Testosterone Assay (REF 33560)	BECKMAN COULTER
Bio-Plex Pro Mouse Cytokine kits	Bio-rad
DNase/RNase-free ddH2O	Gibco/Life Technologies
dNTP mix (10 mM)	Life Technologies
Free testosterone ELISA Kit (ab 178663)	Abcam
FastStart Essential DNA Green Master (MasterMix for SYBR Green I-based qRT-PCR)	Roche
Hoechst 33342 reagent	Thermo Fisher
Human cytokine/chemokine magnetic bead panel (HCYTOMAG-60K)	Millipore
Poly-L-Lysin solution	Sigma-Aldrich/Merck
Precision Plus ProteinTM Dual Core Standards	Bio-Rad
QIAamp Viral RNA Mini Kit	Qiagen
Ribolock RNase Inhibitor (40 U/µl)	Fermentas/Thermo Scientific
SHBG ELISA Kit (ab 260070)	Abcam
SuperscriptTM III Reverse Transcriptase Kit	Invitrogen/Life Technologies
Testosterone ELISA Kit (ab 174569)	Abcam
Testosterone enzyme Immunoassay Kit	DetectX, Arbor Assay
17β-Estradiol ELISA Kit (ab 108667)	Abcam
17β-Estradiol enzyme Immunoassay Kit	DetectX, Arbor Assay

8.1.4. Antibodies

Superblock T20 (Thermo Scientific) was used to dilute all primary antibodies, while Western blot blocking buffer was used to prepare all secondary antibodies, unless otherwise specified.

Primary Antibody	Species/Dilution	Application/Manufacturer/Catalogue number
Anti-GAPDH	Rabbit	Primary antibody for Western Blot
	1:1000	Cell Signaling (#2118)

Anti-nucleoprotein (NP)	Mouse 1:1000	Primary antibody for Western Blot Abcam (#ab128193)
Anti-polymerase basic protein 1 (PB1)	Rabbit 1:1000	Primary antibody for Western Blot ThermoFischer (# PA5-34914)
Maackia Amurensis Lectin II	Biotinylated 10µg/ml in FBS free cell culture median	Lectin for Immunofluorescence Vector Laboratories (B-1265-1)
Sambucus Nigra Lectin	Biotinylated 20µg/ml in FBS free cell culture median	Lectin for Immunofluorescence Vector Laboratories (B-1305)

Secondary Antibody	**Origin/Dilution**	**Application/Manufacturer/Catalogue number**
Anti-goat-HRP	Rabbit 1:20000	Secondary antibody for Western Blot Sigma-Aldrich/Merck (#A5420)
Anti-mouse-HRP	Goat 1:20000	Secondary antibody for Western Blot Sigma-Aldrich/Merck (#A4416)
Alexa Fluor™ 488 conjugate	Streptavidin 1:200	For Immunofluorescence Invitrogen (S11223)

8.1.5. Enzymes

Enzyme	**Manufacturer**
SuperScript III Reverse Transcriptase (part of *Superscript™ III Reverse Transcriptase Kit;*)	Invitrogen/Life Technologies

8.1.6. Plasmid and vectors

Plasmid/Vector	**Application/Description/Reference**
pHW2000-H7N9-NP	Expression vector for A/Anhui/1/2013 (H7N9) NP protein. Generously provided by Hans-Dieter Klenk, University of Marburg, Marburg, Germany

8.1.7. DNA oligonucleotides (qRT-PCR)

Primer/Gene (m, *Mus musculus*)	Sequence 5'-3'
A/Anhui/1/2013 (H7N9)-NP	Forward: CCTGCTTGTGTGTACGGACT
	Reverse: GGCTGTTTTGAAGCAGACGG
mTNF-α	Forward: CAGAAAGCATGATCCGCGAC
	Reverse: GGCCATAGAACTGATGAGAGGG
mMIP-1α	Forward: CAGCCAGGTGTCATTTTCCTG
	Reverse: CTCGATGTGGCTACTTGGCA
mMIP-1β	Forward: AACCTAACCCCGAGCAACAC
	Reverse: GGGTCAGAGCCCATTGGTG
mIFN-γ	Forward: AGGTCAACAACCCACAGGTC
	Reverse: GAATCAGCAGCGACTCCTTT
mIL-1β	Forward: GAGCCCATCCTCTGTGACTC
	Reverse: AGCTCATATGGGTCCGACAG
mIL-10	Forward: GGTTGCCAAGCCTTATCGGA
	Reverse: CACCTTGGTCTTGGAGCTTATT
mIL-6	Forward: CTCCCAACAGACCTGTCTATAC
	Reverse: GTGCATCATCGTTGTTCATAC
mEotaxin	Forward: GAGCTCCACAGCGCTTCTAT
	Reverse: GAAGTTGGGATGGAGCCTGG
mVEGF	Forward: TCTGAGAGAGGCCGAAGTCC
	Reverse: GCGGGGTGCTTTTGTAGACT
mIL-15	Forward: CGCCCAAAAGACTTGCAGTG
	Reverse: GGTGGATTCTTTCCTGACCTCT
mGM-CSF	Forward: AAGGTCCTGAGGAGGATGTGG
	Reverse: GTCTGCACACATGTTAGCTTCTTG
mYwhaz	Forward: CACGCTCCCTAACCTTGCTT
	Reverse: ATCGTAGAAGCCTGACGTGG

8.1.8. Narcotics and supplements

Description	Manufacturer
Forene/Isofluorane (100%)	Abbott
Ketamine (100 mg/ml)	WDT
Sodium chloride (NaCl) (0.9%)	B. Braun Melsungen AG
Xylazine (20 mg/ml)	WDT

8.1.9. Eukaryotic cell lines

Cell line	Description/Origin/Reference
LC540	Rat Fischer Leydig cell testicular tumour *ATCC (CCL 43)*
Madin-Darby Canine Kidney (MDCK)	Immortalized canine MDCK cell line (♀) *ATCC (CCL-34)*

8.1.10. Media and supplements for eukaryotic cell culture

Medium	Composition/Manufacturer
Bovine serum albumin solution (BSA; 35%, in D-PBS)	Sigma-Aldrich/Merck
Bovine serum albumin (powder, A9418-5G)	Sigma-Aldrich/Merck
Cryoconservation medium	FBS 10% DMSO
Collagenase type 1 (C0130)	Sigma-Aldrich/Merck
Dulbecco's Modified Eagle's Medium (DMEM)	Sigma-Aldrich/Merck
Dulbecco's Modified Eagle's Medium/F12 (DMEM/F12, D6434-6X)	Sigma-Aldrich/Merck
Dulbecco's Phosphate Buffered Saline (D-PBS)	Sigma-Aldrich/Merck
Minimum Essential Medium (MEM)	Sigma-Aldrich/Merck
Fetal bovine serum (FBS) superior	Biochrom GmbH
Hanks balanced salt solution (HBSS), Ca/Mg-free, 10X (14185045)	ThermoFischer
Hanks balanced salt solution (HBSS), Ca/Mg-free, 1X (14175053)	ThermoFischer
L-Glutamine (200 mM, L-Glu)	Sigma-Aldrich/Merck
Penicillin-Streptomycin (P/S)	Sigma-Aldrich/Merck
Percoll (GE17-0891-01)	Sigma/GE Healthcare
Trypsin from bovine pancreas, TPCK-treated (TPCK trypsin)	Sigma-Aldrich/Merck
Trypsin-EDTA	Sigma-Aldrich/Merck

Cell growth medium	DMEM or MEM (MDCK) 10% FBS 1% L-Glutamine 1% Penicillin & Streptomycin
Inoculation medium	DMEM or MEM (MDCK) 1% L-Glutamine 1% Penicillin & Streptomycin
Infection medium (MDCK)	MEM 1% L-Glutamine 1% Penicillin & Streptomycin 0.2% BSA 1:1000 TPCK trypsin
Infection medium (LC540)	DMEM 1% L-Glutamine 1% Penicillin & Streptomycin 0.2% BSA 1:2000 TPCK trypsin
Modified Eagle Medium 2x (2x MEM), without Phenol Red	Sigma-Aldrich/Merck
Overlay medium for plaque test	2x MEM (2% L-Glu, 2% P/S, 0.4% BSA) *and* 2.5% Avicel in ddH_2O (*1:1 mixture*)

8.1.11. Virus strains

Virus strain	Origin/Description/References
A/Hamburg/NY1580/09 (H1N1)	Sigrid Baumgarte, Institut für Hygiene und Umwelt, Hamburg, Germany
A/Victoria/03/75 (H3N2)	A clinical isolate also used in our previous study[84]
A/Anhui/1/2013	A clinical isolate (from a 35-year-old women in Anhui, China[85]) kindly provided as a gift from John McCauley (National Institute for Medical Research, London, UK).

8.1.12. Experimental animal lines

Animal line	Background	Description/Reference
Mouse (Wide type)	C57BL/6J	Male mice (10 weeks old) were purchased from Envigo RMS Harlan Laboratories (Rossdorf, Germany)
Rat (Wide type)		Male rats (5 months old) raised in house in LIV

8.1.13. Consumables

Consumable	Manufacturer
6-well tissue culture plate (standard)	Falcon / BD Biosciences
6-well Poly-L-Lysin coated tissue culture plate	Greiner bio-one Cellstar
12-well tissue culture plate (standard)	Greiner bio-one Cellstar
24-well tissue culture plate (standard)	Falcon / BD Biosciences
96-well conical bottom microwell plate	Nunc
96-well lockwell plate	Nunc
96-well tissue culture plate (standard)	Sarstedt
Microlance 3 Cannula (25G x 1'', 0.5x25 mm)	BD Microlance
Microlance 3 Cannula (26G x 3/8'', 0.45x10 mm)	BD Microlance
Microlance 3 Cannula (27G x ¾'', 0.4x19 mm)	BD Microlance
Capillary/EDTA tubes for blood collection (200 µl)	Kabe Labortechnik GmbH

Cell strainer, 70 µm	Corning
Cover glasses (Ø 13 mm, thickness No. 1.5)	VWR International
Cryo vials (1ml)	Sarstedt
Metal beads (Ø 2.0 mm)	RETSCH (#22.455.0010)
Microscope Slides (Art.Nr.H868)	Carl Roth
Nitrocellulose membrane Hybond-C Extra	Amersham Biosciences
PCR tubes (0.2 ml or 0.5 ml, 8-stripes)	Sarstedt
Petri dishes (100mm)	Falcon / BD Biosciences
Pipette tips, with filter (10, 100, 1000 µl)	Sarstedt
Pipette tips, without filter (100, 100, 1000 µl)	Brandt
Precision wipe tissue	Kimtech Science
Reaction tubes (1.5 ml, 2.0 ml)	Sarstedt
SafeSeal reaction tubes (with screw caps)	Sarstedt
Scalpel	BRAUN
Syringe Omnifix® (1 ml / Luer Lock Solo)	B. Braun Melsungen AG
Syringe Omnifix® (3 ml / Luer Lock Solo)	B. Braun Melsungen AG
Syringe Omnifix® (10 ml / Luer Lock Solo)	B. Braun Melsungen AG
Syringe Omnifix® (20 ml / Luer Lock Solo)	B. Braun Melsungen AG
T25 cell culture flask	Falcon / BD Biosciences
T75 cell culture flask	Sarstedt
Tissue culture dish (100 mm)	Falcon / BD Biosciences
Transfer pipettes (2, 5, 10, 25 ml)	Sarstedt
Tube 15 ml (DNA-, DNase-, RNase-free)	Sarstedt
Tube 50 ml (DNA-, DNase-, RNase-free)	Sarstedt
Whatman paper	A. Hartenstein

8.1.14. Safety gear

Safety gear	Manufacturer
Duct tape *Extra Universal*	TESA
Dräger X-plore® 8000 hoods	Dräger
Dräger X-plore® 8000 powered air-purifying respirator	Dräger
Filter/respirator mask, type 9332 FFP3 ventil	3M
Gloves *Biogel*	3M
Gloves Latex	Kimberly-Clark
Gloves Purple Nitrile	Kimberly-Clark
Lab coat	Leiber
Lab shoes Unisex	Suecos
OP mask	Mölnlycke Health Care
OP Nurse Cap	Mölnlycke Health Care
OP pants (green)	Sattelmacher
Overalls (blue)	ProFit
Safety goggles	UVEX
Shoe covers (blue)	Ansell Health Care
TYVEK® boot covers	DuPont
TYVEK® overalls	DuPont

8.1.15. Laboratory equipment

Laboratory equipment	Manufacturer
Scale (available for small animal)	Kern
Biological safety cabinet (HeraSafe KS12)	Thermo Scientific
Biological safety cabinet (HeraSafe KS18)	Thermo Scientific
Centrifuge Avanti J-E	Beckham Coulter
Centrifuge 5417R	Eppendorf
Centrifuge Varifuge 3.0R	Thermo Scientific
Cryo conservation container Mr. Frosty	Nalgene
Documentation System ChemiDoc™ MP	Bio-rad

Double door system autoclave (BSL-3 laboratory)	MMM
Electrophoresis system Mini Trans-Blot Cell	Bio-Rad
Gel documentation system Gel Doc XR	Bio-Rad
Gel electrophoresis system Mini-PROTEAN Tetra Cell	Bio-Rad
Gel electrophoresis system Sub-Cell GT (15 x 15 cm)	Bio-Rad
Heraeus temperature-controlled CO_2 incubator B6120	Kendro
Heraeus temperature-controlled CO_2 incubator BBD 6220	Thermo Scientific
Heraeus temperature-controlled CO_2 incubator Heracell 150	Thermo Scientific
Intelli-Mixer (overhead mixer for falcon tubes)	NeoLab
Isoflurane vaporizer	UNO
LightCycler® 96	Roche
Magnetic stirrer MR3001 (with heating element)	Heidolph
Microliter pipettes Eppendorf Reference (1-10, 10-100, 100-1000 µl)	Eppendorf
Microplate reader Tecan Safire2	Tecan
Microwave Supratomic M754	Miele
Mikrotom HM325	Microm
Mixer mill MM 400	RETSCH
Multichannel pipettes (8-12 channel; 5-50 µl; 20-200 µl)	Brand
NanoDrop Lite	Thermo Scientific
Neubauer counting chamber, bright light	Marienfeld
Nikon Eclipse 80i upright light microscope, coupled with Color Camera Nikon DS-Ri2	Nikon (Japan)
Nikon Eclipse Ti-E spinning disc microscope	Nikon (Japan)
Overhead shaker	Heidolph
Paraffin embedding center EG1160	Leica Biosystems
pH calculation device pHenomenal®	VWR
Pipetus	Hirschmann Laborgeräte
Power Pac HC Power Supply	Bio-Rad
Precision scale Extend ED224S	Sartorius

Precision scale ExtendED3202S-CW	Sartorius
Quadrupole ion trap orbitrap mass spectrometer Fusion	Thermo Scientific
Roller Mixer SRT9	Stuart
Shaker MaxQ 6000	Thermo Scientific
Shaker WT 17	Biometra
Shaking waterbathSW22	Julabo
Small centrifuge (1.5 ml reactions tubes)	Biozym
Small centrifuge (PCR tube, 8-stripes)	Biozym
Sonicator UP100H	Heidolph
Spectrophotometer NanoDrop 1000	Peqlab
Spectrophotometer Spectronic Genesys 10 Bio	Thermo Scientific
Surgical forceps (organ harvesting of animal experiment)	F.S.T.
Surgical scissors (organ harvesting of animal experiment)	F.S.T.
Thermomixer TMix 220V	Analytik Jena
ThermoMixer® C, including Thermoblock	Eppendorf
Thermostat Precitherm PFV	Labora Mannheim
Tissue infiltration system ASP300	Leica Biosystems
Transmitted-light microscope	Zeiss
Ultrapure water system Milli Q Aca	Millipore
UPLC system Dionex Ultimate 3000	Thermo Scientific
Vortex-Mixer 7-2020	neoLab

8.1.16. Software

Software	**Manufacturer/Reference**
Adobe Photoshop CS4	Adobe Systems Inc.
Adobe Illustrator 2019	Adobe Systems Inc.
BD FACS Diva™ Software v.8.0.1	BD Biosciences
GraphPadPrism v.9.4.0	GraphPad Software Inc.
ImageJ	National Center for Biotechnology Information
LightCycler® 96 software, V 1.1.0.1320	Roche

LinRegPCR (version 2018.0)	Academic Medical Center, Amsterdam, the Netherlands
Microsoft Office	Microsoft
Matlab	MathWorks
Mendeley desktop	Mendeley
Nikon NIS-Elements Advanced Research 4.51	Nikon (Japan)

8.2 Methods

8.2.1. Ethics statement

Human Cohort

The Ethics Committee of the National Institute for Viral Disease Control and Prevention, Center for Disease Control and Prevention, China (China CDC) reviewed and approved the sample collection from all study subjects, including laboratory-confirmed H7N9 avian influenza cases, seasonal influenza cases, close contacts of H7N9 cases, and poultry workers. This study obtained informed consents from all participants.

Animal model

The animal experiments were conducted in compliance with the regulations of the German animal protection law, as approved by the Behörde für Gesundheit und Verbraucherschutz, Hamburg, Germany (licensing number: N124/2021, T-2020-11-11).

8.2.2. Study participants

As a retrospective study, stored serum or plasma samples collected previously were used through the influenza surveillance network in the local Center for Disease Control and Prevention (CDC), China. Two study groups were included in this study: 1) H7N9 cases and healthy controls (close contacts of H7N9 cases and epidemiologically linked poultry workers); 2) Seasonal influenza cases (outpatient and hospitalized). This study enrolled individuals who were 18 years of age or older and had complete epidemiological information including age, sex, illness onset date, sample collection date, outcome, and/or antiviral treatment, as well as sufficient amounts of serum or plasma samples.

8.2.2.1. Collection of H7N9 cases and healthy controls samples

Throat swabs were collected and diagnosed for influenza A (H7N9) virus from suspected cases with influenza like illness (ILI) in the local CDCs or the Chinese National Influenza Center (CNIC) by real-time RT-PCR with specific primers and probes targeting the matrix, H7 and N9 genes. Once a patient was confirmed with H7N9 influenza virus, an active surveillance was initiated under the influenza surveillance network of the local CDC by conducting serum and throat swabs collection from patients, their close contacts and poultry worker with direct epidemiological link to contaminated environment or poultry for the diagnosis of H7N9 infection. No H7N9 virus was detected from healthy controls and poultry workers in this study. Obtained samples from study participants were kept at -80°C before further analysis.

8.2.2.2. Collection of seasonal influenza cases samples

Simultaneous collection of plasma samples (EDTA plasma) and throat swabs was performed when patients sought outpatient care or were hospitalized during the 2015-2016 influenza season in China. The plasma samples were stored for archiving purposes when seasonal influenza virus was detected by real-time RT-PCR. All collected samples were kept at -80°C until further analysis.

8.2.3. Animal experiment

The experimental procedures involving animals were carried out in accordance with the German Animal Welfare Act at the Leibniz Institute for Virology (LIV), Hamburg, Germany. Male C57BL/6J mice (10 weeks of age) were obtained from Envigo RMS Harlan Laboratories (Rossdorf, Germany). Male rats (5 months old) used for the isolation of primary Leydig cells were in house animals in LIV.

8.2.3.1. Narcosis of mice

To obtain baseline blood samples before infection, mice were anesthetized with isoflurane delivered via a vaporizer. For the infection experiment, mice were anesthetized with a combination of ketamine (100 mg kg-1) and xylazine (10 mg kg-1) administered by intraperitoneal injection, prepared in a sterile 0.9% sodium chloride solution. The dosage of anesthesia was determined based on the weight of each individual animal, using a 1 ml syringe and a 26G cannula.

8.2.3.2. Infection or treatment of mice

The mice were intranasally administered with either PBS, 5 mg kg^{-1} polyinosinic:polycytidylic acid (poly (I:C)) or 10^3 plaque forming units (p.f.u.) of H7N9 influenza A virus (A/Anhui/1/13). The mice were intranasally carefully inoculated with 50 µl of the inoculum using a pipette. Virus dilution was prepared according to the formula as below.

$$\frac{\text{Infection dose (p.f.u/ml)} * \text{Number of animals} * 1000}{\text{Virus stock titer (p.f.u/ml)}} = \text{µl virus stock in x µl PBS}$$

8.2.3.3. Weight loss and survival experiment

Mice were monitored daily for 6 days after infection. Euthanization of mice was conducted when the weight loss reached the humane endpoint (25% weight loss) or for organ harvesting. Mice were euthanized by cervical dislocation under isoflurane anesthesia, and organs were promptly harvested. To ensure proper disposal, the mouse cadavers were subsequently autoclaved.

8.2.3.4. Bleeding and organ harvesting

Baseline blood before infection and blood after infection were both collected in this study. In accordance with animal welfare regulations, the mice were limited to two blood draws per week. To account for this, the mice were divided into three distinct groups for plasma collection. Group 1 consisted of pre-infection plasma and plasma collected 1 day post-infection from the same animal, Group 2 included pre-infection plasma and plasma collected 3 days post-infection from the same animal, and Group 3 comprised pre-infection plasma and plasma collected 6 days post-infection from the same animal. For the collection of post-infection plasma, the animals were administered with isoflurane anesthesia and blood samples were collected through the retrobulbar route into EDTA tubes. Blood samples were then centrifuged for 10 min at 2000 g, 4°C. For organ harvesting, lungs and testes were collected at each time point.

The left lung was removed into a tube filled up with 4% formalin for histology measurement. The right lung was divided into two parts; one part was removed to a tube filled with sterilized metal beads for homogenization and another tube filled up with 1 ml RNAprotect® at 4°C in order to protect the sample before RNA isolation. For histopathological examination of testes, the left testis was immersed in Bouin's solution for 24 h, then washed with 70% ethanol and finally embedded in paraffin using conventional techniques. Hematoxylin and eosin were used

for the staining of sections. The right testis was divided into two parts for homogenization and RNA isolation, respectively. The initial weight of each tissue sample was recorded before homogenization. Subsequently, the tissue was homogenized in 1 mL of PBS using a RETSCH homogenizer (20 Hz, 10 min), and centrifuged at 6000 x g for 10 min. The supernatant was aliquoted and stored at -80°C until further analysis.

8.2.3.5. Isolation and culture of primary rat Leydig cells

Two male rats were sacrificed under over dose of CO_2 using a vaporizer for harvesting of testes. Decapsulated testical tissues were incubated in a 50 ml falcon tube containing 15 ml MEM-BSA (0.1%) with 2.5 mg/ml of collagenase 1 and mixed at the speed of 90 cycles/min in the tube rotator for 20 min at 37°C. Then filtrated through using the 70 µm filter for three times to new 50 ml falcon tubes. Added 15 ml MEM-BSA (0.1%) and centrifuged at 250 x g for 7 min at room temperature (RT). Carefully removed the supernatant and added 10 ml HBSS-BSA and resuspended crude Leydig cells. Centrifuge at 250 x g for 7 min at RT. Repeated this step once to wash out collagenase 1. Resuspend crude Leydig cell suspension in 8 ml of HBSS-BSA and filtrated through with the 70 µm filter. Carefully laid 4ml of filtrated Leydig cell suspension onto the top of prepared discontinuous Percoll gradient (including 3 ml of 90% Percoll, 10 ml of 60% Percoll, 10 ml of 40% Percoll and 5 ml of 20% Percoll). Then centrifuged at 800 x g for 20 min at RT. Discarded first two bands and collected the third fraction from the top of gradient. Diluted the fraction in 22.5 ml of HBSS-BSA and centrifuged at 350 x g for 10 min at RT. Washed and centrifuged cells twice with 15 ml culture medium (DMEM/F12, 1% L-Glu, 1% P/S, 2% FBS) at 350 g for 8 min at RT. Seeded cells in 6 well Poly-L-Lysine coated plates at 34°C, 5% CO_2 for 48h.

8.2.4. Cell culture techniques

8.2.4.1. Cultivation of eukaryotic cells

The eukaryotic cell lines were maintained in a temperature-controlled incubator under the conditions of 37°C, 5% CO_2, and 95% relative humidity (rH). The growth medium for MDCK II cells was composed of MEM, supplemented with 10% FBS, 1% L-Glu, and 1% P/S, while that for LC540 cells was DMEM, supplemented with 10% FBS, 1% L-Glu, and 1% P/S. To ensure the absence of Mycoplasma spp contamination, regular testing of all cell lines was performed using the Venor®GeM Classic Mycoplasma PCR Detection Kit (Minerva Biolabs GmbH) following the manufacturer's instructions.

8.2.4.2. Cryopreservation and thawing of eukaryotic cells

Eukaryotic cell lines were cryopreserved in liquid nitrogen for long-term storage. To prepare cryopreserved stocks, a confluent flask (70-90% confluency) was trypsinized and centrifuged at 1000 x g for 5 minutes at room temperature. The cell pellet was then resuspended in 10% dimethyl sulfoxide (DMSO) solution (in fetal bovine serum) and aliquoted into 1 ml cryovials. The cryovials were stored in cryopreservation containers at -80°C for at least 24 hours before transferring them to liquid nitrogen for long-term storage. To re-cultivate the frozen cells, cryovials were thawed quickly in a 37°C water bath, followed by a washing step in growth medium (1 ml of cells added into 9 ml growth medium) to remove residual DMSO (centrifugation: 300 x g, 5 min). The pellet was then resuspended in growth medium and seeded into T25 cell culture flasks and further incubated at 37°C, 5% CO_2, 95% rH.

8.2.4.3. Mycoplasma spp detection

It was routinely screened all eukaryotic cell lines used in this research for the presence of mycoplasma spp contamination using the Venor®GeM Classic Mycoplasma PCR Detection Kit (Minerva Biolabs GmbH) following the manufacturer's protocol.

8.2.5. Nucleic acid techniques

8.2.5.1. Extraction of total RNA from murine tissues

Total RNA was extracted from murine lung and testis tissues that had been preserved in RNAprotect® solution. The tissues were placed into sterile 2 ml tubes containing 4-6 metal beads (Ø 2 mm), and 1 ml of Trizol reagent was added to each tube. The tissue was then homogenized for 10 min at 30 Hz in a Mixer RETSCH. After centrifugation at 12000 x g for 15 min at 4°C, the upper aqueous phase was collected and transferred to spin-filter D. RNA extraction was carried out using the innuPrep RNA Mini Kit (Analytik Jena) with slight modifications according to the manufacturer's instructions. After a washing step with HS buffer, a DNase I treatment (RNase-Free DNase Set; Qiagen) was performed to digest genomic DNA. For this purpose, 10 µl DNase I was diluted in 70 µl RDD buffer per sample and applied to the columns. The columns were then washed with 500 µl HS buffer. The isolated RNA was eluted with 30 µl RNase-free ddH2O containing 1 U/µl Ribolock RNase Inhibitor, and the RNA concentration was measured on NanoDrop Lite. The RNA samples were stored at -80°C until further analyses.

8.2.5.2. Quantitative real-time reverse transcription PCR (qRT-PCR)

This study utilized a two-step quantitative reverse transcription polymerase chain reaction (qRT-PCR) technique to measure the expression levels of inflammatory genes or viral RNA in testis tissue from mice experiment. Initially, isolated total RNAs were subjected to a reverse transcription reaction using a random nonamer (p9) primer mix (GeneLink) to generate a pool of complementary DNA (cDNA). Next, specific primer pairs were used to quantify the expression levels of target genes in 96-well plates using the SYBR Green reagent (Roche) and the LightCycler® 96 system (Roche). Murine tyrosine 3-monooxygenase/tryptophan 5-monooxygenase activation protein, zeta polypeptide (Ywhaz) expression was used as a reference and quantified using specific primers. The quantitative RT-PCR data was analyzed using the linear regression method with the help of LinRegPCR software. To quantify viral RNA in testes, the standard curve was generated by analyzing serial dilutions of NheI-linearized pHW2000-H7N9-NP vector construct. More details on cDNA synthesis and quantitative amplification reaction can be found in **Table 2** and **Table 3**, respectively.

Table 2. RT reaction for cDNA synthesis.

Component	**Volume (µl)/Amount (µg)**
ddH_2O	ad 13 µl
Primer (p(dN)9) [50 µM]	1 µl
dNTPs, 10 mM	1 µl
RNA Template	1 µg
Total	**13 µl**
PCR Cycling	**65°C, 5 min**
First Strand Buffer (5x)	4 µl
DTT, 0.1 M	1 µl
Ribolock RNAse Inhibitor	1 µl
Superscript III RT, 200 U/µl	1 µl
Total	**20 µl**

	25°C, 5 min	
PCR Cycling	**55°C, 60 min**	
	70°C, 15 min	

Table 3. Setup of quantitative amplification reaction using SYBR Green reagent.

Component / PCR Cycling	**Volume (µl)**	
ddH_2O	7.4	
Primer forward (20 µM)	0.3	
Primer reverse (20 µM)	0.3	
Fast Start Essential Green Master (2x)	10.0	
cDNA template	2.0	
Total	**20**	
	95°C, 5 min	
	95°C, 15 sec	
	65°C, 10 sec	**45 cycles**
PCR Cycling	**72°C, 20 sec**	
	95°C, 1 sec	
	37°C, 120 sec	

8.2.6. Protein biochemical techniques

8.2.6.1. SDS-PAGE and Western blot

SDS polyacrylamide gel electrophoresis (SDS-PAGE) and Western blot (WB) were conducted using standard procedures. Briefly, SDS gels were prepared and stored at 4°C for 2-3 days or prepared just before use (refer to **Table 4** for details). Mini-PROTEAN Tetra Cell system (Bio-Rad) was used for gel electrophoresis, and 10-15 µl of cell lysates and 2 µl of Precision PlusProteinTM Dual Core Standard (Bio-Rad) were loaded onto the gel as a marker. Electrophoresis was carried out for 1.5 - 2 h at 70 to 125 V. Mini Trans-Blot Cell (Bio-Rad) was used for Western blotting at 250 mA for 70 min. The membrane was blocked for 1 h with blocking solution (3 % BSA in PBS-T) at room temperature (RT) and incubated with primary

antibodies overnight at 4°C. The membrane was then incubated with secondary antibodies for 1 to 1.5 h at RT. Membranes were washed with washing buffer (1 x PBS-T) for at least 30 min between each antibody incubation step and before the final detection. SuperSignal West Femto Chemiluminescent Substrate (Thermo Scientific) and ChemiDocTM MP imaging system (Bio-rad) were used for detection according to the manufacturer's instructions.

Table 4. Preparation of SDS gels (4x).

Compound	Resolving gel (10%)	Stacking gel (4%)
ddH_2O	7.9 ml	6.8 ml
Resolving gel buffer (4x)	5 ml	-
Stacking gel buffer (4x)	-	1.25 ml
SDS (10 %)	200 µl	100 µl
Rotiphorese Gel 30	6.7 ml	1.7 ml
TEMED	8 µl	10 µl
APS (10 %)	200 µl	100 µl
Total	**20 ml**	**10 ml**

8.2.6.2. Sex hormone quantification

For human cohorts, the levels of estradiol (17β-estradiol, E2) and testosterone were quantified in serum samples from H7N9 patients, close contacts, and poultry workers using the Beckman Coulter DxI 800 Access Immunoassay System. The measurements were performed at the clinical laboratory of the Sino-Japan Friendship Hospital located in Beijing, China. The Beckman Coulter DxI 800 Access Immunoassay System, which utilizes a chemiluminescent immunoassay with paramagnetic particles, was used to quantitatively determine total estradiol and testosterone levels, including both bound and unbound forms. Specifically, the Access Estradiol Assay (REF 33540, BECKMAN COULTER) and Access Testosterone Assay (REF 33560, BECKMAN COULTER) were used for this purpose. Since the Access Immunoassay System is only available for serum samples, the study measured plasma (EDTA-plasma) samples collected from seasonal influenza patients in house by using commercial Enzyme-Linked Immunosorbent Assay (ELISA) kits. In brief, the study used Abcam's 17β-Estradiol (ab 108667) and Testosterone (ab 174569) kits, which do not show cross-reaction with EDTA. This study utilized Abcam's SHBG (ab 260070) and free testosterone (ab 178663) ELISA kits to determine the levels of sex hormone binding globulin (SHBG) and free testosterone in all H7N9 and seasonal influenza patients.

The testosterone, free testosterone, and estradiol concentrations were converted to SI units (nmol/L or pmol/L). The conversion was done automatically by the measurement platform or manually using the following formulas: for testosterone values (ng/mL) or free testosterone (pg/mL), the values were multiplied by a factor of 3.467; for estradiol values (pg/mL), the values were multiplied by a factor of 3.671, as per the manufacturer's instructions. To determine the total concentration of estradiol (17β-estradiol) and testosterone in murine samples, the study employed an enzyme immunoassay kit (DetectX, Arbor Assay) using plasma samples that had been extracted with diethyl ether

8.2.6.3. Cytokine and chemokine quantification

For human cohorts, the study used the Luminex bead based multiplex assay using a human cytokine/chemokine magnetic bead panel (HCYTOMAG-60K, Millipore, USA) to access cytokines and chemokines from serum or plasma samples collected from both H7N9 and seasonal influenza cases according to manufacturer's instruction. The panel includes 29 inflammatory biomarkers (EGF, Eotaxin, G-CSF, GM-CSF, IFN-α2, IFN-γ, IL-10, IL12-P40, IL12-P70, IL-13, IL-15, IL-17A, IL-1RA, IL-1α, IL-1β, IL-2, IL-3, IL-4, IL-5, IL-6, IL-7, IL-8, IP10, MCP-1, MIP-1α, MIP-1β, TNF-α, TNF-β, VEGF). And a smaller panel including 21 selected cytokines and chemokines showing significant differences in H7N9 cases (GM-CSF, IFN-α2, IFN-γ, IL-10, IL12-P40, IL12-P70, IL-13, IL-17A, IL-1RA, IL-1α, IL-1β, IL-5, IL-6, IL-7, IL-8, IP10, MCP-1, MIP-1α, MIP-1β, TNF-α, TNF-β) was selected to be measured among control groups including H7N9 close contacts and poultry workers.
In mice experiment, pulmonary cytokine and chemokines response were analyzed for Eotaxin, G-CSF, GM-CSF, IFN-γ, IL-1β, IL-2, IL-3, IL-4, IL-5, IL-6, IL-10, MCP-1, MIP-1α, MIP-1β, TNF-α, IL-15, and VEGF by using Bio-Plex Pro Mouse Cytokine kits (Bio-rad).
For cytokines and chemokines that were not detectable (i.e., below the limit of detection) in all groups, a value of 0.1 was assigned for the purpose of analysis.

8.2.7. Virological techniques

8.2.7.1. Infection of eukaryotic cells with influenza A virus

The study aimed to evaluate the replicative fitness of influenza A viruses in specific cellular conditions by conducting growth kinetics for 72 hours. In preparation for the infection, LC540 cell line was seeded in Poly-L-Lysin coated 6-well plates. To initiate the infection, cells were washed with PBS and then inoculated with virus stock diluted to an MOI of 1.0 in 500 µl of inoculation medium. The required amount of virus was calculated using the following formula:

$$\frac{\text{MOI} * \text{Inoculation volume [x µl]} * \text{Number of cells}}{\text{Virus stock titer}} = \text{µl virus stock in x µl inoculation medium}$$

Viral particles were attached to the cells by incubation at 37°C, 5% CO2 for 30 minutes, after which the inoculation medium was removed and the cells were thoroughly washed three times with acidic PBS (pH 5.5) and once with normal cell culture PBS. Subsequently, added 3 ml infection medium containing TPCK-treated trypsin (1:2000 dilution) to each well. Cell culture supernatants (200 µl /well) were collected at 0h, 24h, 48h and 72h p.i and stored at -80°C. The viral titers were determined using a plaque assay on MDCK cells, as described below.

8.2.7.2. Determination of viral titers by plague assay

Herein, this study performed 10-fold serial dilutions of cell culture supernatants or tissue homogenates in PBS. For determination of the viral titer, seeded MDCK cells in 12-well plates three days before the titration (1:6 diluted from confluent T75 flasks). The cell culture supernatants or tissue homogenates were diluted in 10-fold serial dilutions and incubated with MDCK cells for 30 minutes at 37°C, 5% CO_2 with overlay medium to determine their titers. After 72 hours p.i., cells were rinsed with 1x PBS, fixed using 4% paraformaldehyde, and the formation of plaques was detected by staining with crystal violet. **Table 5** shows an overview of the plague assay parameters is provided based on the corresponding well format utilized. Viral titers from tissue homogenates were normalized by dividing with sample weight accordingly.

Table 5. Parameters of plague assay in different multi-well formats.

Plate format	Seeding volume of MDCK per well	Inoculation volume of virus per well	Overlay medium per well	4% PFA volume per well
6-well plate	3.0 ml	333 µl	3.0 ml	1.5 ml
12-well plate	1.5 ml	150 µl	1.5 ml	1.0 ml
24-well plate	1.0 ml	100 µl	1.0 ml	0.5 ml

$$\frac{\text{Number of plaques} * \text{Dilution factor} * 1000}{\text{Inoculation volume}} = \text{virus titer in PFU/ml}$$

8.2.8. Histology techniques

All histological procedures were performed by collaborating partners in the Institute for Anatomy and Cell Biology, Justus-Liebig University of Gießen, Germany. After fixing the samples in Bouin for 24 h, they were washed with 70% ethanol and then embedded in paraffin using standard protocols. Light microscopy was used to evaluate hematoxylin and eosin (HE) stained paraffin sections from tissue fixed in Bouin.

8.2.9. Microscopy techniques

Expression of α2,3- and α2,6-linked sialic acid (SA) influenza receptors in rodent LC540 Leydig cells was analyzed by immunostaining and confocal fluorescence microscopy. Briefly, $0.1X10^5$ cells/well of LC540 cells were seeded in Poly-L-Lysine coated 24-well plates with cover slips (2 ml/well) at 37°C, 5% CO_2 for 24 h. Cells were incubated at 4°C for 10 min and washed once with cold cell culture D-PBS. 20 µg/ml of biotinylated Maackia Amurensis Lectin II (α2,3-SA) or biotinylated Sambucus Nigra Lectin II (α2,6-SA) prepared with cold FBS free cell culture media were added accordingly to each well (150 µl/well) and incubate for 30 min at 4°C. After two washing steps with cold cell culture D-PBS (5 min each), cells were fixed with 4% PFA for 30 min at 4°C, followed by permeabilization using 0.1% Triton-X-100 (in cell culture D-PBS) for 20 min at RT. After two washing steps with cold cell culture D-PBS (5 min each), 5 µg/ml of streptavidin (Alexa Fluor™ 488 conjugate) including 1:1000 diluted Hoechst 33342 reagent was added together to all wells and incubate at RT for 15 min. The stained cells were washed 2 times with cell culture D-PBS. Cover slips were transferred carefully to flumont G covered slide and dried overnight at RT for further analysis using confocal fluorescence microscopy. Quantification of receptor expression was performed by programing script in Matlab.

8.2.10. Statistical analysis

To compare two groups (paired or unpaired, two-tailed), we used the non-parametric Mann-Whitney test or t-test, and for comparison among three groups (unpaired, two-tailed), we employed the non-parametric Kruskal-Wallis test or one-way ANOVA. Non-normally distributed values were converted to their natural logarithmic form (Ln) to enable linear regression analysis for quantitative analysis. Since the study was exploratory in nature, no correction for multiple hypotheses was applied. The p-values of the statistical tests were utilized as exploratory indicators, with significance levels indicated as follows:* $p < 0.05$, ** $p < 0.01$, *** $p < 0.001$, **** $p < 0.0001$. The statistical analyses were performed using GraphPad Prism 9.0.1 (GraphPad Software, Inc.), SAS®, version 9.4 TS level 1M5 (SAS Institute Inc., Cary, NC, United States) and IBM® SPSS® Statistics 27.

9 Results

9.1 Characteristics and demographics of study subjects

The study participants consist of two groups: one is the main study subjects including individuals diagnosed with H7N9, close contacts of H7N9 patients and poultry workers who tested negative for H7N9; the secondary study subjects were outpatients or hospitalized caused by seasonal influenza viruses **(Table 6)**. A total of 369 subjects were included in this study, which were subdivided in those aged 18-49 years old (yrs) (reproductive age) and ≥50 years old (yrs)(post reproductive age). The median age of H7N9 cases in both groups is 42 yrs and 61 yrs, respectively. Consistent with previous findings from five epidemic waves of H7N9 infections in China[69], the number of males subjects also accounted for over 70% of all included H7N9 patients in this study. The median age and proportion of male subjects in H7N9 healthy controls (close contacts and poultry workers) were similar with H7N9 cases for both age groups **(Table 6)**. For enrolled seasonal influenza cases, the study also found the higher proportion of males in hospitalized patients for both young and elderly. H7N9 patients were mostly enrolled at their acute phases after illness onset for both age groups (18-49 yrs: 6.5 days, ≥50 yrs: 7.5 days) **(Supplemental Table 1)**. Over 80% of H7N9 cases have received antiviral treatment during their hospitalization. Most of them were from southern China and identified from the fifth epidemic during 2017, which was reported with the highest number of laboratory-confirmed H7N9 cases among all epidemics[69].

Table 6. Demographics of study participants.

Age group	Study participants (*n*=369)	Age (years)		Sex (%)	
		Median	Q1-Q3	Male	Female
18-49 years	H7N9 cases (*n*=44)	42	34-46	33 (75%)	11 (25%)
	H7N9 negative close contacts (*n*=40)	35	27-41.3	29 (73%)	11 (27%)
	H7N9 negative poultry workers (*n*=43)	41	36-46.5	32 (74%)	11 (26%)
	Seasonal influenza outpatient (*n*=28)	26.5	23.3-32.8	16 (57%)	12 (43%)
	Seasonal influenza hospitalized (*n*=15)	35	30-45	11(73%)	4 (27%)
≥50 years	H7N9 cases (*n*=54)	61	56-67	38 (70%)	16 (30%)
	H7N9 negative close contacts (*n*=31)	62	54-70.5	16 (52%)	15 (48%)
	H7N9 negative poultry workers (*n*=65)	55	53-62	45 (69%)	20 (31%)
	Seasonal influenza outpatient (*n*=25)	61	56-67	12 (48%)	13 (52%)
	Seasonal influenza hospitalized (*n*=24)	72	63-77	14 (58%)	10 (42%)

Data are median (25 th quartile-75th quartile, Q1-Q3) or *n* (%). Subjects with available testosterone or estradiol levels were included for final analysis.

9.2 Sex difference of dysregulation of sex hormones and inflammatory response in H7N9 influenza cases

9.2.1. H7N9 infection is associated with testosterone reduction in men

Firstly, the study measured testosterone levels from all study groups in order to investigate the contribution of sex hormones to the male predominance in H7N9 infections. In men of both age groups, the median levels of total testosterone from H7N9-nagetive poultry workers and H7N9-negative close contacts were all within the reference range reported from Chinese men[86] **(Figure 11a)**. However in H7N9 male patients, the levels of circulating total testosterone were significantly reduced compared to healthy poultry workers and their close contacts in both age groups (18-49 yrs: $p<0.0001$, $p<0.0001$, ≥50 yrs: $p<0.0001$, $p=0.0117$) **(Figure 11a)**. Furthermore, within men aged 18-49 yrs old, individuals with lower total testosterone levels towards to a higher risk of fatal outcome during the development of H7N9 infection compared to eventually survived patients ($p=0.0399$) **(Figure 11b)**. However, this was not observed in older H7N9 male patients. To furtherly evaluate whether the infection has greater androgenic effects, the study also evaluated concentrations of free testosterone and the sex hormone binding globulin (SHBG) to understand the relationship between total testosterone and potential androgenic activity. The median levels of free testosterone in H7N9 male patients of both ages were under the lower reference limit referring to the manufacturer's instruction **(Supplementary Figure 1a)** which is consistent with the reduced total testosterone levels. Unlike total testosterone levels, we could not observe a significant difference of free testosterone between male H7N9 deaths and survivals. On the other hand, SHBG levels in H7N9 infected males of both ages were all within normal reference range[86] **(Supplementary Figure 1b)** and showed no difference between deaths and survivals. This further indicated that the lack of observed correlation between total testosterone and H7N9 related mortality in males aged 50 yrs and over was not influenced by SHBG levels, which usually increases with aging in some men **(Figure 11b)**.

In female H7N9 study subjects, total testosterone levels were all within reference range in general and showed comparable levels to healthy control groups **(Figure 11c)**. Albeit, there is a tendency of elevated testosterone levels in fatal H7N9 cases compared to those who survived in both age groups **(Figure 11d)**. Consistent with total testosterone, the median level of free testosterone were within normal reference range and a tendency of slightly higher levels of free testosterone were observed in deaths **(Supplementary Figure 1c)**. The SHBG levels in female H7N9 patients were also within normal reference range without significant difference among the assessed groups **(Supplementary Figure 1d)**.

The study took seasonal influenza patients as another study cohort in order to access whether sex hormones correlate with disease severity that caused by the virus circulating widely in

humans. Similar with H7N9 male patients, total testosterone levels of men infected with seasonal H1N1 or H3N2 influenza virus were lower in hospitalized cases compared to outpatients, particularly in those aged of 18-49 yrs (p=0.0128) **(Figure 11e)**. Furthermore, free testosterone levels were distributed at the lower limit of reference range in all seasonal influenza infected patients **(Supplementary Figure 1e)**, whereas the levels of SHBG were inside the reference range[86] **(Supplementary Figure 1f)**. For women infected with seasonal influenza viruses, total testosterone levels showed with a slightly tendency towards elevation in those who were hospitalized compared to outpatients but without significant difference **(Figure 11f)**. The concentrations of free testosterone were inside reference range in all female cases, albeit hospitalized women aged over 50 yrs showed higher levels in comparison with outpatients (p=0.002) **(Supplementary Figure 1g)**. The concentrations of SHBG were inside normal reference range among all females of both age groups **(Supplementary Figure 1h)**.
Taken together, these data indicate that H7N9 infections is associated with reduction of total and free testosterone levels in males of both reproductive and post-reproductive ages. Furthermore, the data support the hypothesis that lower levels of total testosterone in 18-49 yrs old males is associated with their fatal outcome.

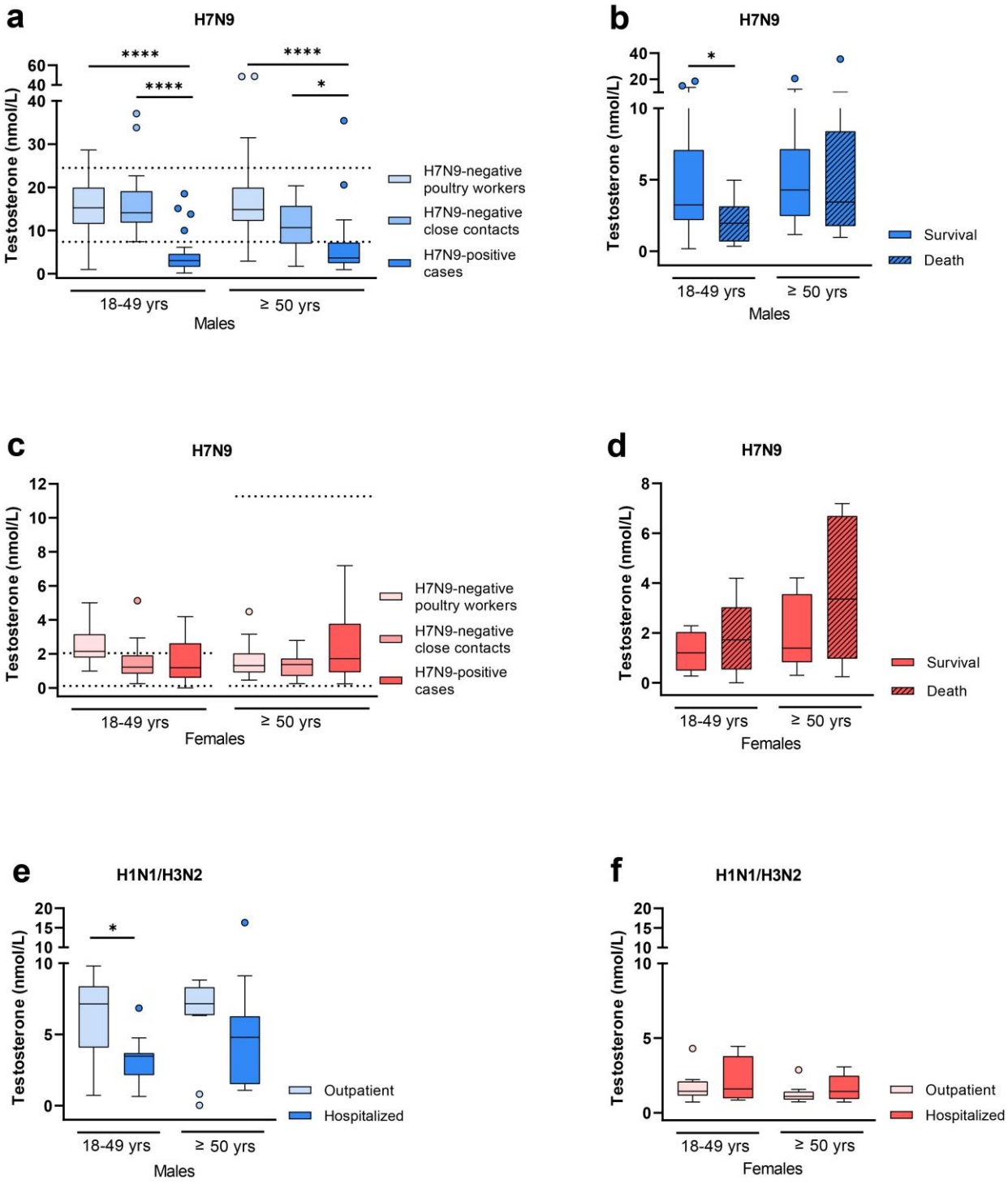

Figure 11. Testosterone levels in H7N9 infected patients compared to control groups.

(a) Total testosterone expression levels were measured in sera from H7N9 IAV-infected male patients (18-49 yrs: n=33, ≥50 yrs: n=38) and compared to male controls as follows: i) H7N9-negative poultry workers (18-49 yrs: n=32, ≥50 yrs: n=45) and ii) H7N9-negative close contacts (18-49 yrs: n=29, ≥50 yrs: n=16); (b) Total testosterone expression levels in H7N9-infected male patients were compared in dependency of disease outcome (18-49 yrs survival/death: n=18/15, ≥50 yrs survival/death: n=27/11); (c) Total testosterone expression levels were measured in sera from H7N9 IAV-infected female patients

(18-49 yrs: n=10, ≥50 yrs: n=16) and compared to female control groups as follows: i) H7N9-negative poultry workers (18-49 yrs: n=11, ≥50 yrs: n=20) and ii) H7N9-negative close contacts (18-49 yrs: n=11, ≥50 yrs: n=15). (d) Total testosterone expression levels in H7N9 IAV-infected female patients were compared in dependency of disease outcome (18-49 yrs survival/death: n=4/6, ≥50 yrs survival/death: n=10/6); (e, f) Total testosterone expression levels were measured in the plasma from seasonal influenza-infected male (18-49 yrs outpatient/hospitalized: n=15/11, ≥50 yrs outpatient/hospitalized: n=12/14) (e) and female patients (18-49 yrs outpatient/hospitalized: n=12/4, ≥50 yrs outpatient/hospitalized: n=13/10) (f) and compared in dependency of disease severity (outpatient vs. hospitalized).(a, c) The age-specific reference range of testosterone in Chinese men and women was added as dotted lines in a and c (no age difference in testosterone in Chinese men)[86]. (a-f) Data are presented as Box-and-whisker plots (Tukey). The horizontal line in each box represents the median value. The 25th-75th percentiles represent the endpoints of the box. The whiskers stretch to the lowest and highest values within 1.5 times the interquartile range (IQR) from the 25th-75th percentiles. Dots represent outliers according to Tukey's definition. Unpaired, two-tailed nonparametric analysis (Mann–Whitney test) was used for comparisons between two groups (b, d, e, f). The Kruskal–Wallis test (a, c) was used for comparisons among the three groups. P values were classified into four groups: * $p < 0.05$, ** $p < 0.01$, *** $p < 0.001$, **** $p < 0.0001$ (adapted from my publication[87]).

9.2.2. H7N9 infection does not show association with altered estradiol levels in men

Secondly, the study evaluated the levels of estradiol, which is another significant sex hormone, among all study subjects. Among males, estradiol levels were all within the normal reference range and the study did not observed significant alterations among H7N9 patients and controls including close contacts and poultry workers in both age groups **(Figure 12a)**. However, some H7N9 male patients displayed increased levels of estradiol than healthy controls. Consistently, several H7N9 fatal cases showed elevated trend of estradiol levels in comparison to survivals **(Figure 12b)**. In women, estradiol levels of all younger subjects were within normal reference range and showed no difference among groups, whereas the elderly showed elevated estradiol levels in comparison to healthy close contacts of H7N9 patients (p=0.0006) **(Figure 12c)**. Nevertheless, the study could not observe the association between elevated estradiol levels and fatal outcome, albeit tendency of increased estradiol levels was observed in some women **(Figure 12d)**.

Among male patients infected with seasonal influenza viruses, levels of estradiol were not altered between outpatients and those being hospitalized, albeit again some hospitalized individuals presented induced estradiol levels **(Figure 12e)**. For women with seasonal influenza infections, estradiol levels showed no difference between outpatients and hospitalized patients **(Figure 12f)**.

Overall, no correlation was observed between H7N9 infections and changes in levels of estradiol from men, whereas H7N9 infections in women aged 50 yrs and above is linked with induced levels of estradiol. However, the increased estradiol is not associated with fatal outcome; the role of estradiol in disease severity in women needs further investigations.

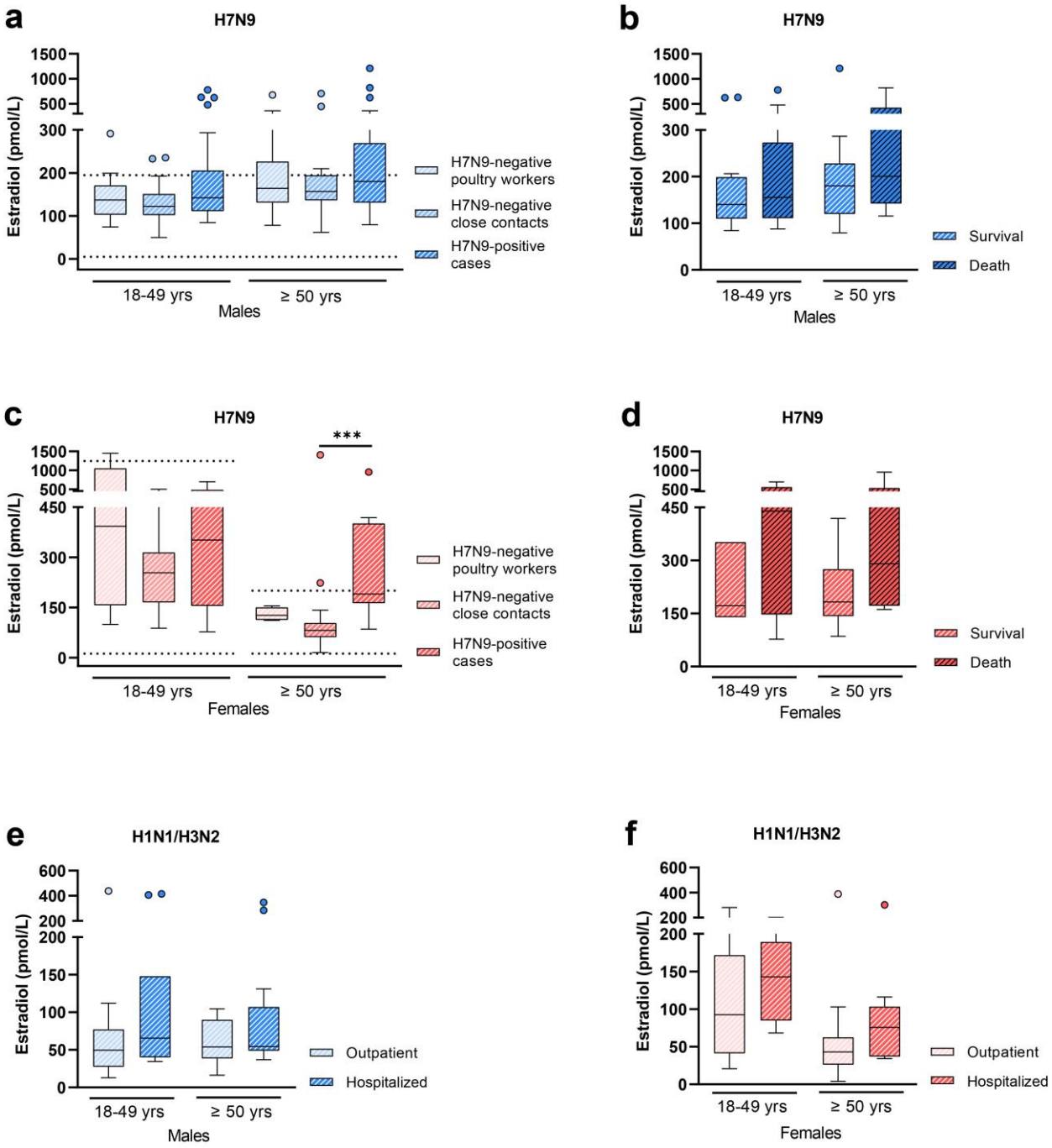

Figure 12. Estradiol levels in H7N9 infected patients compared to control cohorts.

(a) Estradiol levels were measured in sera from H7N9 IAV-infected males (18-49 yrs: n=32, ≥50 yrs: n=27) and compared to male control groups as follows: i) H7N9-negative poultry workers (18-49 yrs:

n=15, ≥50 yrs: n=19) and ii) H7N9-negative close contacts (18-49 yrs: n=29, ≥50 yrs: n=16); (b) Estradiol levels in H7N9 IAV-infected male patients were compared in dependency of disease outcome (18-49 yrs survival/death: n=18/14, ≥50 yrs survival/death: n=17/10); (c) Estradiol levels were measured in sera from H7N9 IAV-infected females (18-49 yrs: n=9, ≥50 yrs: n=12) and compared to female control groups as follows: i) H7N9-negative poultry workers (18-49 yrs: n=8, ≥50 yrs: n=4) and ii) H7N9-negative close contacts (18-49 yrs: n=11, ≥50 yrs: n=15). (d) Estradiol levels in H7N9 IAV-infected female patients were compared in dependency on disease outcome (18-49 yrs survival/death: n=3/6, ≥50 yrs survival/death: n=6/6). (e, f) Estradiol levels were measured in plasma from seasonal influenza-infected male (18-49 yrs outpatient/hospitalized: n=16/11, ≥50 yrs outpatient/hospitalized: n=12/14) (e) and female patients (18-49 yrs outpatient/hospitalized: n=12/4, ≥50 yrs outpatient/hospitalized: n=13/10) (f) and are compared in dependency of disease outcome (outpatient vs. hospitalization). The age-specific reference range of estradiol in Chinese men and women was added as dotted lines in a and c (no age difference in estradiol in Chinese men)[88]. (a-f) Data are presented as Box-and-whisker plots (Tukey). The horizontal line in each box represents the median value. The 25th-75th percentiles represent the endpoints of the box. The whiskers stretch to the lowest and highest values within 1.5 times the interquartile range (IQR) from the 25th-75th percentiles. Dots represent outliers according to Tukey's definition. Unpaired, two-tailed non-parametric analysis (Mann-Whitney test) was used for comparisons between two groups. The Kruskal-Wallis test was used for comparisons among the three groups. P values were classified into four groups: * $p < 0.05$, ** $p < 0.01$, *** $p < 0.001$, **** $p < 0.0001$ (adapted from my publication[87]).

9.2.3. H7N9 male patients with elevated inflammatory cytokine and chemokine have higher risk of mortality.

'Cytokine storms' is one major contributor to disease severity in influenza infections[89,90]. However, analysis of inflammatory response by sex is still lacking. Furthermore, it is known that the sex hormone receptors are widely expressed in immune cells, and the intricate interplay between sex hormones and cytokines/chemokines, along with their interactive regulatory mechanisms, can significantly affect crucial immune pathways[91]. Therefore, the study evaluated the dysregulation of inflammatory markers in H7N9-infected or seasonal influenza-infected male and female patients independency of disease outcome.

In both sexes, H7N9 infection induced significantly higher level of cytokines/chemokines (such as IL-6, TNF-α, IFN-γ, IP-10, MCP-1, etc) comparing with healthy poultry workers and their close contacts **(Supplementary Figure 2)**, which is consistent the observed 'cytokine storms' observed in H7N9 patients from previous studies[92,93]. Furthermore, the study found the distribution of dysregulated inflammatory markers were different between sexes and several of inflammatory markers were related to lethal outcome. In H7N9 male patients, the study observed induced levels of inflammatory markers including G-CSF (18-49 yrs: p=0.0364), GM-CSF (≥50 yrs: p=0.0438), IL-8 (18-49 yrs: p=0.0021, ≥50 yrs: p=0.0381), IL-10 (≥50 yrs:

p=0.0300), IL-15 (18-49 yrs: *p*<0.0001, ≥50 yrs: *p*=0.0322), MCP-1 (≥50 yrs: *p*=0.0116) and TNF-α (18-49 yrs: *p*=0.0182) were related with deaths **(Figure 13a-g)**. However, the study could not observe the association in those inflammatory markers in H7N9-infected females **(Figure 13h-n)**. Conversely, the declined levels of Eotaxin (18-49 yrs: *p*=0.0061) and induced levels of MIP-1ß (18-49 yrs: *p*=0.0121, ≥50 yrs: *p*=0.0216) and EGF (≥50 yrs: *p*=0.0405) were related with lethal outcome in women other than men **(Figure 13o-t)**.

For males infected with seasonal H1N1/H3N2 influenza virus, the study found induced expressions of IL-8 (18-49 yrs: *p*<0.0001, ≥50 yrs: *p*=0.0111), MIP-1α (18-49 yrs: *p*=0.0346), IL-7 (18-49 yrs: *p*=0.0338), IL-15 (18-49 yrs: *p*=0.0291), EGF (18-49 yrs: *p*=0.0390), VEGF (18-49 yrs: *p*=0.0145) and IFN-α2 (≥50 yrs: *p*=0.0102) were related to the need for hospitalization which were not observed in women except for IL 8 (18-49 yrs: *p*=0.0148, ≥50 yrs: *p*=0.0042) **(Figure 14a-n)**. On the other hand, reduction of IFN-γ (≥50 yrs: *p*=0.0202) and MIP-1ß (≥50 yrs: *p*=0.0137) were related to hospitalized women but not men **(Figure 14o-r)**.

These findings show that H7N9 infection induced hypercytokinemia in both sexes but stimulated with different magnitude of inflammatory markers in males and females. In H7N9 male patients, cytokines/chemokines involved in monocyte and granulocyte pathways are more strongly related to negative prognosis compared to females, and this tendency is observed in seasonal influenza-infected males. Herein, unlike female cases either infected with H7N9 or seasonal influenza viruses, excessively expressed cytokines and chemokines such as G-CSF, GM-CSF, IL-10, MCP-1, TNF-α and especially IL-15 are related to deaths in H7N9 male patients.

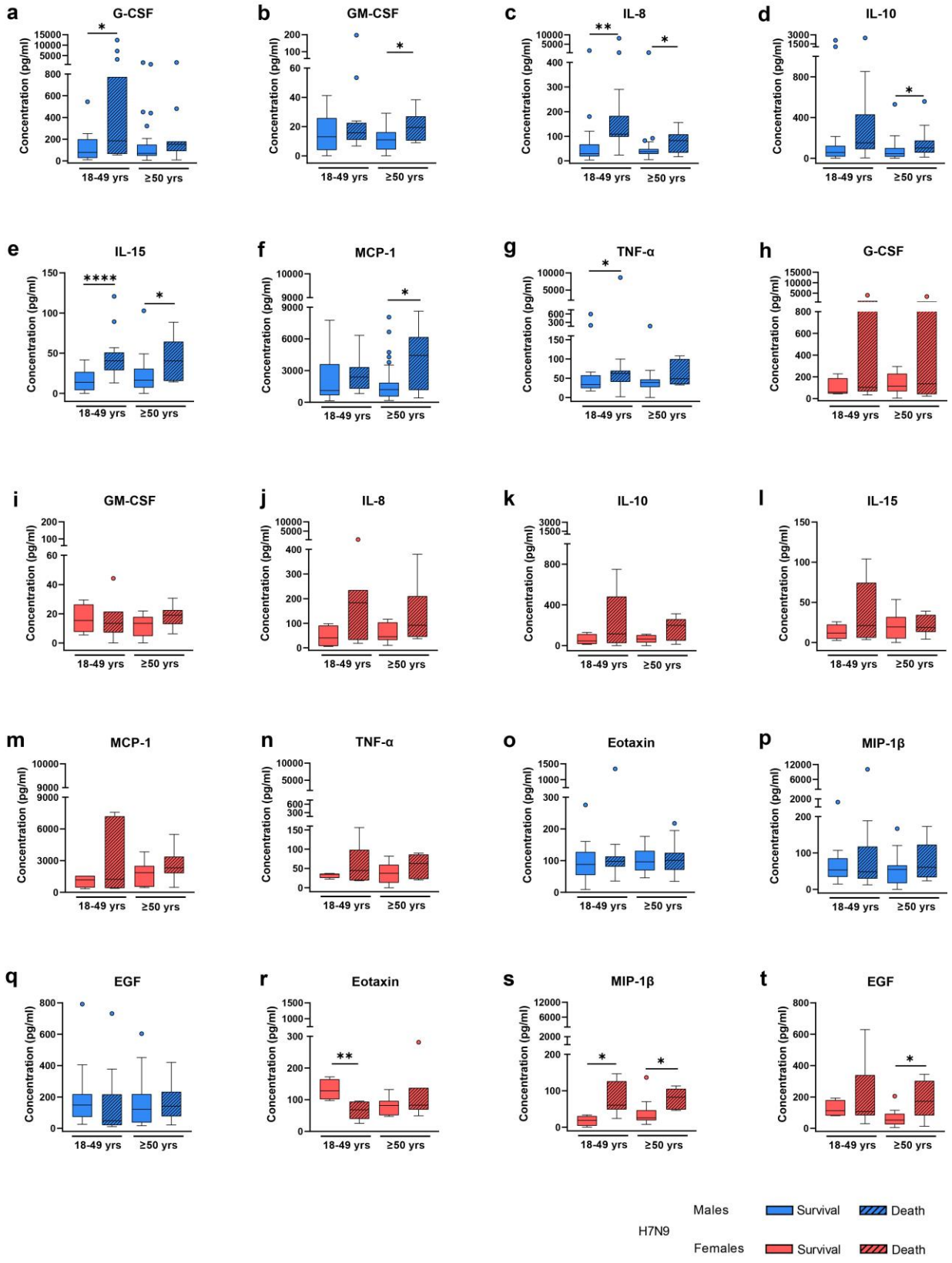

Figure 13. Cytokine and chemokine profiles in H7N9 infected patients in dependency of disease outcome.

(a-t) Shown are the expression levels of cytokines and chemokines in the sera of H7N9 IAV-infected males (18-49 years survival/death: n=18/15, ≥50 years survival/death: n=27/11) and female patients

(18-49 years survival/death: n=4/7, ≥50 years survival/death: n=10/6) who either survived or succumbed to the infection. The measurement was performed using a multiplex immunoassay. Cytokines/chemokines considerably dysregulated in males include: G-CSF (granulocyte colony-stimulating factor; a), GM-CSF (granulocyte-macrophage colony-stimulating factor; b), IL-8 (interleukin 8; c), IL-10 (interleukin 10; d), IL-15 (interleukin 15; e), MCP-1/CCL2 (monocyte chemoattractant protein 1; f), and TNF-α (tumor necrosis factor alpha; g). The same cytokines and chemokines were not altered in female H7N9 patients between both groups (h-n). Cytokines/chemokines considerably dysregulated in females include: Eotaxin (r), MIP-1β/CCL4 (macrophage inflammatory protein 1 beta; p), and EGF (epidermal growth factor; t). These cytokines were not significantly altered in males between both groups (o-q). Data are presented as Box-and-whisker plots (Tukey). The horizontal line in each box represents the median value. The 25th-75th percentiles represent the endpoints of the box. The whiskers stretch to the lowest and highest values within 1.5 times the interquartile range (IQR) from the 25th-75th percentiles. Dots represent outliers according to Tukey's definition. Unpaired, two-tailed non-parametric analysis (Mann-Whitney test) was used for comparisons between two groups. The Kruskal-Wallis test was used for comparisons among the three groups. P values were classified into four groups: * $p < 0.05$, ** $p < 0.01$, *** $p < 0.001$, **** $p < 0.0001$ (adapted from my publication[87]).

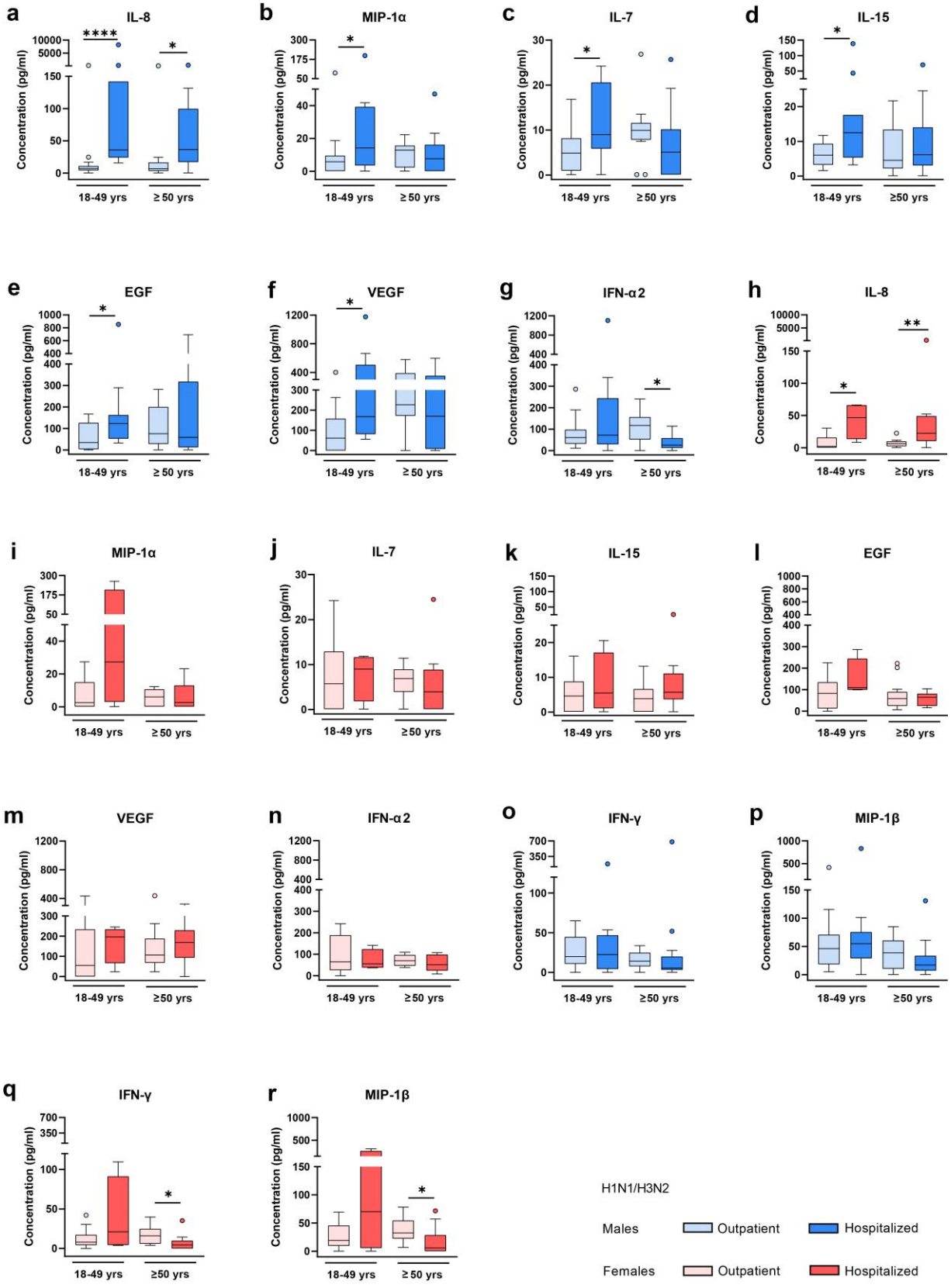

Figure 14. Cytokine and chemokine profiles in seasonal H1N1/H3N2 influenza patients in dependency of disease outcome.

(a-r) Shown are the expression levels of cytokines and chemokines in the plasma from seasonal influenza outpatients and hospitalized patients, each divided into two age groups: 18-49 yrs (male outpatient/hospitalized: n=16/11, female outpatient/hospitalized: n=12/4) and ≥50 yrs (male outpatient/hospitalized: n=12/14, female outpatient/hospitalized: n=13/10). The measurement was carried out using a multiplex immunoassay. Cytokines/chemokines considerably dysregulated in either or both sexes include: IL-8 (interleukin 8; a, h), MIP-1α/CCL3 (macrophage inflammatory protein 1 alpha; b, i), IL-7 (interleukin 7; c, j), IL-15 (interleukin 15; d, k), EGF (epidermal growth factor; e, l), VEGF (vascular epidermal growth factor; f, m), IFN-α2 (interferon alpha 2; g, n), IFN-γ (interferon gamma; o, q), and MIP-1β/CCL4 (macrophage inflammatory protein 1 beta; p, r). Data are presented as Box-and-whisker plots (Tukey). The horizontal line in each box represents the median value. The 25th-75th percentiles represent the endpoints of the box. The whiskers stretch to the lowest and highest values within 1.5 times the interquartile range (IQR) from the 25th-75th percentiles. Dots represent outliers according to Tukey's definition. Unpaired, two-tailed non-parametric analysis (Mann-Whitney test) was used for comparisons between two groups. The Kruskal-Wallis test was used for comparisons among the three groups. P values were classified into four groups: * $p < 0.05$, ** $p < 0.01$, *** $p < 0.001$, **** $p < 0.0001$ (adapted from my publication[87]).

9.2.4. Inflammatory markers show negatively association with testosterone levels in H7N9 infected men

Based on previous analysis, the study have observed low testosterone levels in men were associated with poor disease outcome, and a broader profile of inflammatory markers were induced in male patients with severe or fatal outcomes. Hence, this study looked for potential interactions between the observed male-specific cytokines/chemokines and testosterones in H7N9 or seasonal influenza patients by applying a linear regression model. Herein, the study did not observe any interaction between deaths and survivals. Overall, testosterone levels and cytokines showed a negative association including IL-6 (R^2=0.3672), IL-10 (R^2=0.2387), IL-15 (R^2=0.5049), IL-1RA (R^2=0.2506) and IL-1α (R^2=0.2564) in H7N9-infected men aged 18-49 yrs **(Figure 15a-e)** as well as IL-6 (R^2=0.2355) and IL-10 (R^2=0.2966) in elders aged above 50 yrs **(Figure 15f and g)**. Additionally, the study could only observed the negative association between G-CSF levels and testosterone levels in seasonal H1N1/H3N2-infected men aged 18-49 yrs **(Supplementary Figure 3)**.

Taken together, this study identified the reduced of testosterone levels are associated with induced inflammatory makers in H7N9-infected males, particularly the IL-15, which can explain approximately 50% variation (R^2=0.5049) of testosterone levels.

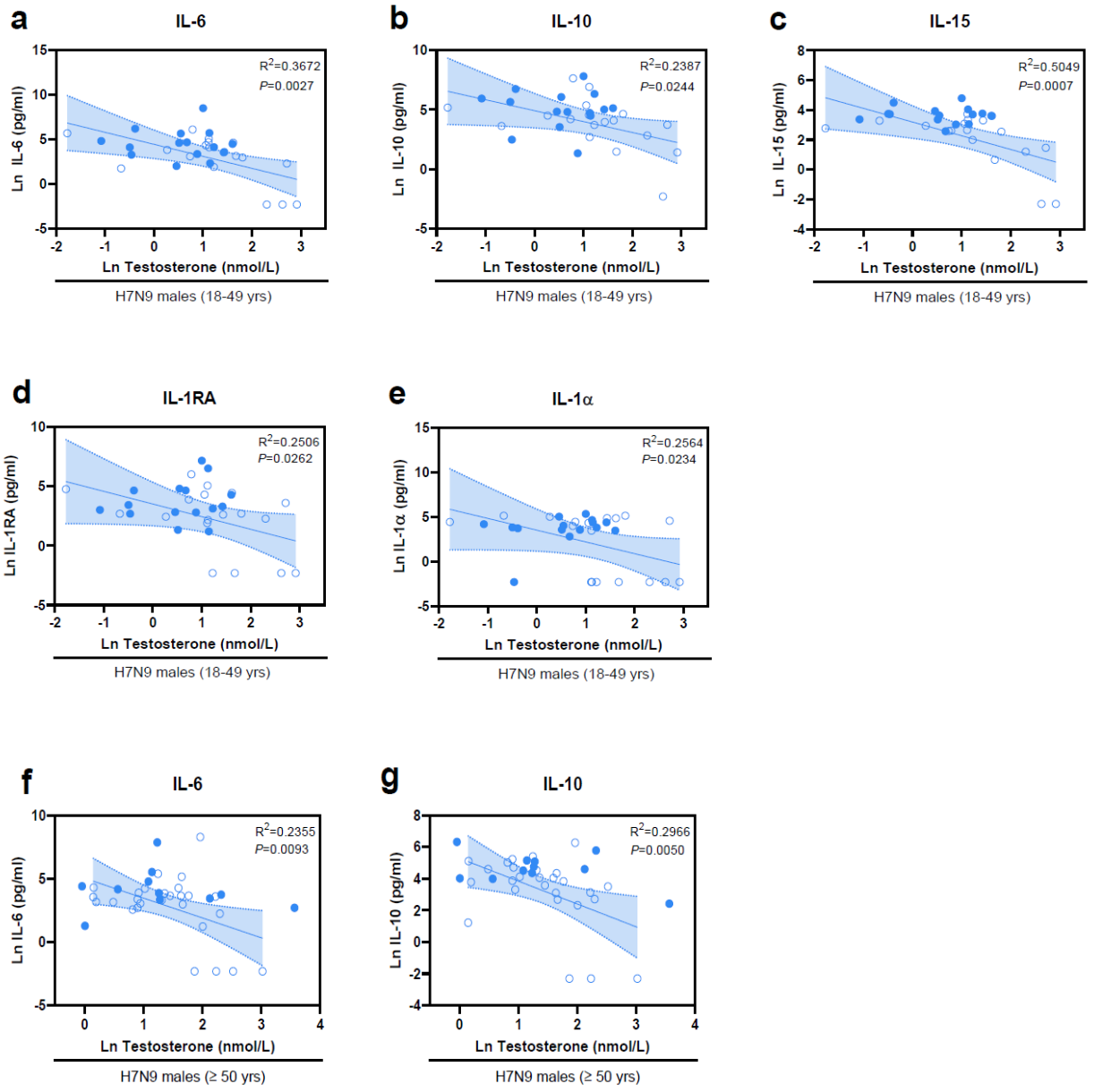

Figure 15. Correlation of testosterone and cytokine/chemokine levels in men infected with H7N9 influenza.

(a-g) Shown is the observed regression between testosterone and cytokine/chemokine levels in H7N9 IAV-infected males. Natural logarithm transformed (Ln) testosterone expression levels measured in the sera from H7N9 males were plotted over the Ln transformed cytokine/chemokines levels. (a-e) Overall regression of testosterone with cytokines IL-6 (interleukin 6; a), IL-10 (interleukin 10; b), IL-15 (interleukin 15; c), IL-1RA (interleukin 1 receptor antagonist; d) and IL-1α (interleukin 1 alpha; e) observed from H7N9 younger males without interaction between deaths and survivors (18-49 yrs survival/death: *n*=18/15); (f-g) Observed overall regression of testosterone with cytokines IL-6 (interleukin 6; f) and IL-10 (interleukin 10; g) in H7N9 older males without interaction between deaths and survivors (≥50 yrs survival/death: *n*=27/11). (a-g) The best-fit line with 95% confidence intervals of the overall regression is shown in each figure. The centre of the error distribution is the regression line.

Two-tailed linear regression was performed. Adjustment for multiple hypotheses was not necessary due to the explorative nature of the study. A hollow blue circle represents survival, and a solid blue circle represents death. R squared values are shown in the figures (adapted from my publication[87]).

9.3 Replication of influenza A virus in Leydig cells

Then the study sought experimental evidence for the potential origin of reduced testosterone levels. Since testosterone is mainly synthesized from the Leydig cells in the testes, the study assessed the replication ability of influenza A virus in the gonadal cells. In the rodent Leydig cell line LC540, H1N1 seasonal influenza virus showed with limited and lowest replication ability, and followed with H3N2. The growth of both seasonal viruses was stagnate after 24h post infection **(Figure 16a)**. However, H7N9 influenza virus replicated more efficient than seasonal influenza viruses at 24h, 48h and 72h post infection. The replication of H7N9 virus was also detected in rodent primary Leydig cells isolated in house **(Figure 16b, supplemental Figure 4a-b)**. However, the viral titer of H7N9 virus in Leydig cells was several logs lower than what observed with relatively high MOI (MOI=1.0) infection in known susceptible cell lines (e.g., MDCK) and was stagnate over time. In order to confirm this was of a productive viral infection, the study measured the viral protein at 6h, 16h, 24h and 48h post infection by Western-blotting. The study could detect expression of PB1 since 6h post infection for both H3N2 and H7N9 viruses and the signals peaked at 16h post infection for all viruses **(Supplemental Figure 4c)**. Furthermore, the study also confirmed both the 'human' (α-2,6 SAs) and 'avian' (α-2,3 SAs) influenza receptors were expressed in rodent Leydig cells which allows influenza virus to enter the cells **(Supplemental Figure 4d)**. Thus, experiments *in vitro* showed that H7N9 influenza virus is able to replicate in Leydig cells indicated further evaluation *in vivo* for the impact of viral infection in testis to the testosterone synthesis is necessary.

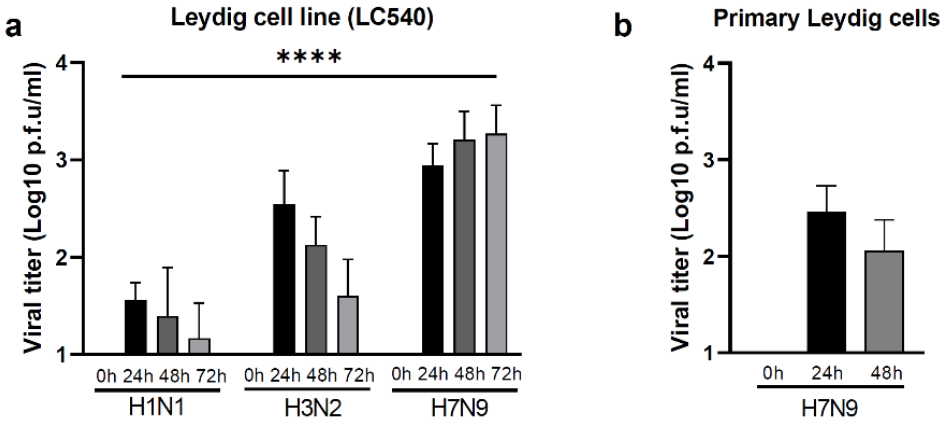

Figure 16. Replication of influenza A virus in Leydig cells.

(a) Replication of seasonal H1N1, H3N2 and H7N9 influenza viruses in rat Leydig cell with the MOI of 1.0 (LC540). The Kruskal-Wallis test was used for comparisons among the three groups. P values were classified into four groups: * $p < 0.05$, ** $p < 0.01$, *** $p < 0.001$, **** $p < 0.0001$; (b) Replication of H7N9 influenza virus with the MOI of 1.0 in primary Leydig cells isolated in house from rat.

9.4 H7N9 spreads to murine testes and causes testosterone depletion

9.4.1. Replication of H7N9 influenza virus in murine testes

Since this study evaluated the dysregulation of sex hormones retrospectively in human cohorts, it is not applicable to address if there is a causal link between H7N9 infection and testosterone depletion. Therefore, the study utilized a male mouse model treated or infected with PBS, poly (I:C) or H7N9 influenza virus. H7N9 infected mice started losing weight at 4 days post infection (d.p.i) while there was no weight loss in PBS or poly(I:C) treated mice **(Supplemental Figure 5a).** The study then measured the viral titer in lung from both poly (I:C) treated or H7N9 infected mice at day 1, 3 and 6 post infection (d.p.i). No viral replication in poly (I:C) treated mice was detected. The replication of H7N9 influenza virus in lung was detected since 1 d.p.i and peaked at 3 d.p.i **(Figure 17a)** which was in line with pulmonary inflammatory response **(Supplemental Figure 6)**. No detectable plagues was found in testes from H7N9 infected mice (data not shown). However, viral mRNA was detected in the testes of some mice (40%, 6/15) at day 1 after infection and later detected from all mice except for one at 3 d.p.i (94%, 15/16) **(Figure 17b)**. The viral mRNA of H7N9 virus was still detectable from over half of infected mice (57%, 4/7) at 6 d.p.i. These results indicated the respiratory H7N9 influenza virus can spread to murine testes and replicate in gonadal organ to some extent.

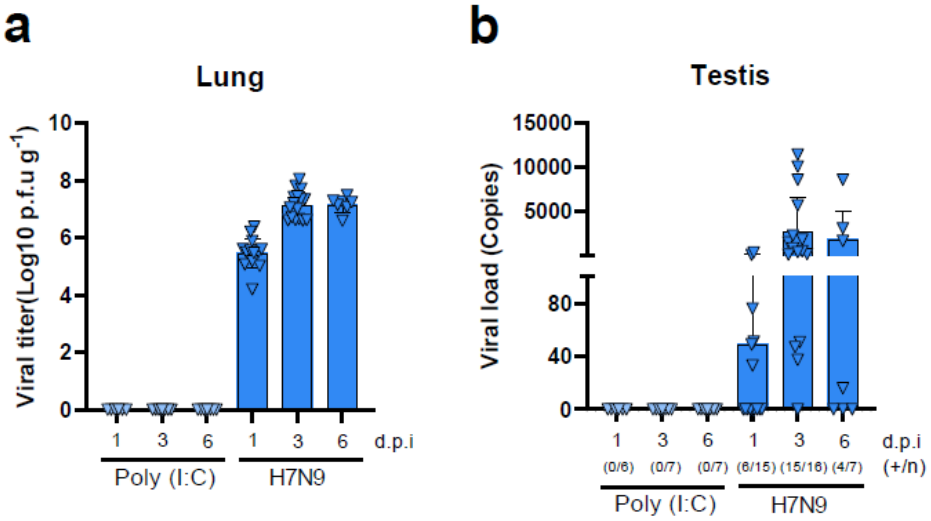

Figure 17. H7N9 influenza virus replicates in murine testes.

(a) Lung viral titres of mice control-treated with Poly (I:C) (n=6, 7 and 7) or infected with H7N9 virus (n=15, 16 and 7) at 1, 3 and 6 d.p.i. (b) Viral NP mRNA expression levels in the testes from mice control-treated with Poly (I:C) or infected with H7N9 virus at 1d.p.i (Poly (I:C): n=6, H7N9: n=15), 3 d.p.i (Poly (I:C): n=7, H7N9: n=16) and 6 d.p.i (Poly (I:C): n=7, H7N9: n=7). Number of mice with detectable H7N9 viral NP mRNA levels and the total number of mice are shown below the graph as (+/n). Data are presented as the mean values+SDs (adapted from my publication[87]).

9.4.2. H7N9 infection causes testosterone reduction in mice

As followed, the study measured the testosterone and estradiol levels from 1 day pre-infection (or pre-treatment) and 1, 3 and 6 days post-infection (or post-treatment) from poly (I:C) or H7N9 infected male mice, respectively. The study detected the reduction of testosterone levels from poly (I:C) treated at 1 d.p.i (p=0.0120) and 3 d.p.i (p=0.0469) **(Figure 18a,b)**. Consistently, testosterone depletions were also detected from H7N9 infected mice at these two time points (1d.p.i: p=0.0137, 3 d.p.i: p=0.0244) **(Figure 18d,e)**. And there is no significant difference in both groups at 6 d.p.i. **(Figure 18c,f)**. On the other hand, the study observed significant down regulation of estradiol levels from poly (I:C) treated mice (p=0.0005) whereas there was an up regulation of estradiols in H7N9 infected mice at 1 d.p.i (p=0.0063). Nevertheless, the estradiol levels reduced at 6 d.p.i (p=0.0019) in H7N9 infected mice **(Supplementary Figure 5 j-o)**. These results confirmed the causality of H7N9 infection and testosterone reduction that observed from male patients. Although poly (I:C) treatment also can cause testosterone reduction in mice, the mechanisms behind the down regulation of testosterone might be different with H7N9 infection as the study also observed the estradiol levels altered in different directions in viral infection and poly (I:C) treated mice.

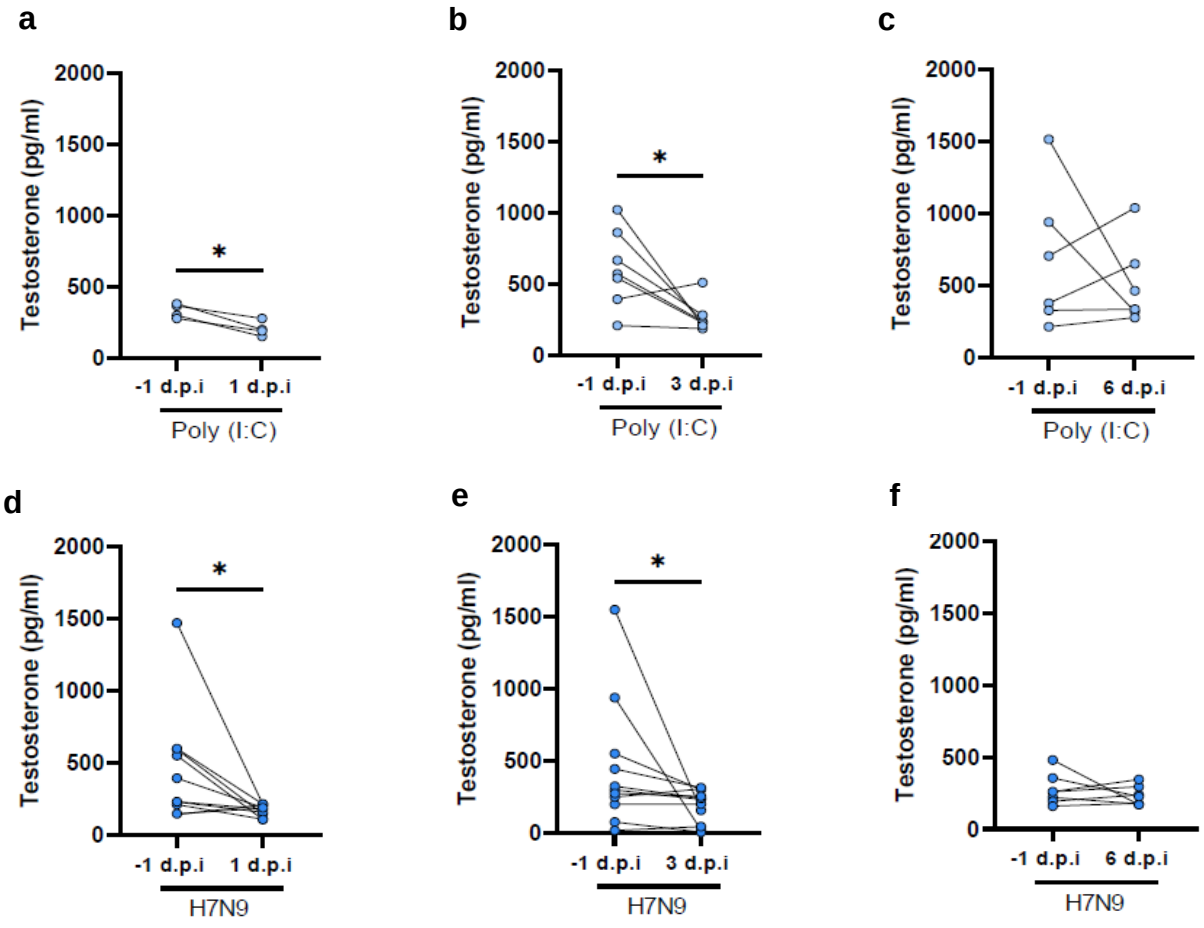

Figure 18. Infection of H7N9 reduced testosterone levels in male mice.

(a-c) Before and post infection testosterone levels are shown from mice treated with Poly (I:C) (n=4, 7 and 6) at 1, 3 and 6 d.p.i. (d-f) Before and post infection, testosterone levels were measured in mice infected with H7N9 virus (n=10, 11 and 7) at 1, 3 and 6 d.p.i. Data are presented as Box-and-whisker plots (Tukey). The horizontal line in each box represents the median value. The 25th-75th percentiles represent the endpoints of the box. The whiskers stretch to the lowest and highest values within 1.5 times the interquartile range (IQR) from the 25th-75th percentiles. Dots represent outliers according to Tukey's definition (adapted from my publication[87]).

9.4.3. H7N9 infection induced testicular inflammatory response in mice

The impact of cytokine or chemokine markers to testosterones synthesis is known from previous studies. However, whether the nasal administrated H7N9 virus can cause inflammatory dysregulation or pathological changes in murine testis is still unknown. In this study, mice infected with H7N9 virus displayed increased testicular pro-inflammatory cytokine/chemokine levels in comparison to PBS- or poly(I:C)-treated mice at 3 d.p.i., which was the point of time when the virus reached the highest titer in lung and testes. These inflammatory markers included MCP-1 (PBS or poly (I:C) vs. H7N9: p=0.0071, p=0.0080), IP-10 (PBS vs. H7N9: p=0.0472), IL-10 (PBS or poly (I:C) vs. H7N9: p<0.0001, p=0.0014), MIP-1ß (PBS or poly (I:C) vs. H7N9: p<0.0001, p=0.0004) and IL-1ß (PBS or poly (I:C) vs. H7N9: p<0.0001, p=0.0079) **(Figure 19a-e)**. Other measured cytokines or chemokines that didn't show significant dysregulation among groups included TNF-α, IL-15, MIP-1α, IFN-γ, IL-6, GM-CSF, VEGF, Eotaxin **(Supplemental Figure 5 b-i)**. Although the study observed the induced testicular inflammatory response in male mice infected with H7N9 virus, there were no apparent impacts at the levels of testicular pathology, which might due to the limited replication of H7N9 in testes **(Figure 19f-h; Supplementary Figure 5p-u)**. Taken together, these data indicated that H7N9 influenza virus infection could cause testicular inflammatory response but not in poly (I:C) treated mice. The upregulated cytokines and chemokines might contribute to the reduction of testosterone synthesis.

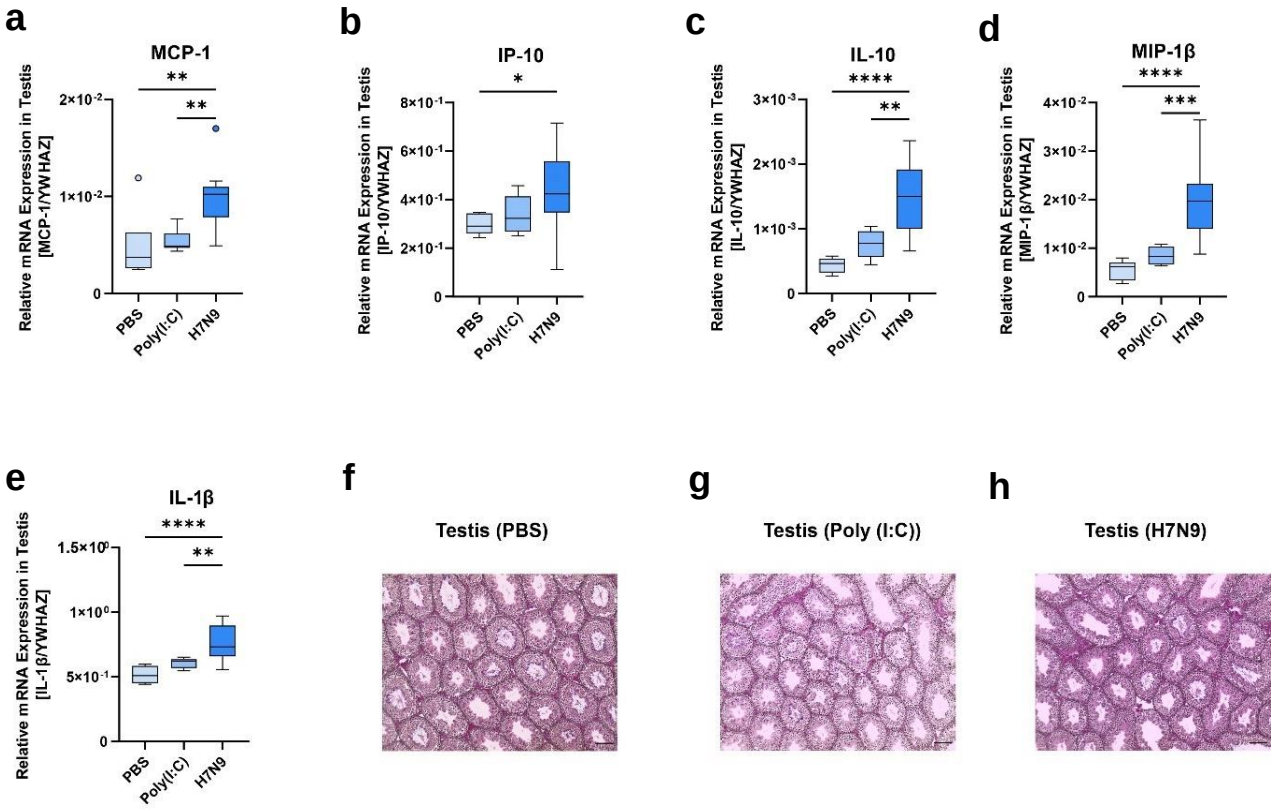

Figure 19. Infection of H7N9 induced inflammatory response in testis in male mice.

(a-e) Significantly increased relative mRNA expression levels of inflammatory markers in the testes of H7N9-infected mice (n=16) compared with PBS (n=7)- or Poly (I:C) (n=7)-treated mice at 3 dpi. Data are presented as Box-and-whisker plots (Tukey). The horizontal line in each box represents the median value. The 25th-75th percentiles represent the endpoints of the box. The whiskers stretch to the lowest and highest values within 1.5 times the interquartile range (IQR) from the 25th-75th percentiles. Dots represent outliers according to Tukey's definition. (f-h) Hematoxylin and eosin (HE)-stained paraffin sections from Bouin fixed tissue were evaluated via light microscopy. Shown are representative histological images of the testes of PBS (n=7)-, or Poly (I:C) (n=7)-control treated and H7N9-infected mice (n=7) at 3 d.p.i. (10X). Scale bars (100 µm) are shown in the bottom right of each micrograph. (c-m) Unpaired or paired, two-tailed non-parametric analysis (Mann-Whitney test) or *t* test was used for comparisons between two groups. One-way ANOVA or the Kruskal-Wallis test was used for comparisons among the three groups. P values were classified into four groups: * $p < 0.05$, ** $p < 0.01$, *** $p < 0.001$, **** $p < 0.0001$ (adapted from my publication[87]).

10 Discussion and outlook

10.1 Risk factors contributing to the sex differences in infection

Genetic factors

Sex chromosomes are considered as the genetic basis for the sexual dimorphism in infectious diseases[94]. In the XY sex-determination system in humans, the Y chromosome is relatively small that contains approximately 100 protein-coding genes, whereas the X chromosome carries over 800 protein-coding genes[95] enriched with loci involved in the immune response[96,97]. Males carrying only a single copy of the X chromosome are mostly affected by X-linked variants, while females are considered as biologically superior as their two copies of X chromosome can compensate the X-linked disorders[98]. The biallelic expression of X-linked genes protects women from recessive mutations and increases the genetic diversity of immune cells[97]. Therefore, females perform better than males against infectious diseases although they are more susceptible to developing autoimmune diseases[97,99–101]. Many X-linked genes play a role in susceptibility or severity to infectious diseases, which differs in males and females. For instance, the nuclear factor kappa-B (*NF-κB*) is an important transcription factor driving the inflammatory response against pathogens[102]. The essential modulator (NEMO) of *NF-κB*, inhibiting an *NF-κB* kinase and upregulating the expression level of *NF-κB,* is encoded by IKBKG gene which harbors in the X chromosome[97]. Mutations in IKBKG gene typically result in impaired immune responses and are related with higher risk of viral and bacterial infections in men with sepsis, pneumonia, otitis or sinusitis[103–105]. The X-linked gene toll-like receptor 7 (TLR7) plays a key role in the innate immune response by specifically recognizing single-stranded RNA and DNA such as influenza viruses[106,107]. Recently, some rare variants identified in TLR7 were found to be associated with critical ill COVID-19 male patients below 60 years old as the type I and II interferons responses was disrupted[108–111]. Besides the disadvantage of males in innate immune response, the adaptive immune responses to vaccination and infection are generally lower in males[112,113]. The underlying mechanisms are still poorly understood. A recent study revealed that GRP174, an X-linked G-protein-coupled receptor suppresses the positioning of male B cells towards to the germinal center but not in females in mouse model[114].

Additionally, females experience random X-chromosome inactivation (XCI) in order to keep identical expression level of X-linked proteins with males. However, about 20-30% of genes can escape the inactivation in humans[115,116]. Therefore, the differential X-linked gene expression between sexes resulted in sex differences in wide conditions. A recent study revealed the expression of the escaping XCI gene *Kdm6a* (encodes the UTX protein) which is

an epigenetic regulator was lower in male NK cells. The deficiency of UTX reduced NK cells effector response and increased lethality to viral infection independent of sex hormones[117].

Sex hormones

It is known that both innate and adaptive immune responses vary between males and females. Females usually generate stronger immune responses against pathogens or vaccination than males based on previous studies *in vitro*, in rodents and in humans[112]. Direct effects of sex hormones on immunological pathways are one of the factors contributing to this sex dimorphism, especially testosterone and estradiol that have been shown to effect the function of immune cells through activating sex hormone receptors-mediated pathway that are widely expressed in different circulating immune cells such as lymphocytes, macrophages, dendritic cells, T cells and B cells[118,119]. Sex hormones and their specific receptors act as a ligand-regulated transcription factor of target genes such as cytokines and chemokines. The classic androgen receptor (AR)[120] and estradiol receptor (ER, including ER-α and ER-β)[121,122] belong to the steroid hormone group of the nuclear receptor superfamily which have a common structure including an N-terminal domain (NTD), DNA-binding domain (DBD), hinge region and ligand-binding domain (LBD)[123]. The classical ligand-regulated pathway is triggered by the binding of free testosterone or estradiol to LBD of intracellular AR or ER respectively, which induces a conformational change of steroid receptors. As followed, the complex of sex hormone-receptors is translocated into the nucleus where the DBD of steroid receptor can bind to the androgen or estrogen response elements (ARE or ERE) in the promoter regions to regulate the expression of target genes **(Figure 20)**[123,124].

Testosterone generally supresses the immune response. Previous studies have revealed that testosterone or dihydrotestosterone (DHT) treatment in human umbilical vein endothelia (HUVECs) or benign prostatic hyperplasia cells (BPH) inhibited NF-κB activity, which is a transcription factor of cytokines and chemokines and therefore suppressed the production of inflammatory factors, such as IL-8 and IL-6[125,126]. In *vivo*, treatment with testosterone in orchiectomized animals attenuated the expression of lipopolysaccharides (LPS)-induced TNF-α and inducible nitric oxide (iNO) in a dose-dependent manner[127]. Delivery of exogenous testosterone to elderly or castrated young male mice can notably improve the consequences of IAV infection in both and pulmonary pathology in young mice[128]. On the other hand, treatment of female mice with testosterone protects them from lethal outcomes caused by 2009 pandemic H1N1 influenza virus infection which is also associated with reduced expression of pro-inflammatory markers such as IL-1β and IL-6 in the lung[129]. Epidemiological and clinical studies have revealed that men with androgen deficiency (hypogonadism) were associated

with higher levels of inflammatory markers such as IL-6, IL-1β, TNF-α and C-reactive protein (CRP)[130–133].

Estradiol levels vary during the menstruation period, with particular high levels during gestation and reduced levels after menopause[112]. It can widely affect innate immunity and the differential effects on the immune response depend on not only the estradiol levels but also the localization of ERs in immune cells. Two classical ERs express differently among immune cells in humans. For instance, T cells exhibit high levels of ER-α expression whereas ER-β is abundantly expressed in B cells[134]. In addition, the non-classical ER signalling also interacts with ERE-independent transcription factors (i.e NF-κB) through protein-protein interactions in immune cells[135]. Estradiol, particularly 17β-estradiol (E2) bidirectionally regulates immune cells such as monocytes function in females of different status[136]. For females during menopause, increased levels of monocytes counts were reported[137,138]. Additionally, women which received hormone replacement therapy (HRT) during their menopause showed reduction of monocytes numbers[138]. Taken together, these reports indicate that estradiol suppresses monocyte function. On the other hand, higher number of monocytes were observed in pregnant women with higher level of estradiol[139–142]. Moreover, evidence suggests that the immune response against viral infection is complicated and varies depending on female sex hormone status during menopause, pregnancy, contraception or receiving HRT[143]. Treatment with high concentration of exogenous E2 in ovariectomized female mice infected with H1N1 influenza virus resulted in reduced morbidity and mortality, and suppressed expression of inflammatory-related biomarkers such as TNF-α and MCP-1[144]. On the other hand, it was shown that elevated estradiol levels are associated with severity (ICU and higher sequential organ failure assessment score (SOFA)) and higher cytokine response (i.e IFN-γ) in SARS-CoV-2 male patients[145].

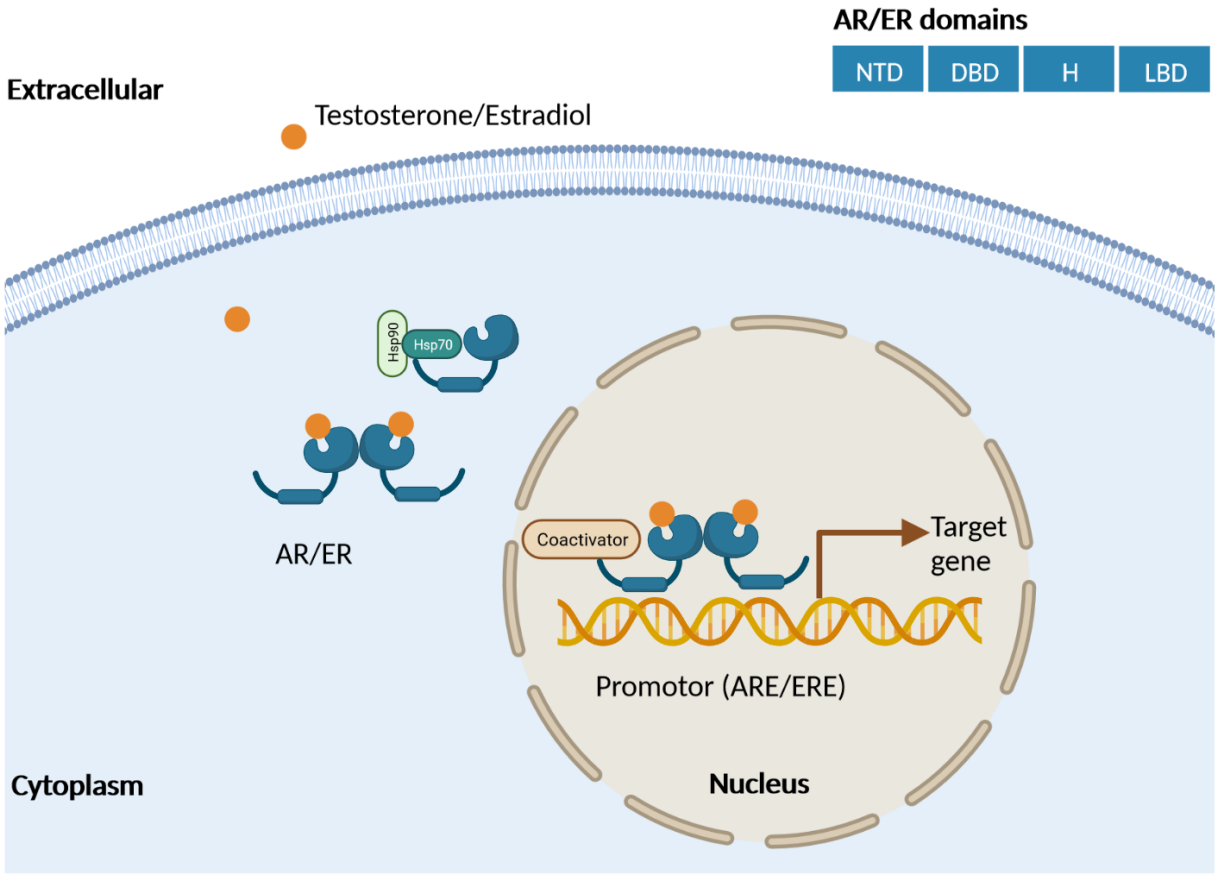

Figure 20. The classic sex hormones and specific receptor-mediated signalling.

A simplified overview of the classic AR or ER (AR/ER)-mediated signalling. The upper right schematic displays the AR/ER domains including NTD, N-terminal domain; DBD, DNA-binding domain; H, Hinge; LBD, Ligand-binding domain. Inactive AR/ER usually binds with heat shock proteins (i.e Hsp70, Hsp90) predominantly distributed in the cytoplasm. Binding free status testosterone or estradiol to the LBD domain of AR/ER triggers the monomers to form a dimer. As followed, this complex is translocated with recruited coactivator proteins to the nucleus where the DBD domain of AR/ER binds to the specific promoter area (ARE/ERE) of target gene to regulate its expression. AR, androgen receptor; ER, estrogen receptor; ARE, androgen receptor elements; ERE, estrogen receptor elements.

Gender differences

Unlike sex that is the biological difference between males and females, gender refers to a sociocultural factor that could shape the different behaviours and practices of both sexes. Chromosomic and sex hormones discussed before are very important factors but could not fully account for the sex differences in incidence, morbidity or mortality of diseases, as the gender difference could be a confounder that needs to be considered.

The disparity social division between men and women resulted in different exposure risk to diseases. For example, females are at higher risk than males for Ebola hemorrhagic fever that is likely due to women are more frequently involved in caretaking and therefore are at increased risk of being exposed to Ebola virus from Ebola hemorrhagic fever patients[146].

The different health behaviours such as health-seeking behaviours could explain the different susceptibility or severity in diseases of both sexes[147]. Some studies revealed that women are more often to seek healthcare facilities than men in developed countries[148,149]. However, specific infectious diseases in women are likely to be underestimated due to less utilization of the healthcare sector in developed countries. For instance, there are more men seeking public healthcare for tuberculosis (TB) diagnosis in some Asian countries as women were more influenced by the stigma and fear of social consequences[150]. The differential healthcare seeking or access behaviour leading to biased surveillance or detection in H7N9 infected men was also discussed in WHO[79]. However, due to high awareness of H7N9 infections and widely distributed influenza surveillance network in China, it is less likely that men always sought to care for ILI more frequently than women did during the five waves of H7N9 epidemics.

Lifestyles and comorbidities could influence disease susceptibility and severity[147]. For example, smoking is commonly believed as a risk factor for infectious lung diseases. The risk towards to progression of pulmonary TB is higher in men, whereas the ratio was reduced when smokers were excluded[151]. Smoking could also be a gender factor to COVID-19 infection and severity as it is related to higher expression of the ACE2 receptor[152,153]. Unhealthy lifestyle could be one of the factors that causes obesity. During the pandemic of COVID-19, patients with obesity defined by a body mass index (BMI) of greater than or equal to 30 were associated with more often being admitted to ICU and fatal outcome[154]. Due to the limitation of data, access to the underlying comorbidities or lifestyle habits of included H7N9 study subjects is not available. However, it might be a confounder when we perform the biological sex difference analysis in male-biased H7N9 infection as coexisting conditions and smoking habit have been reported from H7N9 patients[155].

10.2 The role of sex hormones in male-biased H7N9 infection

The study observed significantly reduced levels of total and bioavailable free testosterone in both young and older H7N9-infected male patients compared to H7N9-negative healthy controls. The lower total testosterone levels in H7N9 male cases was detected from fatal individuals aged 18-49 yrs indicating low testosterone is associated with disease severity. Likewise, the study also observed the association from hospitalized seasonal H1N1/H3N2 influenza-infected men although the overall degree of testosterone reduction was less than H7N9-infected male patients. However, the study could not observe any significant alteration of androgens in H7N9 or seasonal influenza infected-female patients. For estradiol, although it was significantly induced in H7N9-infected female patients at post reproductive stage, the study could not observe its association with death that might be due to the small sample size. Additional evidence supported the causal relationship between H7N9 infection and testosterone depletion by utilizing a murine model in this study. Therefore, the study hypothesized that the infection in general could influence the dysregulation of testosterone levels particularly in males during the course of influenza or other viral infections. Indeed, low testosterone levels were also detected in severe male individuals diagnosed with SARS-CoV-2 infections and was regarded as an indicator for organ failure and poor prognosis in men[14537,156–162]. Besides low testosterone, the increased estradiol levels were observed to have a correlation to disease severity in male patients with COVID-19 as well[145]. However, study did not observe this finding in H7N9 male cases although there might be a tendency for increased estradiol levels in patients who succumbed to the infection.

Since the testosterone is more likely an immunosuppresive transcription factor, lower androgen activity in male-biased H7N9 infection might increase the risk of aggressive releasement of inflammatory cytokines and chemokines, which is associated with disease severity and unfavourable prognosis. Indeed, the study found low testosterone to be negatively associated with several excessively expressed inflammatory markers in men including IL-6, IL-10, IL-15, IL-1RA and IL-1α. Among these markers, the negative association with IL-6 has been observed in men of both ages in this study. This is particularly important as excessive IL-6 and its association with immunopathology was observed in many viral infections including COVID-19[163,164]. Furthermore, the IL-15 that has been reported to be relevant to immunopathology caused by influenza infections, showed the strongest association with low testosterone levels in the linear regression model. It has been shown that IL-15 can partially contribute to the exacerbation of lung damage in influenza virus infected mice by regulating viral specific $CD8^+$ T cell response[165]. IL-15 also influences the proliferation and maintenance of NK cells. The knockout of IL-15 can protect mice from lethal influenza infection which

associated the absence of NK cells that significantly augment pulmonary inflammation in mice[166].

10.3 Testicular infection caused by other viral infections

A number of viruses have been detected in the male genital tract (particularly the testis) and semen which can possibly alter the reproductive and endocrine systems, and allows for sexual transmission[167,168]. In general, viral spreading to the reproductive tract may occur by crossing the blood-testes/epididymis barriers and causing direct damage on target organs or indirect harmful effects via systemic or local pro-inflammatory cytokines and chemokines [169,170]. Viruses may persist long in testes even without effective replication as this organ is immunologically privileged[171]. Many of these viruses can cause chronic or latent infections like human immunodeficiency virus (HIV) and hepatitis B virus (HBV). However, viruses that cause acute infections were also able to effect the genital tract and therefore induce male reproductive illness. In **Table 7**, re-emerging and emerging virus pathogens of public concern that can affect the reproductive health in men are summarized. Due to the scope of this study, discussions as followed focus on emerging viruses that can cause acute and respiratory infections.

The outbreaks of Zika virus (ZIKV), which are mediated by mosquitoes and have been detected in over 80 countries, are considered a global threat to public health[172]. Importantly, it can cause systematic infection as evident by replicative virus which was detected in majority of organs including testes in a murine model for ZIKV infection[173,174]. On the other hand, persistent secretion of virus in semen indicated the potential long-term reproductive deficiency in humans **(Table 7)**.

The current emergence of monkeypox virus infections worldwide since May 2022[175], particularly identified in non-epidemic regions, has raised the public concerns about the transmission and possible impact to human health including risk to infertility. As of 13 March 2023, there were 86,516 laboratory-confirmed cases, including 111 deaths reported from 110 countries across all WHO regions[176]. Repeated and prolonged detection of monkeypox viruses has been reported from different studies **(Table 7)**. Although majority of cases were from those men who have sex with men (MSM) that might be already infertility before exposure to monkeypox virus, available findings could not directly support whether the infection can potentially impair fertility in men. However, the possibility cannot be ignored as the presence of viruses in semen showed association with male reproductive health in other viral infections[168].

The current pandemic of COVID-19 resulting from SARS-CoV-2 virus showed that males have higher risk of being hospitalized, admitted to intensive care unit (ICU) and die from the infection than females[177–180]. These findings raised the concerns of its impact to male reproductive health and fertility. In fact, a previous study on the pathological alteration in testes from fatal cases infected with SARS coronavirus has already indicated that orchitis is a complication in male SARS patients[181]. It will not be a surprise if SARS-CoV-2, which is about 79.5% similar to SARS coronavirus, can also cause testicular infection. A systematic review and meta-analysis evaluated the effect of SARS-CoV-2 on male reproductive physiology and fertility from 25 eligible studies[182]. It found that although the evidence of viral presence in semen was limited, the infection could cause orchitis, alter seminal parameters and hypogonadism, and induce severe histology changes in testes from fatal cases that might due to the local inflammatory response **(Table 7)**. Therefore, the possible adverse effects of COVID-19 infections on male reproductive function and fertility should be considered and further long-term evaluation is required.

Studies on the effects of influenza virus on male reproductive health is scarce. However, potential impacts should not be ignored as alteration in sperm have been documented in humans with influenza virus infections[183]. Furthermore, HPAI H5N1 influenza viruses, which can cause systematic infection, have been detected in the testes of infected poultry **(Table 7)**. For the first time to my knowledge, this study confirms the existence of both 'human' and 'avian' influenza virus receptors in Leydig cells and the replication of seasonal and avian influenza viruses in these cells. Furthermore, viral RNA was also detected from the testes of mice that infected with H7N9 avian influenza virus. Although the presence of viral RNA could not resulted in abnormal testis histology, upregulated testicular cytokines and chemokines were detected. These findings furtherly suggested systematic and/or local inflammatory response induced by H7N9 infection, which could hit the HPG axis and it's underlying, effect on male reproductive health cannot be excluded. Hence, further investigation on the effect of influenza virus infection to reproductive health in men is required.

Table 7. Summary of main viral infections of public concerns that can effect male reproductive health.

	Virus	Family	Genus	Genome	Effect on male reproductive health (Semen+)*	Refer -ence
Non-respiratory disease[#]	EBOV	Filoviridae	Ebolavirus	ssRNA (−)	The testes as an anatomical site for long-term persistence (+)	184–186
	Human CMV	Herpesviridae	Herpesvirales	dsDNA	Sperm parameter alteration and infertility (+)	187,188
	HBV	Hepadnaviridae	Orthohepadnavirus	dsDNA (RT)	Sperm parameter alteration and infertility (+)	189–191
	HCV	Flaviviridae	Hepacivirus	ssRNA (+)	Sperm parameter alteration and infertility (+)	192–196
	HSV	Herpesviridae	Simplexvirus	dsDNA	Inflammation of the prostate, epididymis, impaired fertility, and changes in sperm parameters	187,188, 197
	HIV	Retroviridae	Lentivirus	ssRNA (RT)	Orchitis, “Sertoli-cell only” syndrome, and infertility (+)	188,198 –201
	HPV	Papillomaviridae	Alpha-, beta-, gamma-papillomavirus	dsDNA	Subfertility and infertility (+)	202–204
	Monkeypox	Poxviridae	Orthopoxvirus	dsDNA	Persistent seminal viral shedding (+)	205–209
	ZIKV	Flaviviridae	Flavivirus	ssRNA (+)	Orchitis, epididymo-orchitis, and infertility in mouse models. Persistent seminal viral shedding and sperm parameter alteration in men (+)	173,174, 210–214
Respiratory disease	Influenza virus	Orthomyxoviridae	Influenza virus	ssRNA (−)	Sperm parameter alteration, replication in testes from birds (H5N1)	183,215, 216
	Mumps virus	Paramyxoviridae	Rubulavirus	ssRNA (−)	Epididymo-orchitis and infertility (+)	217,218
	SARS-CoV	Coronaviridae	Betacoronavirus	ssRNA (+)	Orchitis	181
	SARS-CoV-2	Coronaviridae	Betacoronavirus	ssRNA (+)	Orchitis, Sperm parameter alteration (+)	182,219, 220

#: Although some viruses can be transmitted through respiratory droplet, the main transmission route is through direct contact, sexual transmission or vector-borne infection.*: Identified in semen

EBOV: Ebola virus; Human CMV: Human cytomegalovirus; HBV: hepatitis B virus; HCV: hepatitis C virus; HSV: herpes simplex virus; HIV: human immunodeficiency virus; HPV: human papillomavirus; ZIKV: Zika virus;

SARS-CoV: severe acute respiratory syndrome-associated-coronavirus; SARS-CoV-2: severe acute respiratory syndrome-associated-coronavirus type 2; ssRNA (-): negative-sense, single-stranded RNA viruses; ssRNA (+): positive-sense, single-stranded RNA viruses; dsDNA: double-stranded DNA viruses; dsDNA (RT): double-stranded DNA reverse-transcribing viruses; ssRNA (RT): single-stranded DNA reverse-transcribing viruses. (adapted from[198])

10.4 Prospect of the individualized patient treatment

Given increasing evidences from this and other studies that suggest an association of dysregulated sex hormone levels and severity outcomes during the course of infections such as influenza and SARS-CoV-2, it is important to take into account sex and sex hormones into the individualized patient treatment.

Monitoring the levels of sex hormones is recommended. The importance of low testosterone alone or low testosterone with high estradiol as a predict marker of severe disease outcomes particularly in males infected with influenza and SARS-CoV-2 viruses is clear[87,153,157]. On the other hand, a modelling study for the contribution of testosterone to the during of hospitalization of COVID-19 revealed that individuals with higher levels of testosterone at hospital admission have a shorter duration of virus clearance[221]. Therefore, screening of testosterone and extradiol levels of infected patients during the hospital admission and discharge should be part of a routine clinical strategy to identify the risk of poor prognosis that leads to ICU and mortality.

Critical design and patient selection should be considered when performing treatment on the sex hormones and specific receptors-mediated pathway. The levels of sex hormones should be considered as it may play a double-edged role during the course of infection. As there are considerable studies or clinical trials targeting the pathway of testosterone and AR-mediated pathway for COVID-19 patients and low testosterone is also the main hallmark for the male-biased H7N9 infections[222], we will focus on testosterone related individualized treatment by taking COVID-19 patients as an example **(Figure 21)**. For individuals with asymptomatic or mild illness of SARS-CoV-2 infection, their testosterone levels were found to be high or normal. Given the immunosuppression characteristics of testosterone, the immune response from those patients is relatively low. In order to restore the immune response against the inflammation, treatment on reducing testosterone levels could be considered to reduce the risk of disease development and mortality. For instant, the clinical trial using 5α-reductase inhibitor (5-ARI, Dutasteride) blocking the conversion of testosterone to dihydrotestosterone (DHT) was aimed to explore its protection role against COVID-19 (NCT04446429). On the other hand, for those severely or critically ill COVID-19 individuals or infected patients with hypogonadism, their testosterone levels were supposed to be extremely lower with excessively expressed ‘cytokine storm’. Therefore, testosterone replacement therapy could supposed as an immune response modulator for the treatment.

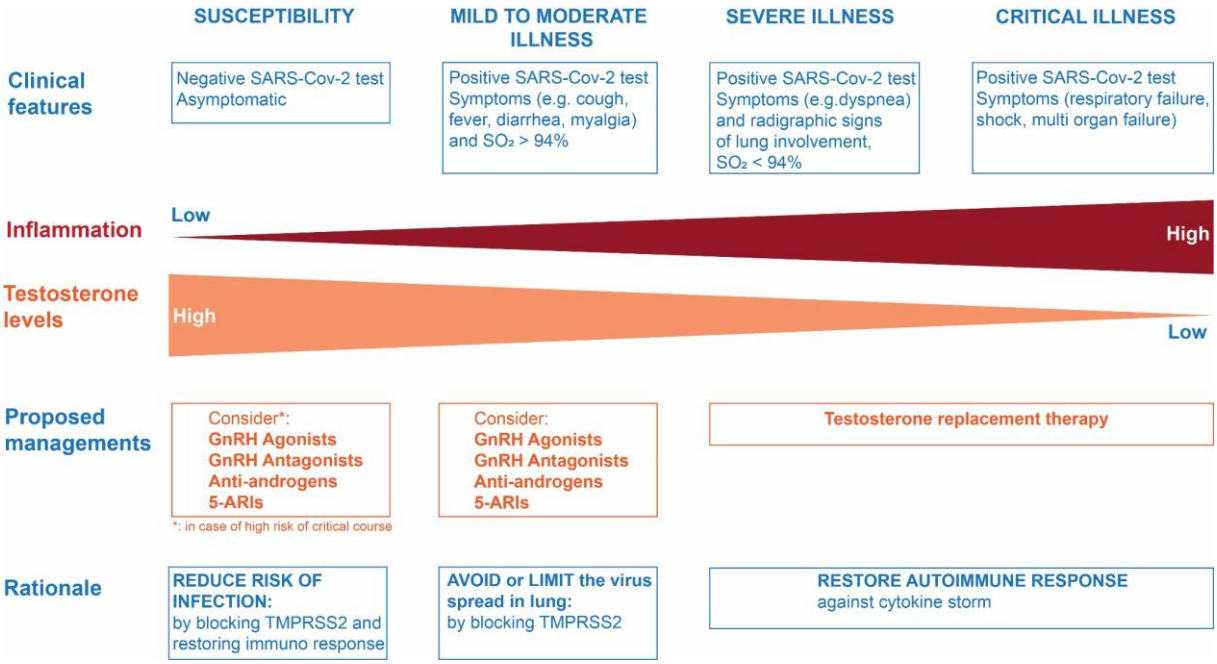

Figure 21. Proposed individualized treatment strategy for SARS-CoV-2 infected patients based on their testosterone levels dynamics and stage of illness.

Shown with an example of proposed personalized treatment of COVID-19 patients in the testosterone and AR-mediated pathway. The treatment considered the levels of testosterone and the stage of disease critically. 5-ARIs, 5α-reductase inhibitors; GnRH, gonadotropin-releasing hormone; SO_2, oxygen saturation; TMPRSS2, transmembrane serine protease 2 (adapted from[223]).

11 Literature

1. Hutchinson, E. C. Influenza Virus. *Trends Microbiol.* **26**, 809–810 (2018).
2. Cheung, T. K. W. & Poon, L. L. M. Biology of influenza a virus. *Ann. N. Y. Acad. Sci.* **1102**, 1–25 (2007).
3. Lener, M. S. Influenza D virus. *Physiol. Behav.* **176**, 139–148 (2016).
4. Wu, Y., Wu, Y., Tefsen, B., Shi, Y. & Gao, G. F. Bat-derived influenza-like viruses H17N10 and H18N11. *Trends Microbiol.* **22**, 183–191 (2014).
5. Tong, S. *et al.* A distinct lineage of influenza A virus from bats. *Proc. Natl. Acad. Sci. U. S. A.* **109**, 4269–4274 (2012).
6. Shaw, M. L. & Palese, P. Orthomyxoviridae. *Fields Virol. 6th ed.* 1151–1185 (2013).
7. Seladi-Schulman, J., Steel, J. & Lowen, A. C. Spherical Influenza Viruses Have a Fitness Advantage in Embryonated Eggs, while Filament-Producing Strains Are Selected In Vivo . *J. Virol.* **87**, 13343–13353 (2013).
8. KILBOURNE, E. D. & MURPHY, J. S. Genetic studies of influenza viruses. I. Viral morphology and growth capacity as exchangeable genetic traits. Rapid in ovo adaptation of early passage Asian strain isolates by combination with PR8. *J. Exp. Med.* **111**, 387–406 (1960).
9. Palese, P. Influenza: Old and new threats. *Nat. Med.* **10**, S82–S87 (2004).
10. Lamb, R. A., Choppin, P. W., Chanock, R. M. & Lai, C. J. Mapping of the two overlapping genes for polypeptides NS1 and NS2 on RNA segment 8 of influenza virus genome. *Proc. Natl. Acad. Sci. U. S. A.* **77**, 1857–1861 (1980).
11. Krammer, F. *et al.* Influenza. *Nat. Rev. Dis. Prim.* **4**, 1–21 (2018).
12. Iwai, A. *et al.* Influenza A virus polymerase inhibits type I interferon induction by binding to interferon β promoter stimulator 1. *J. Biol. Chem.* **285**, 32064–32074 (2010).
13. Yamayoshi, S., Watanabe, M., Goto, H. & Kawaoka, Y. Identification of a Novel Viral Protein Expressed from the PB2 Segment of Influenza A Virus. *J. Virol.* **90**, 444–456 (2016).
14. Pleschka, S. Overview of Influenza virus. *Curr. Top. Microbiol. Immunol.* 1–20 (2013) doi:10.1007/82.
15. Fodor, E. & Velthuis, A. J. W. T. Structure and function of the influenza virus transcription and replication machinery. *Cold Spring Harb. Perspect. Med.* **10**, 1–14 (2020).
16. Zamarin, D., Ortigoza, M. B. & Palese, P. Influenza A Virus PB1-F2 Protein Contributes to Viral Pathogenesis in Mice. *J. Virol.* **80**, 7976–7983 (2006).
17. Varga, Z. T. *et al.* The influenza virus protein PB1-F2 inhibits the induction of type i interferon at the level of the MAVS adaptor protein. *PLoS Pathog.* **7**, (2011).
18. Wise, H. M. *et al.* A Complicated Message: Identification of a Novel PB1-Related Protein

Translated from Influenza A Virus Segment 2 mRNA. *J. Virol.* **83**, 8021–8031 (2009).

19. Tauber, S., Ligertwood, Y., Quigg-Nicol, M., Dutia, B. M. & Elliott, R. M. Behaviour of influenza A viruses differentially expressing segment 2 gene products in vitro and in vivo. *J. Gen. Virol.* **93**, 840–849 (2012).
20. Hu, J. *et al.* PA-X Decreases the Pathogenicity of Highly Pathogenic H5N1 Influenza A Virus in Avian Species by Inhibiting Virus Replication and Host Response. *J. Virol.* **89**, 4126–4142 (2015).
21. Gao, H. *et al.* The contribution of PA-X to the virulence of pandemic 2009 H1N1 and highly pathogenic H5N1 avian influenza viruses. *Sci. Rep.* **5**, 1–11 (2015).
22. Shi, M. *et al.* Evolutionary Conservation of the PA-X Open Reading Frame in Segment 3 of Influenza A Virus. *J. Virol.* **86**, 12411–12413 (2012).
23. Wang, Q. *et al.* Host interaction analysis of PA-N155 and PA-N182 in chicken cells reveals an essential role of UBA52 for replication of H5N1 Avian influenza virus. *Front. Microbiol.* **9**, 1–11 (2018).
24. Muramoto, Y., Noda, T., Kawakami, E., Akkina, R. & Kawaoka, Y. Identification of Novel Influenza A Virus Proteins Translated from PA mRNA. *J. Virol.* **87**, 2455–2462 (2013).
25. Bui, M., Wills, E. G., Helenius, A. & Whittaker, G. R. Role of the Influenza Virus M1 Protein in Nuclear Export of Viral Ribonucleoproteins. *J. Virol.* **74**, 1781–1786 (2000).
26. Pinto, L. H., Holsinger, L. J. & Lamb, R. A. Influenza virus M2 protein has ion channel activity. *Cell* **69**, 517–528 (1992).
27. Wise, H. M. *et al.* Identification of a Novel Splice Variant Form of the Influenza A Virus M2 Ion Channel with an Antigenically Distinct Ectodomain. *PLoS Pathog.* **8**, (2012).
28. Ayllon, J.; Garcia-Sastre, A. *The NS1 protein: A multitasking virulence factor*. *Current Topics in Microbiology and Immunology* vol. 386 (2015).
29. Hale, B. G., Randall, R. E., Ortin, J. & Jackson, D. The multifunctional NS1 protein of influenza A viruses. *J. Gen. Virol.* **89**, 2359–2376 (2008).
30. Pereira, C. F., K.C.Read, E., Wise, H. M., J., A. M. & Digard, P. Influenza A Virus NS1 Protein Promotes Efficient Nuclear Export of Unspliced Viral M1 mRNA. *J. V* **91**, e00528-17 (2017).
31. Neumann, G., Hughes, M. T. & Kawaoka, Y. Influenza A virus NS2 protein mediates vRNP nuclear export through NES-independent interaction with hCRM1. *EMBO J.* **19**, 6751–6758 (2000).
32. Yasuda, J., Nakada, S., Kato, A., Toyoda, T. & Ishihama, A. Molecular assembly of influenza virus: Association of the ns2 protein with virion matrix. *Virology* vol. 196 249–255 (1993).
33. O'Neill, R. E., Talon, J. & Palese, P. The influenza virus NEP (NS2 protein) mediates the nuclear export of viral ribonucleoproteins. *EMBO J.* **17**, 288–296 (1998).

34. Robb, N. C., Smith, M., Vreede, F. T. & Fodor, E. NS2/NEP protein regulates transcription and replication of the influenza virus RNA genome. *J. Gen. Virol.* **90**, 1398–1407 (2009).
35. Selman, M., Dankar, S. K., Forbes, N. E., Jia, J. J. & Brown, E. G. Adaptive mutation in influenza A virus non-structural gene is linked to host switching and induces a novel protein by alternative splicing. *Emerg. Microbes Infect.* **1**, 0 (2012).
36. Walther, T. *et al.* Glycomic Analysis of Human Respiratory Tract Tissues and Correlation with Influenza Virus Infection. *PLoS Pathog.* **9**, (2013).
37. Matrosovich, M. *et al.* Early Alterations of the Receptor-Binding Properties of H1, H2, and H3 Avian Influenza Virus Hemagglutinins after Their Introduction into Mammals. *J. Virol.* **74**, 8502–8512 (2000).
38. Pinto, L. H. & Lamb, R. A. The M2 proton channels of influenza A and B viruses. *J. Biol. Chem.* **281**, 8997–9000 (2006).
39. White, J., Helenius, A. & Gething, M. J. Haemagglutinin of influenza virus expressed from a cloned gene promotes membrane fusion. *Nature* vol. 300 658–659 (1982).
40. Yoshimura, A. & Ohnishi, S. Uncoating of influenza virus in endosomes. *J. Virol.* **51**, 497–504 (1984).
41. Bullough, P. A., Hughson, F. M., Skehel, J. J. & Wiley, D. C. Structure of influenza HA at the pH of membrane fusion. *Nature* **371**, 37–43 (1994).
42. York, A., Hengrung, N., Vreede, F. T., Huiskonen, J. T. & Fodor, E. Isolation and characterization of the positive-sense replicative intermediate of a negative-strand RNA virus. *Proc. Natl. Acad. Sci. U. S. A.* **110**, 1–8 (2013).
43. Newcomb, L. L. *et al.* Interaction of the Influenza A Virus Nucleocapsid Protein with the Viral RNA Polymerase Potentiates Unprimed Viral RNA Replication. *J. Virol.* **83**, 29–36 (2009).
44. Dou, D., Revol, R., Östbye, H., Wang, H. & Daniels, R. Influenza A virus cell entry, replication, virion assembly and movement. *Front. Immunol.* **9**, 1–17 (2018).
45. Plotch, S. J., Bouloy, M., Ulmanen, I. & Krug, R. M. A unique cap(m7GpppXm)-dependent influenza virion endonuclease cleaves capped RNAs to generate the primers that initiate viral RNA transcription. *Cell* **23**, 847–858 (1981).
46. Guilligay, D. *et al.* The structural basis for cap binding by influenza virus polymerase subunit PB2. *Nat. Struct. Mol. Biol.* **15**, 500–506 (2008).
47. Dias, A. *et al.* The cap-snatching endonuclease of influenza virus polymerase resides in the PA subunit. *Nature* **458**, 914–918 (2009).
48. Robertson, J. S., Schubert, M. & Lazzarini, R. A. Polyadenylation sites for influenza virus mRNA. *J. Virol.* **38**, 157–163 (1981).
49. Poon, L. L. M., Pritlove, D. C., Fodor, E. & Brownlee, G. G. Direct Evidence that the

Poly(A) Tail of Influenza A Virus mRNA Is Synthesized by Reiterative Copying of a U Track in the Virion RNA Template. *J. Virol.* **73**, 3473–3476 (1999).

50. Satterly, N. *et al.* Influenza virus targets the mRNA export machinery and the nuclear pore complex. *Proc. Natl. Acad. Sci. U. S. A.* **104**, 1853–1858 (2007).
51. Shimizu, T., Takizawa, N., Watanabe, K., Nagata, K. & Kobayashi, N. Crucial role of the influenza virus NS2 (NEP) C-terminal domain in M1 binding and nuclear export of vRNP. *FEBS Lett.* **585**, 41–46 (2011).
52. Amorim, M. J. *et al.* A Rab11- and Microtubule-Dependent Mechanism for Cytoplasmic Transport of Influenza A Virus Viral RNA. *J. Virol.* **85**, 4143–4156 (2011).
53. Stieneke-Grober, A. *et al.* Influenza virus hemagglutinin with multibasic cleavage site is activated by furin, a subtilisin-like endoprotease. *EMBO J.* **11**, 2407–2414 (1992).
54. Compans, R. W. & Oldstone, M. B. A. *Influenza Pathogenesis and Control - Volume I*. *Current Topics in Microbiology and Immunology* vol. 385 (2014).
55. Webster, R. G. & Laver, W. G. Preparation and properties of antibody directed specifically against the neuraminidase of influenza virus. *J. Immunol.* **99**, 49–55 (1967).
56. Yang, X. *et al.* A beneficiary role for neuraminidase in influenza virus penetration through the respiratory mucus. *PLoS One* **9**, 1–11 (2014).
57. Cohen, M. *et al.* Influenza A penetrates host mucus by cleaving sialic acids with neuraminidase. *Virol. J.* **10**, 1 (2013).
58. Tong, S. *et al.* New World Bats Harbor Diverse Influenza A Viruses. *PLoS Pathog.* **9**, (2013).
59. Yoon, S. W., Webby, R. J. & Webster, R. G. Evolution and ecology of influenza a viruses. *Curr. Top. Microbiol. Immunol.* **385**, 359–375 (2014).
60. Subbarao, E. K., London, W. & Murphy, B. R. A single amino acid in the PB2 gene of influenza A virus is a determinant of host range. *J. Virol.* **67**, 1761–1764 (1993).
61. Hatta, H., Gao, P., Halfmann, P. & Kawaoka, Y. Molecular basis for high virulence of Hong Kong H5N1 influenza a viruses. *Science (80-.).* **293**, 1840–1842 (2001).
62. Gabriel, G. *et al.* The viral polymerase mediates adaptation of an avian influenza virus to a mammalian host. *Proc. Natl. Acad. Sci. U. S. A.* **102**, 18590–18595 (2005).
63. Joseph, U., Su, Y. C. F., Vijaykrishna, D. & Smith, G. J. D. The ecology and adaptive evolution of influenza A interspecies transmission. *Influenza Other Respi. Viruses* **11**, 74–84 (2017).
64. Claas, E. C. J. *et al.* Human influenza A H5N1 virus related to a highly pathogenic avian influenza virus. *Lancet* **351**, 472–477 (1998).
65. World Health Organization. Cumulative number of confirmed human cases for avian influenza A(H5N1) reported to WHO, 2003-2023, 5 January 2023. (2023).
66. Wang, D., Zhu, W., Yang, L. & Shu, Y. The epidemiology, virology, and pathogenicity of

human infections with avian influenza viruses. *Cold Spring Harb. Perspect. Med.* **11**, (2021).

67. Gao, R. *et al.* Human Infection with a Novel Avian-Origin Influenza A (H7N9) Virus. *N. Engl. J. Med.* **368**, 1888–1897 (2013).
68. CDC. Summary of Influenza Risk Assessment Tool (IRAT) Results. (2020).
69. Wang, X. *et al.* Epidemiology of avian influenza A H7N9 virus in human beings across five epidemics in mainland China, 2013–17: an epidemiological study of laboratory-confirmed case series. *Lancet Infect. Dis.* **17**, 822–832 (2017).
70. Yu, H. *et al.* Effect of closure of live poultry markets on poultry-to-person transmission of avian influenza A H7N9 virus: An ecological study. *Lancet* **383**, 541–548 (2014).
71. Cowling, B. J. *et al.* Comparative epidemiology of human infections with avian influenza A H7N9 and H5N1 viruses in China: A population-based study of laboratory-confirmed cases. *Lancet* **382**, 129–137 (2013).
72. Zhou, L. *et al.* Sudden increase in human infection with avian influenza A(H7N9) virus in China, September-December 2016. *West. Pacific Surveill. response J. WPSAR* **8**, 6–14 (2017).
73. Ke, C. *et al.* Human infection with highly pathogenic avian influenza a(H7N9) virus, China. *Emerg. Infect. Dis.* **23**, 1332–1340 (2017).
74. Zhang, F. *et al.* Human infections with recently-emerging highly pathogenic H7N9 avian influenza virus in China. *Journal of Infection* vol. 75 71–75 (2017).
75. Qi, W. *et al.* Emergence and Adaptation of a Novel Highly Pathogenic H7N9 Influenza Virus in Birds and Humans from a 2013 Human-Infecting Low-Pathogenic Ancestor. *J. Virol.* 1–12 (2018).
76. Tanner, W. D., Toth, D. J. A. & Gundlapalli, A. V. The pandemic potential of avian influenza A(H7N9) virus: A review. *Epidemiology and Infection* vol. 143 3359–3374 (2015).
77. Food and Agriculture Organization. H7N9 situation update (2021). (2021).
78. Wang, X. *et al.* Assessment of human-to-human transmissibility of avian influenza A(H7N9) virus across 5 waves by analyzing clusters of case patients in Mainland China, 2013-2017. *Clin. Infect. Dis.* **68**, 623–631 (2019).
79. Arima, Y., Zu, R., Murhekar, M., Vong, S. & Shimada, T. Human infections with avian influenza A(H7N9) virus in China: preliminary assessments of the age and sex distribution. *West. Pacific Surveill. response J. WPSAR* **4**, 9–11 (2013).
80. Li, Q. *et al.* Epidemiology of human infections with avian influenza A(H7N9) virus in China. *N. Engl. J. Med.* **370**, 520–532 (2014).
81. Rivers, C., Lum, K., Lewis, B. & Eubank, S. Estimating human cases of avian influenza A(H7N9) from poultry exposure. *PLoS Curr.* **5**, 1–12 (2013).

82. Zeng, X. *et al.* Vaccination of poultry successfully eliminated human infection with H7N9 virus in China. *Science China Life Sciences* vol. 61 1465–1473 (2018).
83. Li, C. & Chen, H. H7N9 influenza virus in china. *Cold Spring Harb. Perspect. Med.* **11**, 1–18 (2021).
84. Gabriel, G. *et al.* Differential use of importin-α isoforms governs cell tropism and host adaptation of influenza virus. *Nat. Commun.* **2**, (2011).
85. Gao, R. *et al.* Human infection with a novel avian-origin. *N. Engl. J. Med.* **368**, 1888–1897 (2013).
86. Yu, S. *et al.* Establishing reference intervals for sex hormones and SHBG in apparently healthy Chinese adult men based on a multicenter study. *Clin. Chem. Lab. Med.* **56**, 1152–1160 (2018).
87. Bai, T. *et al.* H7N9 avian in fl uenza virus infection in men is associated with testosterone depletion. *Nat. Commun.* **13**, 1–14 (2022).
88. Yu, H. *et al.* Plasma sex steroid hormones and breast cancer risk in Chinese women. *Int. J. Cancer* **105**, 92–97 (2003).
89. Guo, J. *et al.* The serum profile of hypercytokinemia factors identified in H7N9-infected patients can predict fatal outcomes. *Sci. Rep.* **5**, 1–10 (2015).
90. Zhou, J. *et al.* Biological features of novel avian influenza A (H7N9) virus. *Nature* **499**, 500–503 (2013).
91. Mills, I. G. Maintaining and reprogramming genomic androgen receptor activity in prostate cancer. *Nat. Rev. Cancer* **14**, 187–198 (2014).
92. Chi, Y. *et al.* Cytokine and chemokine levels in patients infected with the novel avian influenza a (H7N9) virus in China. *J. Infect. Dis.* **208**, 1962–1967 (2013).
93. Zhou, J. *et al.* Biological features of novel avian influenza A (H7N9) virus. *Nature* **499**, 500–503 (2013).
94. Hay, M., Kumar, V. & Ricaño-Ponce, I. The role of the X chromosome in infectious diseases. *Brief. Funct. Genomics* **21**, 143–158 (2022).
95. National Center for Biotechnology Information. *Genes (Basel).* (2023).
96. Wise, A. L., Gyi, L. & Manolio, T. A. EXclusion: Toward integrating the X chromosome in genome-wide association analyses. *Am. J. Hum. Genet.* **92**, 643–647 (2013).
97. Libert, C., Dejager, L. & Pinheiro, I. The X chromosome in immune functions: When a chromosome makes the difference. *Nat. Rev. Immunol.* **10**, 594–604 (2010).
98. Migeon, B. R. X-linked diseases: susceptible females. *Genet. Med.* **22**, 1156–1174 (2020).
99. Schurz, H. *et al.* The X chromosome and sex-specific effects in infectious disease susceptibility. *Hum. Genomics* **13**, 2 (2019).
100. Di Palo, A. *et al.* What microRNAs could tell us about the human X chromosome. *Cell.*

Mol. Life Sci. **77**, 4069–4080 (2020).

101. Bianchi, I., Lleo, A., Gershwin, M. E. & Invernizzi, P. The X chromosome and immune associated genes. *J. Autoimmun.* **38**, J187–J192 (2012).
102. Baldwin, J. The transcription factor NF-κB and human disease. *J. Clin. Invest.* **107**, 3–6 (2001).
103. Orange, J. S. *et al.* The presentation and natural history of immunodeficiency caused by nuclear factor κB essential modulator mutation. *J. Allergy Clin. Immunol.* **113**, 725–733 (2004).
104. Orange, J. S., Levy, O. & Geha, R. S. Human disease resulting from gene mutations that interfere with appropriate nuclear factor-κB activation. *Immunol. Rev.* **203**, 21–37 (2005).
105. Orange, J. S. *et al.* Human nuclear factor κb essential modulator mutation can result in immunodeficiency without ectodermal dysplasia. *J. Allergy Clin. Immunol.* **114**, 650–656 (2004).
106. Pang, I. K., Pillai, P. S. & Iwasaki, A. Efficient influenza A virus replication in the respiratory tract requires signals from TLR7 and RIG-I. *Proc. Natl. Acad. Sci. U. S. A.* **110**, 13910–13915 (2013).
107. Stegemann-Koniszewski, S. *et al.* Respiratory influenza A virus infection triggers local and systemic natural killer cell activation via toll-like receptor 7. *Front. Immunol.* **9**, 1–13 (2018).
108. Fallerini, C. *et al.* Association of toll-like receptor 7 variants with life-threatening COVID-19 disease in males: Findings from a nested case-control study. *Elife* **10**, 1–15 (2021).
109. Asano, T. *et al.* X-linked recessive TLR7 deficiency in ~ 1 % of men under 60 years old with life-threatening COVID-19. *Sci. Immunol.* **4348**, 1–31 (2021).
110. Van Der Made, C. I. *et al.* Presence of Genetic Variants among Young Men with Severe COVID-19. *JAMA - J. Am. Med. Assoc.* **324**, 663–673 (2020).
111. Solanich, X. *et al.* Genetic Screening for TLR7 Variants in Young and Previously Healthy Men With Severe COVID-19. *Front. Immunol.* **12**, 1–10 (2021).
112. Klein, S. L. & Flanagan, K. L. Sex differences in immune responses. *Nature Reviews Immunology* (2016) doi:10.1038/nri.2016.90.
113. Ghosh, S. & Klein, R. S. Sex Drives Dimorphic Immune Responses to Viral Infections. *J. Immunol.* **198**, 1782–1790 (2017).
114. Zhao, R. *et al.* A GPR174–CCL21 module imparts sexual dimorphism to humoral immunity. *Nature* **577**, 416–420 (2020).
115. Talebizadeh, Z., Simon, S. D. & Butler, M. G. X chromosome gene expression in human tissues: Male and female comparisons. *Genomics* **88**, 675–681 (2006).
116. Fang, H., Disteche, C. M. & Berletch, J. B. X Inactivation and Escape: Epigenetic and

Structural Features. *Front. Cell Dev. Biol.* **7**, 1–12 (2019).

117. Cheng, M. I. *et al.* The X-linked epigenetic regulator UTX controls NK cell-intrinsic sex differences. *Nat. Immunol.* (2023) doi:10.1038/s41590-023-01463-8.
118. Gilliver, S. C. Sex steroids as inflammatory regulators. *J. Steroid Biochem. Mol. Biol.* **120**, 105–115 (2010).
119. Klein, S. L. & Roberts, C. W. *Sex hormones and immunity to infection*. *Sex Hormones and Immunity to Infection* (2010). doi:10.1007/978-3-642-02155-8.
120. Lubahn, D. B. *et al.* Cloning of Human Androgen Rector Complentry. *Science (80-.).* **240**, 327–330 (2014).
121. Mosselman, S., Polman, J. & Dijkema, R. ERβ: Identification and characterization of a novel human estrogen receptor. *FEBS Lett.* **392**, 49–53 (1996).
122. Kuiper, G. G. J. M., Enmark, E., Pelto-Huikko, M., Nilsson, S. & Gustafsson, J. Å. Cloning of a novel estrogen receptor expressed in rat prostate and ovary. *Proc. Natl. Acad. Sci. U. S. A.* **93**, 5925–5930 (1996).
123. Mangelsdorf, D. J. *et al.* The nuclear receptor superfamily: The second decade. *Cell* **83**, 835–839 (1995).
124. Beato, M., Herrlich, P. & Schütz, G. Steroid hormone receptors: Many Actors in search of a plot. *Cell* **83**, 851–857 (1995).
125. Jin, H. *et al.* Testosterone alleviates tumor necrosis factor-alpha-mediated tissue factor pathway inhibitor downregulation via suppression of nuclear factor-kappa B in endothelial cells. *Asian J. Androl.* **11**, 266–271 (2009).
126. Vignozzi, L. *et al.* Antiinflammatory effect of androgen receptor activation in human benign prostatic hyperplasia cells. *J. Endocrinol.* **214**, 31–43 (2012).
127. Chen, C. W. *et al.* Role of testosterone in regulating induction of TNF-α in rat spleen via ERK signaling pathway. *Steroids* **111**, 148–154 (2016).
128. Vom Steeg, L. G. *et al.* Age and testosterone mediate influenza pathogenesis in male mice. *Am. J. Physiol. - Lung Cell. Mol. Physiol.* **311**, L1234–L1244 (2016).
129. Tuku, B. *et al.* Testosterone Protects Against Severe Influenza by Reducing the Pro-Inflammatory Cytokine Response in the Murine Lung. *Front. Immunol.* **11**, 1–7 (2020).
130. Burney, B. O. *et al.* Low testosterone levels and increased inflammatory markers in patients with cancer and relationship with cachexia. *J. Clin. Endocrinol. Metab.* **97**, 700–709 (2012).
131. Tremellen, K., McPhee, N. & Pearce, K. Metabolic endotoxaemia related inflammation is associated with hypogonadism in overweight men. *Basic Clin. Androl.* **27**, 1–9 (2017).
132. Ng, M. K. C. *et al.* Prospective study of effect of androgens on serum inflammatory markers in men. *Arterioscler. Thromb. Vasc. Biol.* **22**, 1136–1141 (2002).
133. Kupelian, V. *et al.* Association of sex hormones and C-reactive protein levels in men.

Clin. Endocrinol. (Oxf). **72**, 527–533 (2010).

134. Phiel, K. L., Henderson, R. A., Adelman, S. J. & Elloso, M. M. Differential estrogen receptor gene expression in human peripheral blood mononuclear cell populations. *Immunol. Lett.* **97**, 107–113 (2005).
135. Kovats, S. Estrogen receptors regulate innate immune cells and signaling pathways. *Cell. Immunol.* **294**, 63–69 (2015).
136. Bouman, A., Jan Heineman, M. & Faas, M. M. Sex hormones and the immune response in humans. *Hum. Reprod. Update* **11**, 411–423 (2005).
137. Bouman, A., Schipper, M., Heineman, M. J. & Faas, M. M. Gender difference in the non-specific and specific immune response in humans. *Am. J. Reprod. Immunol.* **52**, 19–26 (2004).
138. Ben Hur H, Mor G, Insler V, Blickstein I, Amir-Zaltsman Y, Sharp A, G. A. and K. F. Menopause is associated with a sig- nificant increase in blood monocyte number and a relative decrease in the expression of estrogen receptors in human peripheral monocytes. *Am J Reprod Immunol* **34**, 363–369 (1995).
139. Mathur, S., Mathur, R. S., Goust, J. M., Williamson, H. O. & Fudenberg, H. H. Cyclic variations in white cell subpopulations in the human menstrual cycle: Correlations with progesterone and estradiol. *Clin. Immunol. Immunopathol.* **13**, 246–253 (1979).
140. Bouman, A., Moes, H., Heineman, M. J., De Leij, L. F. M. H. & Faas, M. M. The immune response during the luteal phase of the ovarian cycle: Increasing sensitivity of human monocytes to endotoxin. *Fertil. Steril.* **76**, 555–559 (2001).
141. Elenkov, I. J. *et al.* IL-12, TNF-α, and hormonal changes during late pregnancy and early postpartum: Implications for autoimmune disease activity during these times. *J. Clin. Endocrinol. Metab.* **86**, 4933–4938 (2001).
142. Baum, M. Variations in Leucocyte Count During Menstrual Cycle. *Br. Med. J.* **3**, 102 (1975).
143. S.L., K. In Sex and gender differences in pharmacology (ed Regitz-Zagrosek,V.). *Springer* (2012).
144. Robinson, D. P., Lorenzo, M. E., Jian, W. & Klein, S. L. Elevated 17β-estradiol protects females from influenza a virus pathogenesis by suppressing inflammatory responses. *PLoS Pathog.* **7**, (2011).
145. Schroeder, M. *et al.* High estradiol and low testosterone levels are associated with critical illness in male but not in female COVID-19 patients: a retrospective cohort study. *Emerg. Microbes Infect.* **10**, 1807–1818 (2021).
146. McElroy, A. K. *et al.* Ebola hemorrhagic fever: Novel biomarker correlates of clinical outcome. *J. Infect. Dis.* **210**, 558–566 (2014).
147. Gay, L. *et al.* Sexual Dimorphism and Gender in Infectious Diseases. *Front. Immunol.*

12, 1–16 (2021).

148. Verbrugge, L. M. The twain meet: Empirical explanations of sex differences in health and mortality. *J. Health Soc. Behav.* **30**, 282–304 (1989).
149. Kandrack, M. A., Grant, K. R. & Segall, A. Gender differences in health related behaviour: Some unanswered questions. *Soc. Sci. Med.* **32**, 579–590 (1991).
150. Weiss, M. *et al.* Gender and tuberculosis : Cross-site analysis and implications of a multi-country study in Bangladesh , India , Malawi,. *Monogr. Geneva,* 2–100 (2006).
151. Balasubramanian, R. *et al.* Gender disparities in tuberculosis: Report from a rural DOTS programme in south India. *Int. J. Tuberc. Lung Dis.* **8**, 323–332 (2004).
152. Cai, H. Sex difference and smoking predisposition in patients with COVID-19. *Lancet Respir. Med.* **8**, e20 (2020).
153. Guan, W. *et al.* Clinical Characteristics of Coronavirus Disease 2019 in China. *N. Engl. J. Med.* **382**, 1708–1720 (2020).
154. Ambrosino, I. *et al.* Gender differences in patients with COVID-19: A narrative review. *Monaldi Arch. Chest Dis.* **90**, 318–324 (2020).
155. Gao, H. N. *et al.* Clinical findings in 111 cases of influenza A (H7N9) virus infection. *N. Engl. J. Med.* **368**, 2277–2285 (2013).
156. Alexander, D. J. A review of avian influenza in different bird species. *Vet. Microbiol.* **74**, 3–13 (2000).
157. Rowland, S. P. & O'Brien Bergin, E. Screening for low testosterone is needed for early identification and treatment of men at high risk of mortality from Covid-19. *Crit. Care* **24**, 4–5 (2020).
158. Dhindsa, S. *et al.* Association of circulating sex hormones with inflammation and disease severity in patients with COVID-19. *JAMA Netw. Open* 1–15 (2021) doi:10.1001/jamanetworkopen.2021.11398.
159. Van Zeggeren, I. E. *et al.* Sex steroid hormones are associated with mortality in COVID-19 patients: Level of sex hormones in severe COVID-19. *Med. (United States)* **100**, E27072 (2021).
160. Camici, M. *et al.* Role of testosterone in SARS-CoV-2 infection: A key pathogenic factor and a biomarker for severe pneumonia. *Int. J. Infect. Dis.* **108**, 244–251 (2021).
161. Pagano, M. T. *et al.* Predicting respiratory failure in patients infected by SARS-CoV-2 by admission sex-specific biomarkers. *Biol. Sex Differ.* **12**, 1–12 (2021).
162. Rastrelli, G. *et al.* Low testosterone levels predict clinical adverse outcomes in SARS-CoV-2 pneumonia patients. *Andrology* **9**, 88–98 (2021).
163. Tay, M. Z., Poh, C. M., Rénia, L., Macary, P. A. & Ng, L. F. P. The trinity of COVID-19: immunity, inflammation and intervention. *Nat. Rev. Immunol.* (2020) doi:10.1038/s41577-020-0311-8.

164. Gubernatorova, E. O., Gorshkova, E. A., Polinova, A. I. & Drutskaya, M. S. IL-6: Relevance for immunopathology of SARS-CoV-2. *Cytokine Growth Factor Rev.* **53**, 13–24 (2020).
165. Nakamura, R. *et al.* Interleukin-15 Is Critical in the Pathogenesis of Influenza A Virus-Induced Acute Lung Injury. *J. Virol.* **84**, 5574–5582 (2010).
166. Abdul-Careem, M. F. *et al.* Critical role of natural killer cells in lung immunopathology during influenza infection in mice. *J. Infect. Dis.* **206**, 167–177 (2012).
167. Dejucq, N. & Jégou, B. Viruses in the Mammalian Male Genital Tract and Their Effects on the Reproductive System. *Microbiol. Mol. Biol. Rev.* **65**, 208–231 (2001).
168. Salam, A. P. & Horby, P. W. The breadth of viruses in human semen. *Emerg. Infect. Dis.* **23**, 1922–1924 (2017).
169. Guazzone, V. A., Jacobo, P., Theas, M. S. & Lustig, L. Cytokines and chemokines in testicular inflammation: A brief review. *Microsc. Res. Tech.* **72**, 620–628 (2009).
170. Bhushan, S., Schuppe, H. C., Fijak, M. & Meinhardt, A. Testicular infection: microorganisms, clinical implications and host-pathogen interaction. *J. Reprod. Immunol.* **83**, 164–167 (2009).
171. Li, N., Wang, T. & Han, D. Structural, cellular and molecular aspects of immune privilege in the testis. *Front. Immunol.* **3**, 1–12 (2012).
172. Dahiya, N., Yadav, M., Singh, H., Jakhar, R. & Sehrawat, N. ZIKV: Epidemiology, infection mechanism and current therapeutics. *Front. Trop. Dis.* **3**, (2023).
173. Rossi, S. L. *et al.* Characterization of a novel murine model to study zika virus. *Am. J. Trop. Med. Hyg.* **94**, 1362–1369 (2016).
174. Lazear, H. M. *et al.* A Mouse Model of Zika Virus Pathogenesis. *Cell Host Microbe* **19**, 720–730 (2016).
175. Mitjà, O. *et al.* Monkeypox. *Lancet* **401**, 60–74 (2023).
176. World Health Organization. 2022-23 Mpox (Monkeypox) Outbreak:Global Trends. (2023).
177. Team NCPERE. Vital Surveillances; The Epidemiological Characteristics Of An Outbreak Of 2019 Novel Coronavirus Disease (COVID-19). *China CDC Wkly.* **2**, 113–122 (2020).
178. Salje, H. *et al.* Estimating the burden of SARS-CoV-2 in France. *Science (80-.).* **369**, 208–211 (2020).
179. Jin, J.-M. *et al.* Gender differences in patients with COVID-19: Focus on severity and mortality. *Front. Public Heal.* **8**, (2020).
180. Peckham, H. *et al.* Male sex identified by global COVID-19 meta-analysis as a risk factor for death and ITU admission. *Nat. Commun.* **11**, 1–10 (2020).
181. Xu, J. *et al.* Orchitis: A complication of severe acute respiratory syndrome (SARS). *Biol.*

Reprod. **74**, 410–416 (2006).

182. Sengupta, P., Leisegang, K. & Agarwal, A. The impact of COVID-19 on the male reproductive tract and fertility: A systematic review. *Arab J. Urol.* **19**, 423–436 (2021).
183. Sergerie, M., Mieusset, R., Croute, F., Daudin, M. & Bujan, L. High risk of temporary alteration of semen parameters after recent acute febrile illness. *Fertil. Steril.* **88**, 970.e1-970.e7 (2007).
184. Nicastri, E. *et al.* Ebola Virus Disease: Epidemiology, Clinical Features, Management, and Prevention. *Infect. Dis. Clin. North Am.* **33**, 953–976 (2019).
185. Martines, R. B., Ng, D. L., Greer, P. W., Rollin, P. E. & Zaki, S. R. Tissue and cellular tropism, pathology and pathogenesis of Ebola and Marburg viruses. *J. Pathol.* **235**, 153–174 (2015).
186. The PREVAIL III Study Group. A Longitudinal Study of Ebola Sequelae in Liberia. *N. Engl. J. Med.* **380**, 924–934 (2019).
187. Bezold, G. *et al.* Prevalence of sexually transmissible pathogens in semen from asymptomatic male infertility patients with and without leukocytospermia. *Fertil. Steril.* **87**, 1087–1097 (2007).
188. Gimenes, F. *et al.* Male infertility: A public health issue caused by sexually transmitted pathogens. *Nat. Rev. Urol.* **11**, 672–687 (2014).
189. Moretti, E., Federico, M. G., Giannerini, V. & Collodel, G. Sperm ultrastructure and meiotic segregation in a group of patients with chronic hepatitis B and C. *Andrologia* **40**, 286–291 (2008).
190. Su, F. H. *et al.* Hepatitis B virus infection and the risk of male infertility: A population-based analysis. *Fertil. Steril.* **102**, 1677–1684 (2014).
191. Kang, X. J. *et al.* Effects of hepatitis B virus S protein exposure on sperm membrane integrity and functions. *PLoS One* **7**, (2012).
192. Lorusso, F. *et al.* Impact of chronic viral diseases on semen parameters. *Andrologia* **42**, 121–126 (2010).
193. La Vignera, S., Condorelli, R. A., Vicari, E., D'Agata, R. & Calogero, A. E. Sperm DNA damage in patients with chronic viral C hepatitis. *Eur. J. Intern. Med.* **23**, e19–e24 (2012).
194. Hofny, E. R. M. *et al.* Semen and hormonal parameters in men with chronic hepatitis C infection. *Fertil. Steril.* **95**, 2557–2559 (2011).
195. Hofer, H. *et al.* Seminal fluid ribavirin level and functional semen parameters in patients with chronic hepatitis C on antiviral combination therapy. *J. Hepatol.* **52**, 812–816 (2010).
196. Durazzo, M. *et al.* Alterations of seminal and hormonal parameters: An extrahepatic manifestation of HCV infection? *World J. Gastroenterol.* **12**, 3073–3076 (2006).

197. Gianella, S. *et al.* Shedding of HIV and human herpesviruses in the semen of effectively treated HIV-1-infected men who have sex with men. *Clin. Infect. Dis.* **57**, 441–447 (2013).
198. Israel, B., Hospi-, N. Y. & Cancer, M. S. Testicular Dysfunction in Human Immunodeficiency Virus-Infected Men. *Metabolism* **44**, 946–953 (1995).
199. De, M. E. & Waxman, M. Original Contributions Testicular Atrophy in AIDS: A Study of 57 Autopsy Cases. *Testic. atrophy AIDS* 210–214 (1988).
200. Kushnir, V. A. & Lewis, W. Human immunodeficiency virus/acquired immunodeficiency syndrome and infertility: Emerging problems in the era of highly active antiretrovirals. *Fertil. Steril.* **96**, 546–553 (2011).
201. Croxson, T. S. *et al.* Changes in the hypothalamic-pituitary-gonadal axis in human immunodeficiency virus-infected homosexual men. *J. Clin. Endocrinol. Metab.* **68**, 317–321 (1989).
202. Kohn, J. R., Gabrielson, A. T. & Kohn, T. P. Human papilloma virus: to what degree does this sexually transmitted infection affect male fertility? *Fertil. Steril.* **113**, 927–928 (2020).
203. Foresta, C. *et al.* Mechanism of human papillomavirus binding to human spermatozoa and fertilizing ability of infected spermatozoa. *PLoS One* **6**, 1–9 (2011).
204. Souho, T., Benlemlih, M. & Bennani, B. Human papillomavirus infection and fertility alteration: A systematic review. *PLoS One* **10**, 1–9 (2015).
205. du Plessis, S. S., Cardona Maya, W. D. & Omolaoye, T. S. Monkeypox and Male Fertility: Is There Any Looming Danger? *J. Reprod. Infertil.* **23**, 314–317 (2022).
206. Lapa, D. *et al.* Monkeypox virus isolation from a semen sample collected in the early phase of infection in a patient with prolonged seminal viral shedding. *Lancet Infect. Dis.* **22**, 1267–1269 (2022).
207. Bragazzi, N. L., Kong, J. D. & Wu, J. Is monkeypox a new, emerging sexually transmitted disease? A rapid review of the literature. *J. Med. Virol.* **95**, 1–8 (2023).
208. Antinori, A. *et al.* Epidemiological, clinical and virological characteristics of four cases of monkeypox support transmission through sexual contact, Italy, May 2022. *Eurosurveillance* **27**, 1–6 (2022).
209. Liu, J. *et al.* Retrospective detection of monkeypox virus in the testes of nonhuman primate survivors. *Nat. Microbiol.* **7**, 1980–1986 (2022).
210. Joguet, G. *et al.* Effect of acute Zika virus infection on sperm and virus clearance in body fluids: a prospective observational study. *Lancet Infect. Dis.* **17**, 1200–1208 (2017).
211. Uraki, R. *et al.* Zika virus causes testicular atrophy. *Sci. Adv.* **3**, 1–7 (2017).
212. Tsetsarkin, K. A. *et al.* Zika virus tropism during early infection of the testicular

interstitium and its role in viral pathogenesis in the testes. *PLoS Pathog.* **16**, (2020).

213. Govero, J. *et al.* Zika virus infection damages the testes in mice. *Nature* **540**, 438–442 (2016).
214. Ma, W. *et al.* Zika Virus Causes Testis Damage and Leads to Male Infertility in Mice. *Cell* **167**, 1511-1524.e10 (2016).
215. Tanimura, N. *et al.* Pathology of fatal highly pathogenic H5N1 avian influenza virus infection in large-billed crows (Corvus macrorhynchos) during the 2004 outbreak in Japan. *Vet. Pathol.* **43**, 500–509 (2006).
216. Hagag, I. T. *et al.* Pathogenicity of highly pathogenic avian influenza virus H5N1 in naturally infected poultry in Egypt. *PLoS One* **10**, 1–15 (2015).
217. Gazibera, B. *et al.* Spermiogram part of population with the manifest orchitis during an ongoing epidemic of mumps. *Med. Arh.* **66**, 27–29 (2012).
218. Casella, R., Leibundgut, B., Lehmann, K. & Gasser, T. C. Mumps orchitis: Report of a mini-epidemic. *J. Urol.* **158**, 2158–2161 (1997).
219. Selvaraj, K. *et al.* Testicular Atrophy and Hypothalamic Pathology in COVID-19: Possibility of the Incidence of Male Infertility and HPG Axis Abnormalities. *Reprod. Sci.* **28**, 2735–2742 (2021).
220. Yang, M. *et al.* Pathological Findings in the Testes of COVID-19 Patients: Clinical Implications. *Eur. Urol. Focus* **6**, 1124–1129 (2020).
221. Salciccia, S. *et al.* Modeling the contribution of male testosterone levels to the duration of positive covid testing among hospitalized male covid-19 patients. *Diagnostics* **11**, (2021).
222. Lott, N. *et al.* Sex hormones in SARS-CoV-2 susceptibility: key players or confounders? *Nat. Rev. Endocrinol.* (2022) doi:10.1038/s41574-022-00780-6.
223. Salciccia, S. *et al.* Testosterone target therapy: focus on immune response, controversies and clinical implications in patients with COVID-19 infection. *Ther. Adv. Endocrinol. Metab.* **12**, 1–8 (2021).

12 Declaration under oath

Eidesstattliche Versicherung

I hereby declare, under oath, that I have written the present dissertation independently and on my own. Any content taken from other sources are clearly marked as such and listed in the reference section.

Hiermit erkläre ich an Eides statt, dass ich die vorliegende Dissertation unabhängig und eigenständig verfasst habe. Jeglicher Inhalt fremder Quellen ist als deutlich als solcher markiert und in der Referenzliste angegeben.

Hamburg, 10.05.2023

City and Date

Ort und Datum

Signature

Unterschrift

13 Appendix

13.1 List of hazardous substances according to GHS classification

Table 8. Hazardous contaminants with applicable P and H phrases.

Chemical, Reagent or Kit	H Statement	P Statement	Harzard Pictogram
2-mercaptoethanol	H301 + H331, H310, H315, H317, H318, H361fd, H373, H410	P201, P262, P280, P301 + P310 + P330, P302 + P352 + P310, P305 + P351 + P338 + P310	05, 06, 08, 09
2-propanol (isopropanol)	H225, H319, H336	P210, P280, P305 + P351 + P338, P337 + P313	02, 07
3,3'-diaminobenzidin (DAB)	H302, H319, H341, H350	P201, P280, P301 + P312 + P330, P305 + P351 + P338, P308 + P313, P337 + P313	07, 08
Ammoniumperoxodisulfate (APS)	H272, H302, H315, H317, H319, H334, H335	P210, P280, P301 + P012 + P030, P302+P352, P305 + P351 + P338	02, 07, 08
Ampicillin sodium-salt	H317, H334	P261, P280, P342 + P311	08
Citrate Plus Buffer (10x)	H315, H319, H335	P280, P302 + P352, P304 + P340, P305 + P351 + P338	07, 08
Crystal violet	H226, H319, H351, H411	P273, P281, P305 + P351 + P338	02, 07, 08, 09
Diethylpyrocarbonate (DEPC)	H226	P210, P370 + P378	02
Dithiothreitol (DTT)	H302, H412	P264, P270, P273, P301 + P312 + P330, P501	07
Dual-Luciferase® Reporter Assay System	H225	P241, P243, P280, P303 + P361 + P353, P370 + P378, P403 + P235	02
Eosin-Y solution	H225, H290, H319	P210, P280, P305 + P351 + P338, P337 + P313, P403 + P235	02, 05
Ethanol (denatured), for disinfection	H225, H319	P210, P233, P305 + P351 + P338	02, 07
Ethanol (pure)	H225, H319	P210, P233, P305 + P351 + P338	02, 07

Ethidium bromide solution (10 mg/ml)	H331, H341	P261, P281, P311	06, 08
Eukitt	H226, H304, H312 + H332, H315, H319, H335, H373	P210-P260-P280-P301 + P310-P305 + P351 + P338-P370 + P378	02, 07, 08
Forene/Isofluorane (100%)	H336	P261, P271, P303 + P340, P312, P403 + P233, P405, P501	07, 08
Formaldehyde (20 or 37%)	H226, H301 + H311 + H331, H314, H317, H335, H341, H350, H370	P201, P210, P260, P280, P301 + P310 + P330, P303 + P361 + P353, P304 + P340 + P310, P305 + P351 + P338 + P310, P308 + P311, P370 + P378, P403 + P233	02, 05, 06, 08
Glacial acetic acid	H226, H314	P210 + P233 + P240 + P241 + P242 + P243 + P264 + P280	02
Halt™ Protease & Phosphatase Inhibitor Cocktail (100x), including EDTA	H317	P280	07
Hematoxylin	H302	P301 + P312 + P330	07
Hydrochloric acid (37 %)	H290, H314, H335	P280, P303 + P361 + P353, P304 + P340, P305 + P351 + P338, P310	05, 07
Hydrogen peroxide	H302, H318, H412	P280, P301 + P312 + P330, P305 + P351 + P338 + P310	05, 07
Igepal (NP 40)	H302, H315, H318, H410	P280, P301 + P312 + P330, P305 + P351 + P338 + P310	05, 07, 09
innuprep RNA Mini Kit	H302, H314, H412	P101, P102, P103, P260, P303 + P361 + P353, P305 + P351 + P338, P310, P405, P501	05, 07
Ketamine (100 mg/ml)	H302, H332	P261, P264, P301 + P312, P304 + P340, P330	07
Mayer’s hemalum solution	H302, H319, H373	P260 + P264 + P270 + P280	08
Methanol	H225, H301, H311, H331, H370	P210.3, P270, P280.7, P303 + P361 + P353, P304 + P340, P308 + P311	02, 06, 08

Multiplex mouse immunoassay, custom-designed (IL-1b, IL6, TNF-a, IL-10, IFN-a, MCP-1, IL-17A, IL21)	-	P273, P280, P302 + P352, Ü305 + P351 + P338, P313	07
NucleoBond Xtra Maxi	H226, H315, H319, H334	P210, P261, P280, P342 + P311	02, 07, 08
Ottix Plus	H224, H319, H336, H411	P210, P233, P273, P280, P370 + P378, P403 + P235	02, 07, 09
Ottix Shaper	H225	P210, P233, P241, P242, P370 + P378, P501	02
Paraformaldehyde	H228, H302 + H332, H315, H317, H318, H335, H351	P210, P261, P280, P301 + P312 + P330, P305 + P351 + P338 + P310, P370 + P378	02, 05, 07, 08
Passive Lysis Buffer (5x)	H360	P201, P202, P280, P308 + P313, P405, P501	08
Penicillin-Streptomycin (P/S)	H302, H317, H361	P280, P302 + P352, P308 + P313	07, 08
Phenylmethanesulfonyl fluoride (PMSF)	H301, H314	P280, P301 + P310 + P330, P303 + P361 + P353, P304 + P340 + P310, P305 + P351 + P338	05, 06
Polyethylenimine (PEI)	H302, H317, H319, H411	P273, P280, P305 + P351 + P338	07, 09
Potassium dihydrogene phosphate	H315, H319	P264, P280, P305 + P351 + P338, P321, P332 + P313, P337 + P313	07
Proteinase K	H315, H319, H334, H335	P261, P284, P305 + P351 + P338, P342 + P311, P405, P501	07, 08
Pursept-A Xpress, for disinfection	H225, H319	P210, P271, P305 + P351 + P338, P337 + P313, P403 + P233	02, 07
QIAprep Spin Miniprep Kit	H225, H290, H315, H317, H319, H334, H336	P210, P261, P280, P284, P304 + P340, P342 + P311	02, 05, 07, 08
QIAquick Gel Extraction Kit	H302, H318, H412	P280, P305 + P351 + P338 + P310	05, 07

QIAquick PCR Purification Kit	H225, H315, H319, H336	P210, P280	02, 07
RNAlater RNA Stabilization Reagent	H302, H402	P301 + P312, P330, P270, P264, P273	07
RNase-Free DNase Set	H317, H334	P261, P280, P284, P304 + P340, P342 + P311	08
Rotiphorese Gel 30 (Acrylamide)	H302, H315, H317, H319, H340, H350, H361f, H372	P201 P280.7 P301+P312.0 P302+P352.1 P305+P351+P338 P308+P313 i	07, 08
Sodium azide	H300 + H310 + H330, H373, H410	P262, P273, P280, P301 + P310 + P330, P302 + P352 + P310, P304 + P340 + P310	06, 08, 09
Sodium dodecylsulfate (SDS)	H315, H318, H335	P261, P280, P302 + P352, P304 + P340 + P312, P305 + P351 + P338 + P310	05, 07
Sodium hydroxide (NaOH)	H290, H314	P233, P280, P303 + P361 + P353, P305 + P351 + P338, P310	05
Sodium pyruvate solution (Na-pyruvate; 100 mM)	H317, H319	P280, P302 + P352, P305 + P351 + P338	07
Sterilium, for hand disinfection	H226, H319, H336	P102, P210, P305 + P351 + P338, P337 + P313, P301 + P310, P501	02, 07
Superscript™ III Reverse Transcriptase Kit	H302, H412	P264, P270, P273, P301 + P312 + P330, P501	07
Tetramethylethylenediamine (TEMED)	H225, H302 + H332, H314	P210, P280, P301 + P330 + P331, P303 + P361 + P353, P304 + P340 + P312, P305 + P351 + P338	02, 05, 07
Triton X-100	H318	P280, P305 + P351 + P338, P313	05
Trizol Reagent	H301, H311, H331, H314, H335, H341, H373, H412	P201, P261, P264, P280, P273, P301 + P310, P302 + P352, P303 + P361 + P353, P304 + P340, P305 + P351 + P338, P403 + P233, P501	05, 06, 08
Trypsin from bovine pancreas, TPCK-treated (TPCK trypsin)	H315, H319, H334, H335	P261, P280, P284, P304 + P340, P337 + P313, P342 + P311	07, 08

Virkon S, for disinfection (BSL-3 work)	H302, H314, H318, H334, H317, H410	P260, P280, P285, P270, P301 + P330 + P331, P303 + P361 + P353, P304 + P340, P305 + P351 + P338, P405, P501	05, 07, 08, 09
Xylazine (20 mg/ml)	H301	P264, P301 + P310, P330	06
Xylol	H226, H304, H312 + H332, H315, H319, H373	P210, P301 + P330 + P331, P302 + P352, P305 + P351 + P338, P314,	02, 07, 08
ZytoChemPlus (HRP) Broad Spectrum (DAB) Kit	H341, H350	P201, P281, P308+P313	08

Figure 22. GHS codes of Hazard pictograms.

Shown are the 9 hazard pictograms, accompanying Table 8

13.2 Supplemental information

Supplementary Table 1. qRT-PCR primers for murine cytokines/chemokines and the host gene used in this study

Gene	Sequence 5'-3'
TNF-α	Forward: CAGAAAGCATGATCCGCGAC
	Reverse: GGCCATAGAACTGATGAGAGGG
MIP-1α	Forward: CAGCCAGGTGTCATTTTCCTG
	Reverse: CTCGATGTGGCTACTTGGCA
MIP-1β	Forward: AACCTAACCCCGAGCAACAC
	Reverse: GGGTCAGAGCCCATTGGTG
IFN-γ	Forward: AGGTCAACAACCCACAGGTC
	Reverse: GAATCAGCAGCGACTCCTTT
IL-1β	Forward: GAGCCCATCCTCTGTGACTC
	Reverse: AGCTCATATGGGTCCGACAG
IL-10	Forward: GGTTGCCAAGCCTTATCGGA
	Reverse: CACCTTGGTCTTGGAGCTTATT
IL-6	Forward: CTCCCAACAGACCTGTCTATAC
	Reverse: GTGCATCATCGTTGTTCATAC
Eotaxin	Forward: GAGCTCCACAGCGCTTCTAT
	Reverse: GAAGTTGGGATGGAGCCTGG
VEGF	Forward: TCTGAGAGAGGCCGAAGTCC
	Reverse: GCGGGGTGCTTTTGTAGACT
IL-15	Forward: CGCCCAAAAGACTTGCAGTG
	Reverse: GGTGGATTCTTTCCTGACCTCT
GM-CSF	Forward: AAGGTCCTGAGGAGGATGTGG
	Reverse: GTCTGCACACATGTTAGCTTCTTG
YWHAZ	Forward: CACGCTCCCTAACCTTGCTT
	Reverse: ATCGTAGAAGCCTGACGTGG

Supplemental Table 2. Characteristic of H7N9 patients

Characteristic	18-49 years (*n*=44)	≥50 years (*n*=54)
Time from illness onset to sampling (days)		
Median	6.5	7.5
Q1-Q3	5-8.3	6-9
Antiviral treatment (%)		
Yes	39 (89%)	46 (85%)
No	5 (11%)	8 (15%)
Year (%)		
2014-2016	10 (23%)	10 (19%)
2017	34 (77%)	44 (81%)
Region (%)		
South	32 (73%)	33 (61%)
North	12 (27%)	21 (39%)

Data are median (25th quartile-75th quartile, Q1-Q3) or *n* (%).

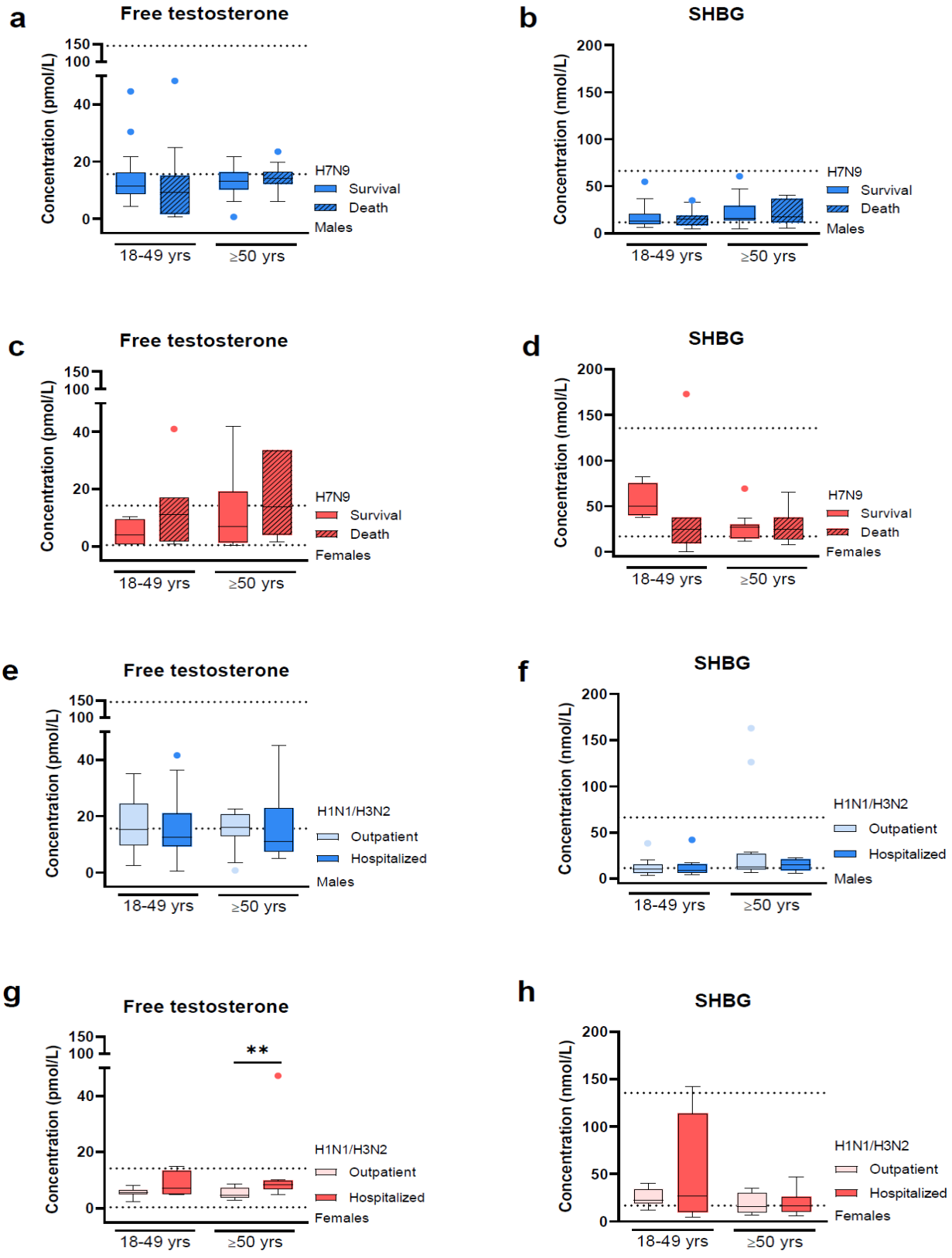

Supplementary Figure 1. Free testosterone and SHBG levels in H7N9 and seasonal influenza cases.

(a, b) Shown are the free testosterone and sex hormone binding globulin (SHBG) levels from H7N9-infected male patients in dependency of disease outcome in each age group (18-49 yrs survival/death:

n=18/15, ≥50 yrs survival/death: n=27/11); (c, d) Shown are the free testosterone and SHBG levels from H7N9-infected female patients in dependency of disease outcome in each age group (18-49 yrs survival/death: n=4/7, ≥50 yrs survival/death: n=10/6); (e, f) Shown are the free testosterone (18-49 yrs outpatient/hospitalized: n=15/11, ≥50 yrs outpatient/hospitalized: n=12/14) and SHBG levels (18-49 yrs outpatient/hospitalized: n=16/11, ≥50 yrs outpatient/hospitalized: n=12/14) from seasonal influenza-infected male patients in both age groups; (g, h) Shown are the free testosterone and SHBG levels from seasonal influenza-infected female patients in both age groups (18-49 yrs outpatient/hospitalized: n=12/4, ≥50 yrs n=13/10). (a-g) Data are presented as Box-and-whisker plots (Tukey). The horizontal line in each box represents the median value. The 25th-75th percentiles represent the endpoints of the box. The whiskers stretch to the lowest and highest values within 1.5 times the interquartile range (IQR) from the 25th-75th percentiles. Dots represent outliers according to Tukey's definition. The two dotted lines in each figure represent the reference ranges for free testosterone (a, e: 15.6-145.6 (pmol/L); c, g: 0.35-14.21 (pmol/L)) and SHBG (b, f: 11.5-66.3 (nmol/L); d, h: 16.8-135.5 (nmol/L)). Statistically significant differences between groups were determined using unpaired, two-tailed non-parametric analysis (Mann-Whitney test), and a P value of < 0.05 was considered significant (* $p < 0.05$, ** $p < 0.01$, *** $p < 0.001$, **** $p < 0.0001$) (adapted from my publication[87]).

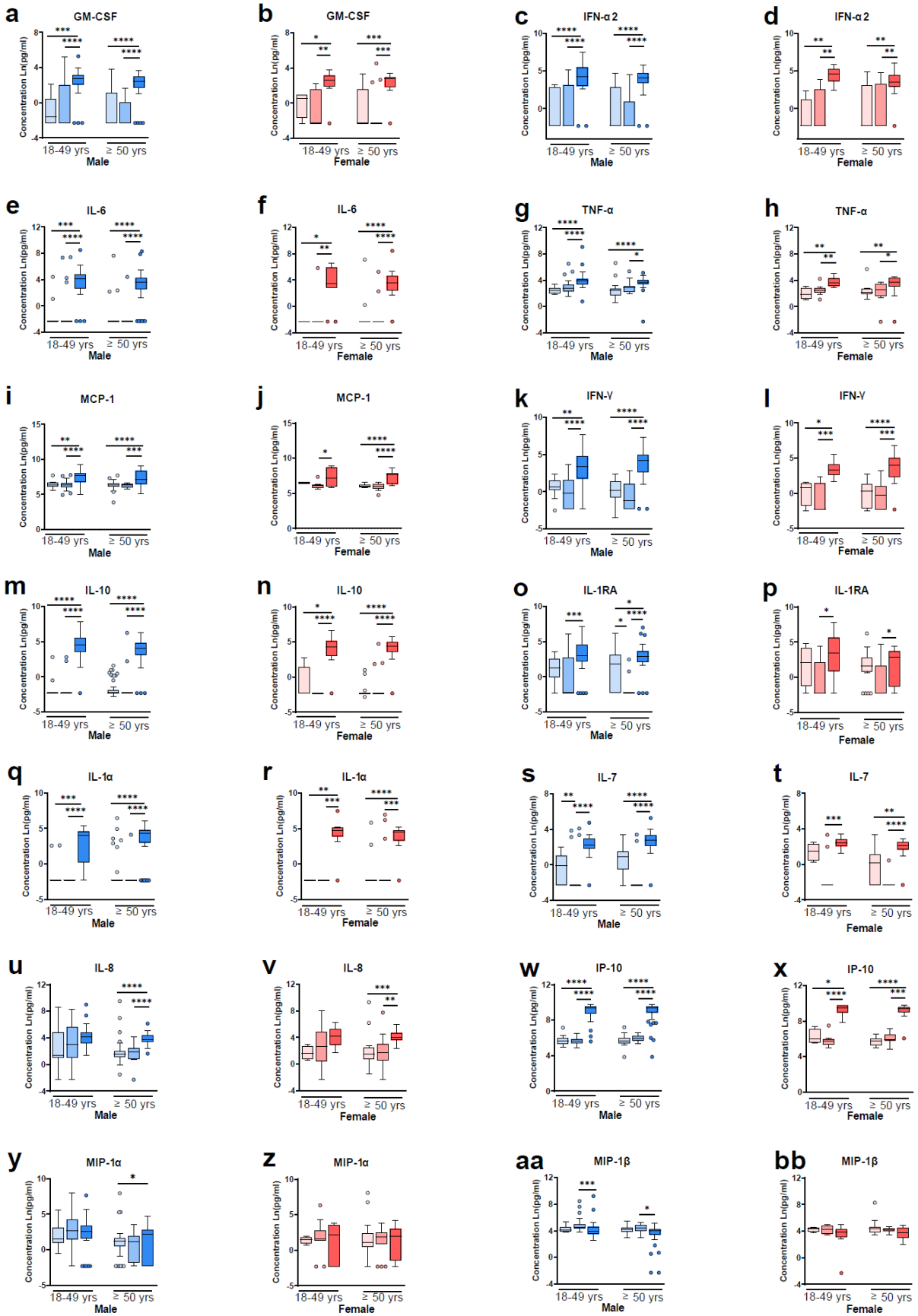
a GM-CSF
b GM-CSF
c IFN-α2
d IFN-α2
e IL-6
f IL-6
g TNF-α
h TNF-α
i MCP-1
j MCP-1
k IFN-γ
l IFN-γ
m IL-10
n IL-10
o IL-1RA
p IL-1RA
q IL-1α
r IL-1α
s IL-7
t IL-7
u IL-8
v IL-8
w IP-10
x IP-10
y MIP-1α
z MIP-1α
aa MIP-1β
bb MIP-1β
Concentration Ln(pg/ml)
18-49 yrs
≥ 50 yrs
Male
Female
Males
H7N9-negative poultry workers
H7N9-negative close contacts
H7N9 cases
Females
H7N9-negative poultry workers
H7N9-negative close contacts
H7N9 cases

Supplementary Figure 2. Cytokine and chemokine response in H7N9 IAV-infected patients compared to control groups.

(a-bb) Shown are the expression levels of cytokines and chemokines in the sera from H7N9 IAV-infected male and female patients who were significantly altered compared to control groups, each divided into two groups based on age: 18-49 years (yrs) and ≥ 50 years old. The number of samples in males were as follows: poultry workers (18-49 yrs: n=12, ≥50 yrs: n=45), H7N9 close contacts (18-49 yrs: n=29, ≥50 yrs: n=16), and H7N9 cases (18-49 yrs: n=33, ≥50 yrs: n=38). The number of samples in females were as follows: poultry workers (18-49 yrs: n=4, ≥50 yrs: n=20), H7N9 close contacts (18-49 yrs: n=11, ≥50 yrs: n=15), and H7N9 cases (18-49 yrs: n=10, ≥50 yrs: n=16). Cytokine/chemokine expression values were used after Ln (natural logarithm) transformation. The measurement was carried out using a multiplex immunoassay. The following analytes were included: GM-CSF (granulocyte-macrophage colony-stimulating factor; a, b), IFN-α2 (interferon alpha 2; c, d), IL-6 (interleukin 6; e, f), TNF-α (tumor necrosis factor alpha; g, h), MCP-1/CCL2 (monocyte chemoattractant protein 1; i, j), IFN-γ (interferon gamma; k, l), IL-10 (interleukin-10; m, n), IL-1RA (interleukin 1 receptor antagonist; o, p), IL-1α (interleukin 1 alpha; q, r), IL-7 (interleukin 7; s, t), IL-8 (interleukin 8; u, v), IP10/CXL10 (interferon gamma-induced protein 10; w, x), MIP-1β/CCL4 (macrophage inflammatory protein 1 beta; y, z) and MIP-1α/CCL3 (macrophage inflammatory protein 1 alpha; aa, bb). Data are presented as Box-and-whisker plots (Tukey). The horizontal line in each box represents the median value. The 25th-75th percentiles represent the endpoints of the box. The whiskers stretch to the lowest and highest values within 1.5 times the interquartile range (IQR) from the 25th-75th percentiles. Dots represent outliers according to Tukey's definition. Statistically significant differences between groups were determined using the Kruskal-Wallis test and Dunn's post hoc test. A P value of < 0.05 was considered a significant difference (* $p < 0.05$, ** $p < 0.01$, *** $p < 0.001$, **** $p < 0.0001$) (adapted from my publication[87]).

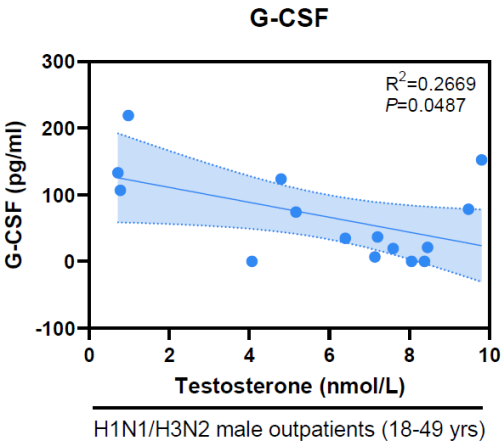

Supplementary Figure 3. Linear regression analysis of testosterone-modulated inflammatory immune responses in seasonal influenza-infected males.

Shown is the observed regression between testosterone and G-CSF (granulocyte colony-stimulating factor) in seasonal influenza male outpatients aged 18-49 years (n=15). Testosterone expression levels measured in the plasma from seasonal IAV-infected male outpatients were plotted over the respective G-CSF levels. Two-tailed linear regression analysis was performed from outpatients and hospitalized patients, and no adjustment for multiple hypotheses was performed due to the explorative nature of the study. The best-fit line with 95% confidence intervals is shown. The measure of centre for the error bands is the regression line. The R squared and P values are shown in the graph (adapted from my publication[87]).

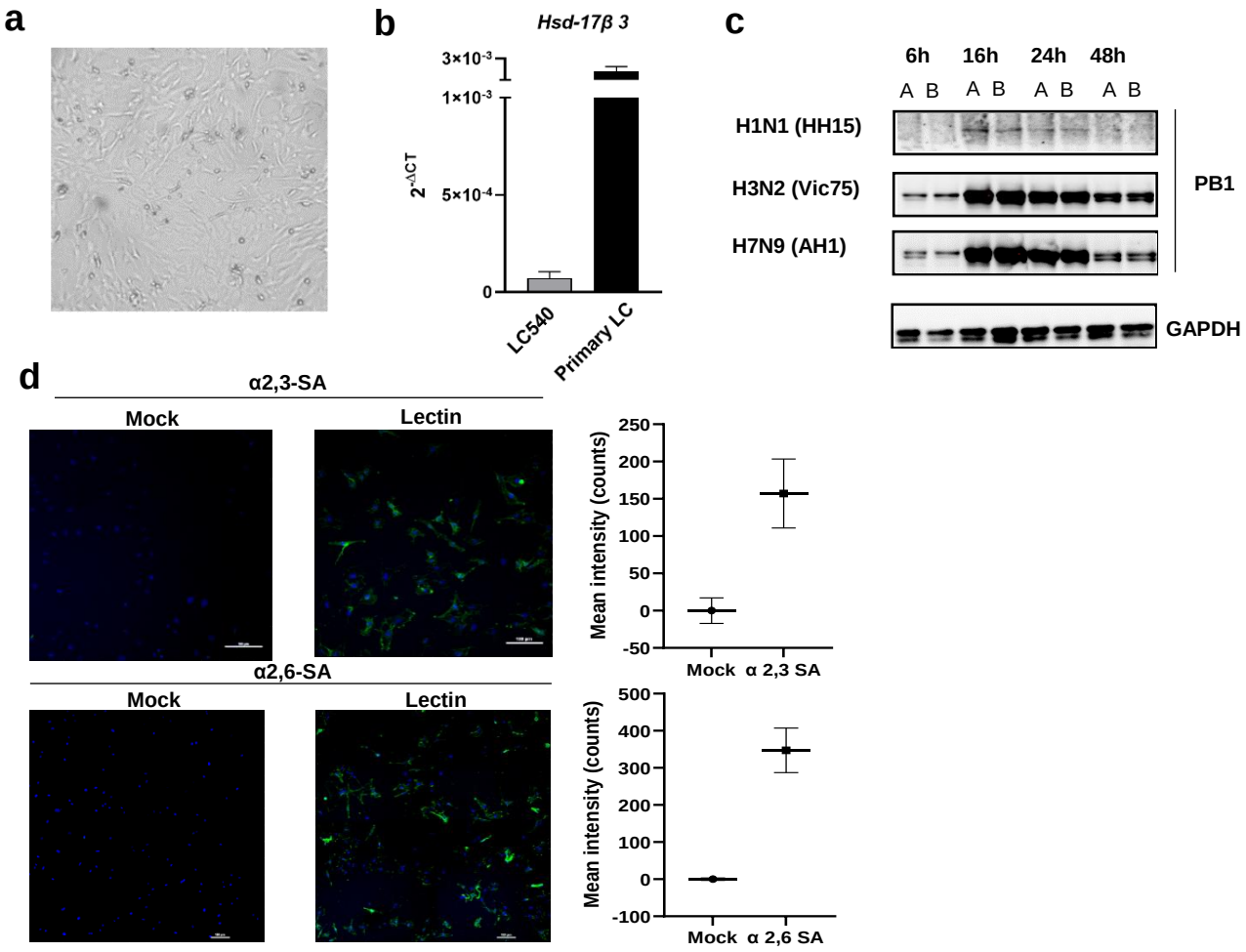

Supplementary Figure 4. Confirmation of the replication of influenza A virus in Leydig cell and primary rat Leydig cells.

(a) Expression of viral polymerase basic protein 1 (PB1) in H1N1, H3N2 and H7N9 infected Leydig cell lines was analyzed by Western blotting at 6h, 16h, 24 h and 48 h p.i. (in duplicates, A and B). GAPDH was detected as loading control; (b) Microscopic image of primary rat Leydig cells cultured for 6 days after isolation (10X); (c) Normalized mRNA expression levels of the Leydig cell marker 17β-Hydroxysteroid dehydrogenase 3 (HSD-17β 3) in the rat tumor Leydig cell line (LC540) and primary rat Leydig cells; (d) Cells were fixed in 4 % PFA solution at 4 c° and nuclei of cells were stained with Hoechst dye. Cells were subjected to immunostaining without (Mock) or with the primary lectin (α 2,3-SA: Biotinylated Maackia Amurensis Lectin II or α 2,6-SA: Sambucus Nigra Lectin), followed by staining with a secondary streptavidin (Alexa Fluor™ 488 conjugate). Images were acquired on a confocal spinning disc microscope at 20x magnification. Scale bars represent 100 µm. Quantification of both receptors was conducted through MATLAB program. Codes were provided the Methods.

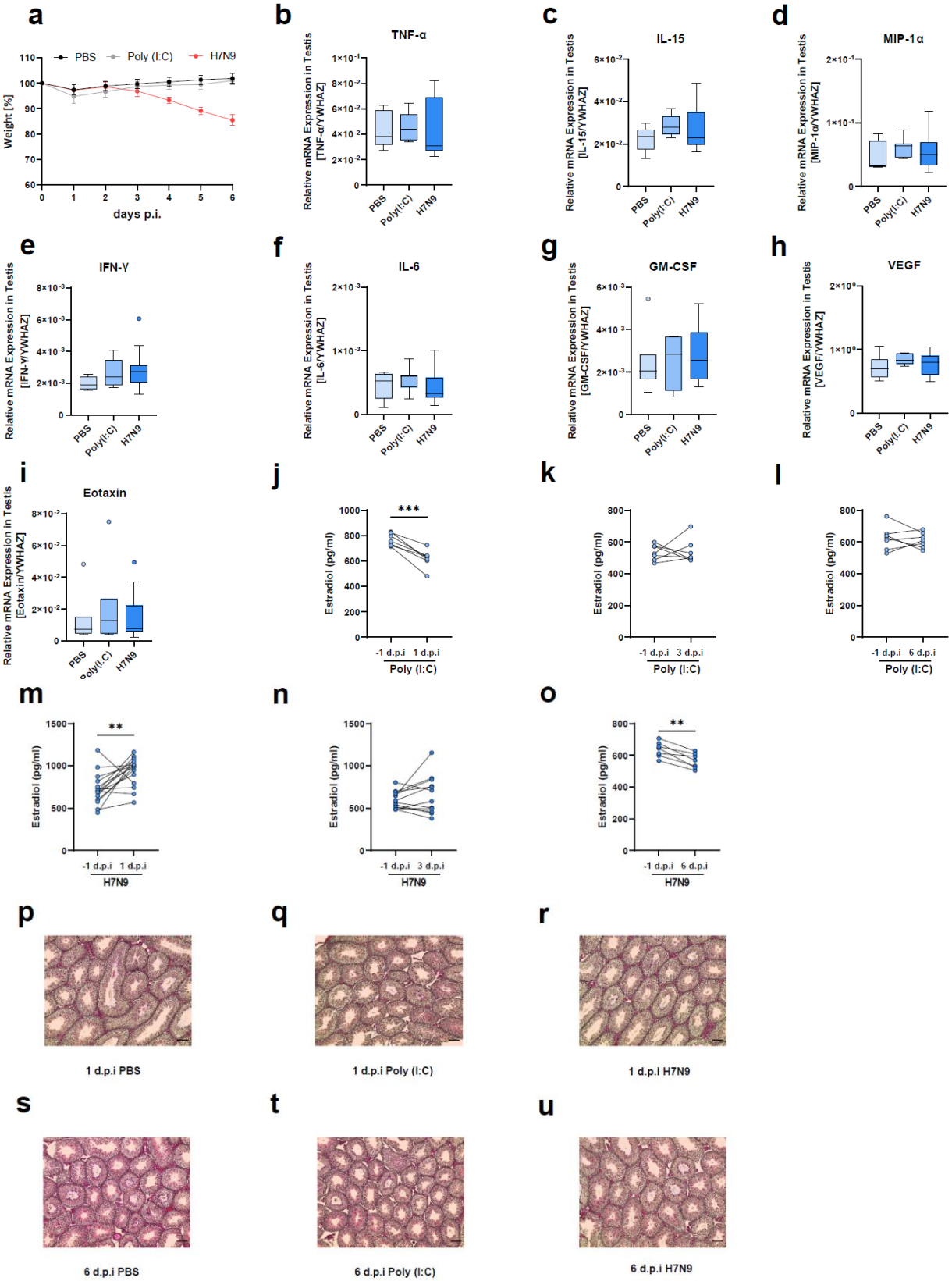

Supplementary Figure 5. Weight loss, testicular inflammation, histopathology and estradiol levels in H7N9 infected mice.

(a) Weight loss of PBS-, Poly (I:C)- and H7N9-treated mice up to 6 d.p.i (b-i) Cytokine and chemokine levels without significant differences in the testes from PBS (n=7)-, Poly (I:C)- (n=7)- and H7N9 (n=16)-treated mice at 3 d.p.i. Data are presented as Box-and-whisker plots (Tukey). The horizontal line in each box represents the median value. The 25th-75th percentiles represent the endpoints of the box. The whiskers stretch to the lowest and highest values within 1.5 times the interquartile range (IQR) from the 25th-75th percentiles. Dots represent outliers according to Tukey's definition. (j-l) Estradiol levels in Poly (I:C)-treated mice at 1 day before treatment (-1 d.p.i) vs. treated mice at 1 day (n=7 vs. n=7), 3 days (n=7 vs. n=7) and 6 days (n=7 vs. n=7) post treatment. (m-o) Estradiol levels in H7N9-infected mice at 1 day before infection (-1 d.p.i) vs. infected mice at 1 day (n=15 vs. n=15), 3 days (n=12 vs. n=12) and 6 days post infection (n=7 vs. n=7). (p-u) Hematoxylin and eosin (HE)-stained paraffin sections from Bouin fixed testis tissue at 1 (p-r) and 6 d.p.i (s-u) were evaluated via light microscopy. Shown are representative histological images of the testes of PBS (1 d.p.i., n=6; 6 d.p.i., n=7)- or Poly (I:C) (1 d.p.i., n=6; 6 d.p.i., n=7)-control treated and H7N9-infected (1 d.p.i., n=6; 6 d.p.i., n=7) mice (10X). Scale bars (100 µm) are shown in the bottom right of each micrograph. (b-i) Statistically significant differences among the three groups were determined using either two-tailed one-way ANOVA or the Kruskal-Wallis test (b-i). (j-o) Statistically significant differences in estradiol were determined by paired, two-tailed t test or non-parametric analysis (j-o). A P value of < 0.05 was considered a significant difference (* $p < 0.05$, ** $p < 0.01$, *** $p < 0.001$, **** $p < 0.0001$) (adapted from my publication[87]).

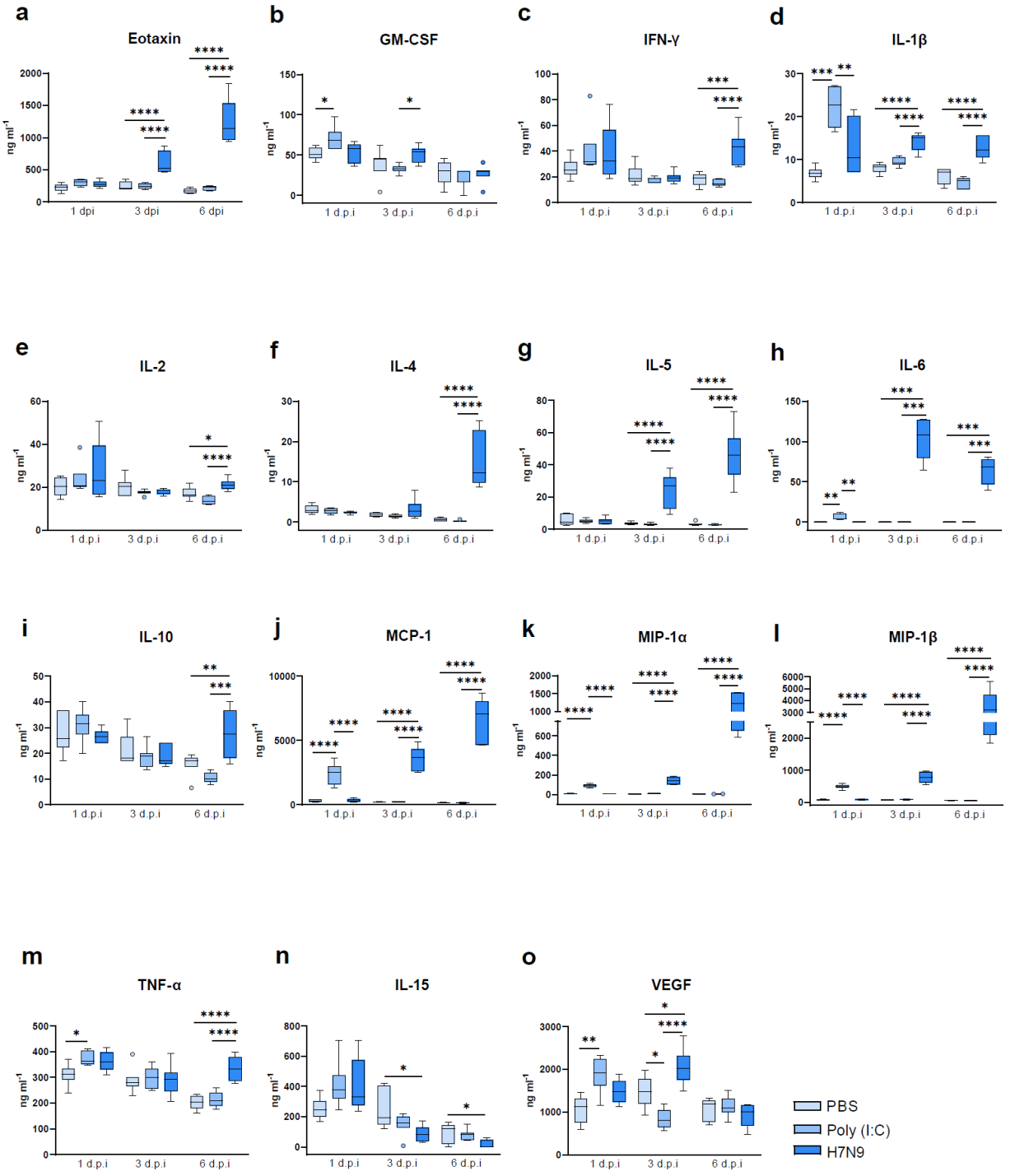

Supplementary Figure 6. Pulmonary inflammatory response in H7N9-infected mice.

(a-o) Cytokines and chemokines were measured in the lungs of PBS and Poly (I:C) control-treated or H7N9 infected mice at 1d.p.i (PBS: n=6, Poly (I:C): n=6, H7N9:n=6), 3 d.p.i (PBS: n=7, Poly (I:C):n=7, H7N9: n=7) and 6 d.p.i (PBS: n=7, Poly (I:C): n=7, H7N9:n=7) using a Bio-Plex Pro Mouse Cytokine multiplex assay. The following analytes were included: Eotaxin (a), GM-CSF (Granulocyte-macrophage colony-stimulating factor; b), IFN-γ (interferon gamma; c), IL-1β (interleukin 1 beta; d), IL-2 (interleukin 2; e), IL-4 (interleukin 4; f), IL-5 (interleukin 5; g), IL-6 (interleukin 6; h), IL-10 (interleukin 10; i), MCP-1

(monocyte chemoattractant protein 1; j), MIP-1α (macrophage inflammatory protein 1 alpha; k), MIP-1β (macrophage inflammatory protein 1 beta; l), TNF-α (tumor necrosis factor alpha; m), IL-15 (interleukin 15; n), and VEGF (vascular epidermal growth factor; o). Data are presented as box-and-whisker plots (Tukey). The horizontal line in each box represents the median value. The 25th-75th percentiles represent the endpoints of the box. The whiskers stretch to the lowest and highest values within 1.5 times the interquartile range (IQR) from the 25th-75th percentiles. Dots represent outliers according to Tukey's definition. Statistically significant differences among groups were determined using either two-tailed ANOVA or the Kruskal-Wallis test. A P value of < 0.05 was considered a significant difference (* $p < 0.05$, ** $p < 0.01$, *** $p < 0.001$, **** $p < 0.0001$) (adapted from my publication[87]).

14 Acknowledgement

This work is a very successful story would not have been achieved without a great teamwork and a productive environment. I am extremely grateful for the great ideas, inspirations, support and fun from everyone in the lab throughout the last 3 and half years with its ups and downs. I will use these lines to especially thank the following people:

Prof. Dr. Gülşah Gabriel

I would like to express my deepest gratitude to your strong belief, guidance, support and encouragement throughout my PhD journey. All your insightful feedback have been instrumental in shaping the direction and scope of this thesis. Without your persistence and strong belief, I think we could not achieve this successful story.

Prof. Dr. Thomas Dobner

Thank you very much for being a reviewer of this thesis the feedback you have given in project meetings.

Prof. Yuelong Shu

Thank you very much for facilitating my PhD program and cooperation with Gülşah in Germany. Thanks very much for your great support, input throughout the entire process of my project from distance.

Dr. Sebastian Beck

The wonder of fate is indescribable. I really appreciate working with you again after your two visits in Beijing. Thanks so much for your excellent guidance, support and critical thinking during the ups and downs of this project. I enjoyed every discussions and brainstormings with you and it was always helpful to me.

Prof. Yongkun Chen

I would like to extend my heartfelt thanks to your unwavering support, trust and encouragement from the very beginning of this project and throughout every steps of this long journey. Particularly, thank you very much for organizing everything, conducting measurement and providing your inputs from distance.

Dr. Stephanie Stanelle-Bertram

So happy to work together again from Beijing to Hamburg. Thanks very much for your great support and guidance in the lab and my project. I have learnt a lot from your experience and the organized performance particularly in all animal experiments.

Dr. Nancy Mounogou Kouassi

Thank you very much for great support in my thesis such as the primer designing and animal experiment. I really like your optimism, your good mood, true, laughs, and tears. I always enjoy our discussion and hope my endless questions did not bother you that much.

Martin Zickler

Thank you for all great support in the lab, the great working atmosphere, the beers and the loud music in S3.

Fabian Stoll

Thank you for the great working atmosphere and always trying to find solutions and discussing all problems. Thank for your attention to detail and perfectionism, whether they are important or not. Thank you for all the fun before or after drinking some beers.

Dr. Zoé Schmal

Thanks for your optimism and your ability to always find something funny in any situation. I enjoyable for our conversations and those colorful LED lights in your Mini Cooper.

Victoria Pfordt

Thank you very much for helping me with the Germany language checking of my thesis.

Dr. Aljawazneh Amirah

Thank you very much for experience sharing for the preparing the PhD thesis and defence. Thanks for the fun during our lunchtime.

Hanna Jania

Thank you very much for all your great help in the lab, for always being calm and collected. I always enjoy working with you. Thanks very much for your accompany and fun for almost every lunch in Mensa.

Annette Gries

Thanks very for all you excellent support and guidance in the lab. I learnt a lot from your experience. I really enjoy all the conversations, your fruitful stories, and your words of encouragement.

Anna Lüttjohann

Thank you so much for your great support in my thesis. I really appreciate your proactive attitude and cheery mood. Thanks for all the fun off work.

Jenny Ruschinski and Britta Weseloh

Thank you for all the scientific support and good conversations in the office.

Ursula Müller
Thank you for the excellent help with all animal-related projects and general guidance in all questions regarding animals. Thanks for all the fun during our lunchtime.
Ute Neumann
Thank you for support in all office-related questions and organizational matters.
Bahaaeldin Alhammady
Thank you for all support and fun during work and off work.

In addition, I would like to express my appreciation to all the people that I did not mention by name who have provided me with an intellectual community, and moral support. Their insightful conversations, brainstorming sessions, and constructive feedback have been invaluable to me.

I would like to extend my heartfelt thanks to my family and friends for their unwavering support and encouragement. Their love, patience, and understanding have been a constant source of strength and inspiration for me throughout this challenging journey.

Lastly, I would like to acknowledge the research participants who have generously given their time, expertise, and insights. Their contributions have made this study possible, and I am grateful for their willingness to share their experiences and knowledge.